Chemical Science

ROYAL SOCIETY OF CHEMISTRY

REVIEW

View Article Online
View Journal | View Issue

Cite this: *Chem. Sci.*, 2026, **17**, 2932

Mitigation strategies for Li_2CO_3 contamination in garnet-type solid-state electrolytes: formation mechanisms and interfacial engineering

Bin Hao,[a] Qiushi Wang,[a] Fangyuan Zhao,[a] Jialong Wu,[a] Weiheng Chen,[b] Zhong-Jie Jiang *[c] and Zhongqing Jiang *[a]

Garnet-type solid-state electrolytes (SSEs) are promising candidates for next-generation solid-state batteries (SSBs) owing to their high ionic conductivity, robust mechanical strength, and broad electrochemical stability window. However, exposure to ambient air results in the formation of a Li_2CO_3 passivation layer on the surface, significantly reducing ionic conductivity and deteriorating interfacial wettability, thereby severely impairing the electrochemical performance of SSBs. This review systematically analyzes the formation mechanisms and influencing factors of Li_2CO_3 contamination on garnet-type SSE surfaces. It summarizes recent strategies for suppressing Li_2CO_3 formation, including sintering process optimization, elemental doping, and grain boundary/interface engineering. Among these approaches, interfacial treatments have attracted considerable attention owing to their cost-effectiveness and operational efficiency. This review focuses on categorizing diverse treatment strategies for improving electrode/electrolyte interfacial contact, including physical cleaning, chemical treatment and conversion, and modification with interfacial interlayers—specifically detailing types such as inorganic, organic, and organic–inorganic composite interlayers. Finally, the future prospects of garnet-type SSEs in high-performance SSBs are discussed, pointing out the need for in-depth research into the formation and evolution mechanisms of Li_2CO_3 and the development of more efficient interface control strategies. This review systematically examines interfacial challenges in garnet-type SSEs, with the ultimate goal of facilitating the development of stable all-solid-state lithium metal batteries and accelerating their commercialization.

Received 10th December 2025
Accepted 13th January 2026

DOI: 10.1039/d5sc09699e

rsc.li/chemical-science

[a]*Zhejiang Key Laboratory of Quantum State Control and Optical Field Manipulation, Department of Physics, Zhejiang Sci-Tech University, Hangzhou 310018, P. R. China. E-mail: zhongqingjiang@zstu.edu.cn*

[b]*Vehicle Energy and Safety Laboratory, Department of Mechanical Engineering, Ningbo University of Technology, Ningbo 315336, Zhejiang, P. R. China*

[c]*Guangzhou Key Laboratory for Surface Chemistry of Energy Materials, Guangdong Engineering and Technology Research Center for Surface Chemistry of Energy Materials, College of Environment and Energy, South China University of Technology, Guangzhou 510006, P. R. China. E-mail: eszjiang@scut.edu.cn*

1 Introduction

Lithium-ion batteries (LIBs) represent one of the most advanced energy storage technologies and have found widespread applications in daily life.[1,2] After three decades of development, the energy density of conventional graphite-anode LIBs is approaching its theoretical limit, with commercial LIBs

Bin Hao

Bin Hao received his Bachelor of Science (BS) degree from Tangshan University in 2022 and his Master's degree from Zhejiang Sci-Tech University in 2025. He is currently pursuing a doctoral degree at Shandong University. His main research direction is the interface engineering of solid-state batteries based on garnet-type solid electrolytes.

Qiushi Wang

Qiushi Wang earned his Bachelor of Science (BS) degree from the Central South University of Forestry and Technology in 2022. He is currently a Master's candidate under the supervision of Professor Zhongqing Jiang at Zhejiang Sci-Tech University. His primary research focus centers on plasma preparation of electrode materials for proton exchange membrane fuel cells and silicon carbon anode materials for lithium ion batteries.

achieving only 80–240 Wh kg^{-1}. This severely limits their application in electric vehicles and other high-energy-density devices. Furthermore, the flammable organic solvents in liquid electrolytes pose significant safety risks. Lithium dendrite formation and growth in these electrolytes can cause severe safety hazards and performance degradation, ultimately compromising battery longevity and potentially leading to thermal runaway (Fig. 1a).[3,4] In recent years, with advancements in new technologies, lithium metal batteries (LMBs), which offer a substantially higher theoretical energy density than LIBs, have regained significant research interest.[5] Consequently, solid-state lithium metal batteries (SSLMBs) have emerged as a highly promising alternative to conventional liquid LIBs, combining lithium metal anodes with nonflammable solid electrolytes to simultaneously achieve high energy density and enhanced safety (Fig. 1b).[6,7] Recent years have witnessed significant exploration and development of various solid-state electrolytes (SSEs), accelerating the progress of SSLMBs. These electrolytes encompass lithium phosphorus oxynitride (LiPON),[8] sodium superionic conductor (NASICON)-type,[9] lithium superionic conductor (LISICON)-type,[10] sulfide-type,[11] perovskite-type,[12] and garnet-type materials.[13] Among these, garnet-type oxide SSEs have emerged as particularly promising due to their high ionic conductivity (10^{-4}–10^{-3} S cm^{-1} at room temperature), wide electrochemical stability window, exceptional shear modulus (56–61 GPa, exceeding that of Li metal by sevenfold), and excellent lithium metal compatibility. These superior characteristics position garnet-type electrolytes as leading candidates for SSLMB applications.[14,15] However, numerous studies have shown that the poor interface contact performance of Li/garnet-type SSEs is a major challenge

Fangyuan Zhao

Fangyuan Zhao obtained her Bachelor of Engineering degree from Luoyang Normal University in 2022. She is presently enrolled in a Master's program at Zhejiang Sci-Tech University under the supervision of Professor Zhongqing Jiang. Her primary area of research focuses on the modification and optimization of polymer solid electrolytes utilizing the electrospinning technique.

Jialong Wu

Jialong Wu earned his Bachelor of Science (BS) degree from Shaoxing University in 2023. He is currently a Master's candidate under the supervision of Professor Zhongqing Jiang at Zhejiang Sci-Tech University. His primary research focus centers on interface engineering and performance optimization in solid-state batteries employing garnet-type solid electrolytes.

Weiheng Chen

Weiheng Chen is a PhD student majoring in Mechanical Engineering at Zhejiang Sci-Tech University and obtained his MS degree in Chemistry from Zhejiang Normal University in 2020. His research involves materials development for energy conversion and storage devices. Recently, he mainly focuses on the analysis of chemical and mechanical degradation mechanisms of all-solid-state Li metal batteries and corresponding density functional theoretical simulations.

Zhong-Jie Jiang

Zhong-Jie Jiang has served as a professor in the College of Environment and Energy, South China University of Technology since 2013. He received his PhD degree in Chemistry from the Technical Institute of Chemistry and Physics, Chinese Academy of Science (2005). Before being the professor, he spent 2 years at the Chemnitz University of Technology as a Humboldt Research Fellow (2005–2008), 3 years at the University of California as a Postdoctoral Fellow (2008–2010), and 2 years at the University of California as an Assistant Project Scientist (2011–2013). His research interests include low temperature plasma application, nanoscience, fuel cells, lithium ion batteries, etc.

Zhongqing Jiang

Zhongqing Jiang is a professor in the Department of Physics at Zhejiang Sci-Tech University. Dr Jiang received his PhD in 2010 in Plasma Physics from the Institute of Plasma Physics, Chinese Academy of Sciences. He was a Postdoctoral Fellow at the University of Texas at Austin from 2011 to 2013. His research interests include synthesis and modification of electrode materials and polymer electrolyte membranes using low temperature plasma for applications in fuel cells, all-solid-state Li metal batteries, zinc–air batteries, sodium ion batteries, etc.

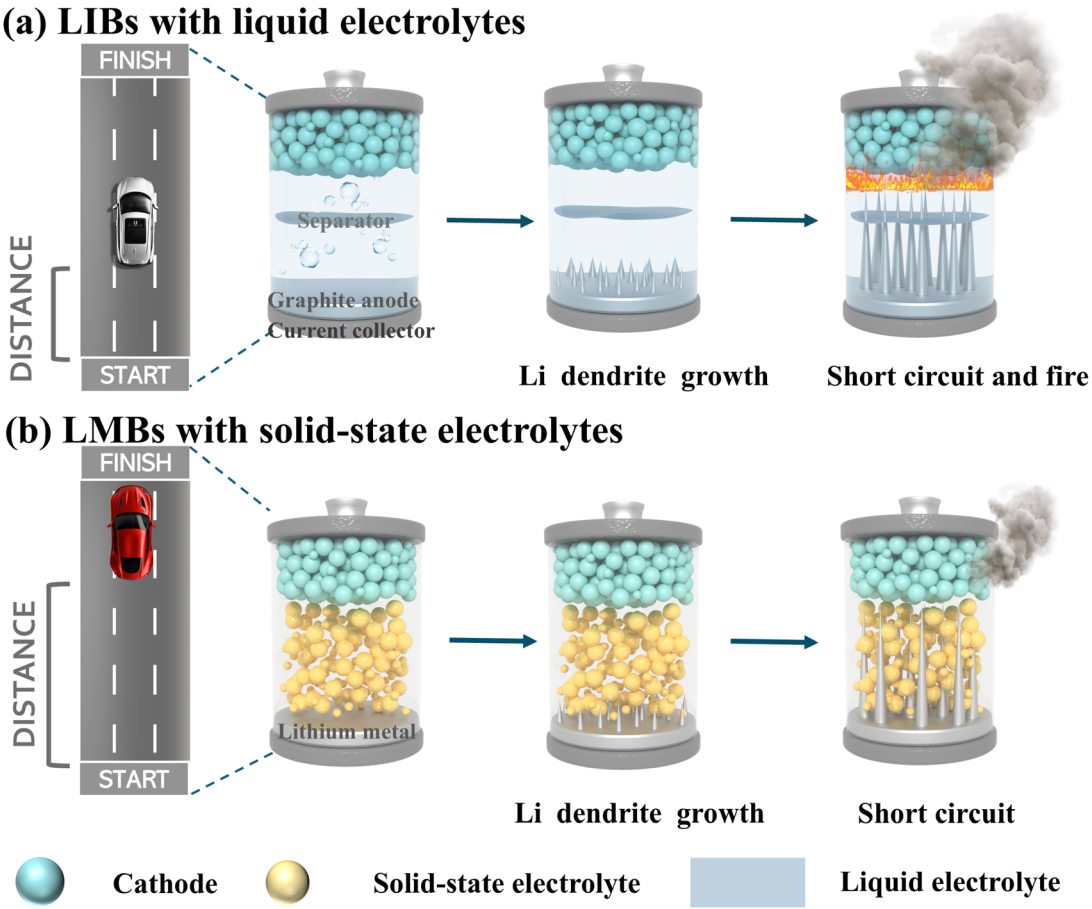

Fig. 1 Comparison of energy output and safety performance between (a) conventional LIBs and (b) SSLMBs.

hindering their large-scale application. The poor air stability of garnet-type SSEs is a primary cause of this issue. Exposure to ambient air induces reactions with moisture and CO_2, forming lithiophobic contaminants (Li_2CO_3 and LiOH) on garnet surfaces. These impurities significantly degrade both the lithium metal/garnet electrolyte interfacial contact and lithium-ion transport across the interface, ultimately impairing battery performance.[16,17]

The garnet-type oxide SSE $Li_7La_3Zr_2O_{12}$ (LLZO) was first reported in 2007. After years of exploration, it was found that substituting part of Zr^{4+} with Ta^{5+} cations to form $Li_{7-x}La_3Zr_{2-x}Ta_xO_{12}$ (LLZTO) could enhance its lithium-ion conductivity by stabilizing the high-conductivity cubic phase structure, while maintaining its stability with Li metal. Although LLZO is chemically stable in air for short periods, recent studies have demonstrated that prolonged air exposure leads to the gradual formation of a lithiophobic Li_2CO_3 passivation layer on its surface. The impact of surface Li_2CO_3 on garnet electrolytes was largely overlooked for a long time. This changed when researchers discovered that Li_2CO_3 induces lithiophobicity, which contrasts sharply with the lithiophilicity of a pristine garnet surface. Consequently, the formation mechanism and detrimental effects of Li_2CO_3 began to be widely studied.[18] The generation of Li_2CO_3 depletes lithium from the LLZO structure, degrading the ionic conductivity of the garnet SSE and increasing grain boundary (GB) resistance, which consequently deteriorates the interfacial impedance.[19] Numerous modification strategies and interfacial engineering approaches have been developed to mitigate Li_2CO_3-related issues in garnet-based solid-state batteries (SSBs). Furthermore, Li foil surfaces readily oxidize due to their high reactivity, forming a composite passivation layer (Li_2CO_3, Li_3N, LiOH, and Li_2O) during processing and storage. This layer reduces battery energy density by impeding ion transfer at the Li anode/electrolyte interface. Both Li_2CO_3 contamination on LLZO surfaces and Li foil passivation significantly hinder the advancement of garnet-based SSBs. The main issues are as follows: (1) the lithiophobic nature and low Li^+ conductivity of Li_2CO_3 severely impede intimate contact between Li metal and LLZO, as well as Li^+ transport across the interface, thereby reducing the overall energy density of the battery; (2) the lithiophobic nature of Li_2CO_3 leads to poor molten lithium wettability, causing both high interfacial resistance (ranging from hundreds to thousands of Ω cm^2) and lithium dendrite formation, which consequently reduces the critical current density (CCD); (3) due to the poor interface contact, the current or charge distribution at the interface becomes uneven, leading to an uneven point-to-point physical connection between the

rigid garnet-type SSE and the lithium metal anode.[24,25] Li metal preferentially deposits at interfaces exhibiting high local current densities, generating excessive localized pressure and inducing thermal instability;[26] (4) Li_2CO_3 impurities degrade the microstructure of LLZO, reducing the particle density and inducing the formation of non-negligible electron conduction pathways inside, which promote lithium nucleation and growth, ultimately increasing the risk of battery short-circuiting;[27] (5) the opaque nature of garnet SSEs makes it difficult to directly observe the interfacial evolution between the SSE and the electrode using common *in situ* non-destructive characterization techniques, creating a bottleneck in comprehensively understanding the interface structure. Therefore, constructing effective strategies to eliminate the Li_2CO_3 passivation layer and exploring diversified interface reconstruction techniques are crucial for enhancing the performance of SSLMBs. These are also key issues that need to be solved to realize the practical application of LLZO.

This review systematically examines the mechanistic impacts of spontaneously formed Li_2CO_3 layers on the interfacial structure and properties of garnet-type SSEs. We will systematically explain the generation pathways of Li_2CO_3 and its core determining factors, explaining how it detrimentally limits the electrochemical performance of garnet-based SSLMBs. Furthermore, we will explore effective strategies for improving the air stability of garnet SSBs. Interfacial stability plays a crucial role in the long-term cycling and high-energy-density operation of SSBs, particularly under high-voltage conditions. Effectively suppressing interfacial side reactions and improving electrolyte stability remain pressing challenges to be addressed.[28] The review will also analyze the core challenges faced by the Li/LLZO interface and the cathode active material/LLZO interface induced by Li_2CO_3, and evaluate the diversified interfacial engineering approaches and regulation mechanisms developed in recent years to address these two types of interface issues. At the end of this review, we conclude with forward-looking perspectives on the future research directions for garnet SSBs, aiming to provide fundamental insights into their surface chemistry and theoretical guidance for the precise manipulation of interfacial properties.

2 Interfacial chemistry and degradation mechanisms in garnet-type SSEs

2.1 Interfacial Li_2CO_3 at the electrode/garnet-type SSE interface

2.1.1 Formation mechanism of Li_2CO_3. The protonation of the garnet-type SSE surface may have occurred as early as during the cooling process after calcination in a high-temperature furnace. As a result, the formation of Li_2CO_3 contaminants might be inevitable. Understanding the formation mechanism of Li_2CO_3 is of significant guiding importance for improving the air stability of garnet-type SSEs. Multiple reaction pathways have been identified for the air–garnet interface (Fig. 2a).[20] Several studies propose a one-step reaction mechanism wherein garnet SSEs directly react with dry CO_2 to form Li_2CO_3 (eqn (1), shown for LLZO). This direct reaction pathway depends critically on the crystal structure and surface characteristics of the garnet-type SSE. Active sites within the crystal structure of the garnet-type SSE can adsorb CO_2 molecules and promote the chemical reaction. Furthermore, surface defects and impurities can increase the reactivity of the surface, facilitating the reaction between CO_2 and the electrolyte to form Li_2CO_3.

$$Li_7La_3Zr_2O_{12} + xCO_2 \rightarrow Li_{7-x}La_3Zr_2O_{12} + xLi_2CO_3 \quad (1)$$

However, first-principles calculations indicate that the one-step reaction pathway is energetically unfavorable, a result that has been experimentally verified. Therefore, some researchers have proposed a two-step reaction pathway. Specifically, when exposed to humid air, water molecules can either directly insert into the garnet structure or react with LLZO *via* a Li^+/H^+ exchange mechanism, resulting in the formation of a surface LiOH layer. The LiOH subsequently reacts with atmospheric CO_2 to form Li_2CO_3 (eqn (2) and (3)). This two-step pathway is considered more prevalent under realistic ambient conditions, which typically contain both moisture and CO_2. In environments with higher relative humidity, the proton exchange reaction between the garnet electrolyte and water is facilitated, thereby accelerating Li_2CO_3 formation. Furthermore, Cheng *et al.*[29] demonstrated that garnet and LiOH form directly through hydration, independent of Li^+/H^+ proton exchange. This occurs when there is sufficient H_2O, leading to the generation of Li_2CO_3.

$$Li_7La_3Zr_2O_{12} + xH_2O \rightarrow Li_{7-x}H_xLa_3Zr_2O_{12} + xLiOH \quad (2)$$

$$2LiOH + CO_2 \rightarrow Li_2CO_3 + H_2O \quad (3)$$

Moreover, these reactions are not limited to the surface but can also proceed within the LLZO bulk, propagating along GBs, especially in inadequately densified pellets. Both LiOH and Li_2CO_3 demonstrate poor lithium-ion conductivity, leading to elevated interfacial resistance at the LLZO/lithium metal interface. Xia *et al.* investigated Ta-doped LLZO pellets (0.5Ta-LLZO) exposed to dry (~5% RH) and humid (~80% RH) air environments for six weeks.[30] Raman spectroscopy revealed characteristic peaks of Li_2CO_3 impurities on the surface of pellets exposed to humid air, whereas no such peaks were detected on those exposed to dry air. Furthermore, Raman mapping images demonstrated that Li_2CO_3 was not only distributed unevenly across the surface of pellets exposed to humid air but also preferentially accumulated at specific surface sites. It has been substantiated that Li_2CO_3 tends to nucleate preferentially around GBs, primarily attributable to the inherently high interfacial energy of these regions. Consequently, the areas highlighted in red on the Raman surface maps of pellets exposed to humid air likely correspond to GBs. In contrast, negligible Li_2CO_3 was observed on the pellets exposed to dry air. These results unequivocally demonstrate that ambient humidity is a critical factor governing the formation of Li_2CO_3.

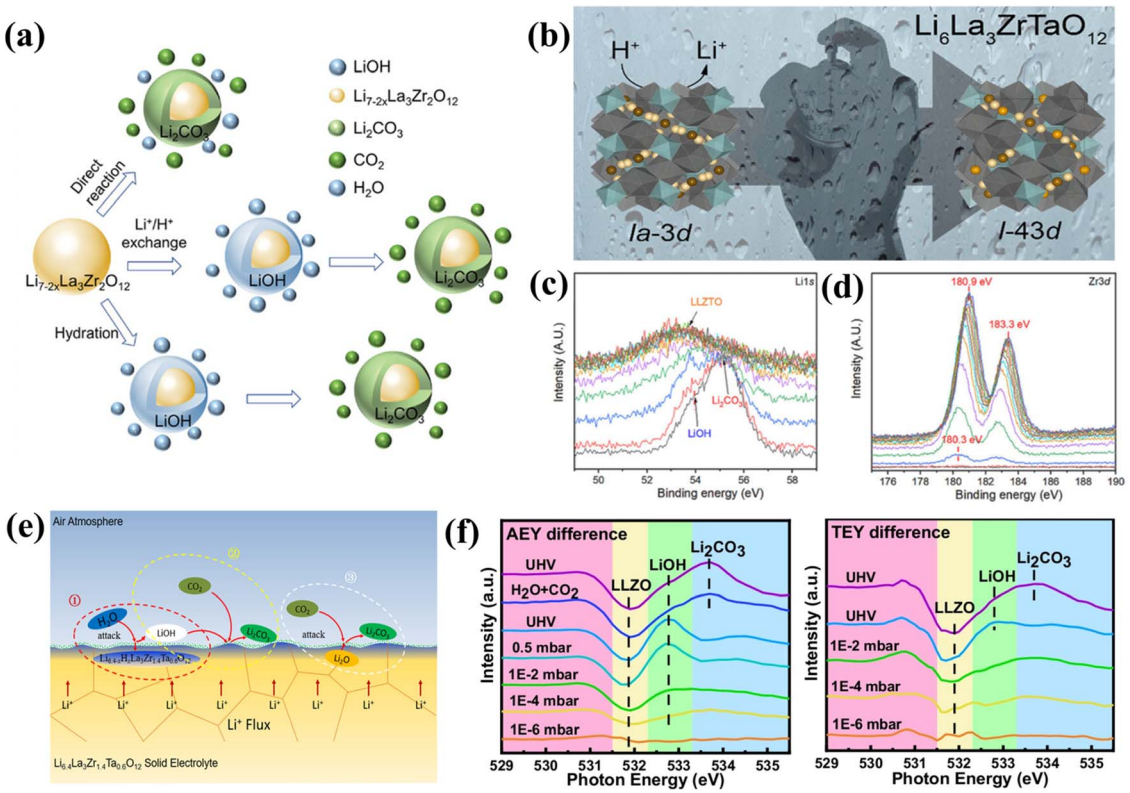

Fig. 2 (a) Reaction pathways of garnet electrolytes with air. Reproduced from ref. 20. Copyright 2024, Wiley-VCH GmbH. (b) Schematic illustration of $Li_6La_3ZrTaO_{12}$ space group transformation following Li^+/H^+ exchange. Reproduced with permission from ref. 21. Copyright 2020, American Chemical Society. XPS depth profiling of the freshly dissociated sample after 24 h air exposure: (c) Li 1s and (d) Zr 3d spectra. (e) Proposed APL formation mechanism on LLZTO surfaces. Reproduced with permission from ref. 22. Copyright 2022, American Chemical Society. (f) Comparative AEY and TEY spectra under varying H_2O/CO_2 pressures. Reproduced from ref. 23. Copyright 2024, Springer Nature.

In addition, atmospheric exposure significantly alters lattice parameters and lithium site occupancy. Lu *et al.*[31] observed that Nb-LLZO's lattice parameters increased progressively from 12.95753 Å to 12.96244 Å following 1–22 days of environmental exposure. For $Li_{6.5}La_3Zr_{1.5}Nb_{0.5}O_{12}$, atmospheric exposure induced complete redistribution of lithium occupancy between the 24d (Li1) and 96h (Li2) sites, resulting from Li^+/H^+ exchange and subsequent Li_2CO_3 formation. Zhang *et al.*[32] employed neutron powder diffraction (NPD) and neutron pair distribution function (nPDF) analyses to demonstrate that Li^+ in $Li_{6.25}La_3Zr_2Al_{0.25}O_{12}$ crystals is located at the 24d (Li1) and 96h (Li2) positions.

Recently, Redhammer *et al.* also discovered that Li^+/H^+ preferentially appears at the 24d (Li1) position of single-crystal LLZTO.[21] This is likely because Ta substitution causes Li^+ to shift from the 24d position to the 96h position, increasing the mobility of Li^+ at the 24d position. The study revealed that $Li_6La_3ZrTaO_{12}$ undergoes Li^+/H^+ exchange primarily at the 24d site during degradation in various environments (air, humid air, water, and acetic acid). As illustrated in Fig. 2b, progressive Li^+/H^+ exchange induces lattice distortion, driving a structural transition from the $Ia\bar{3}d$ to $I\bar{4}3d$ space group and accelerating the transformation to the tetragonal phase. This phase transition significantly reduces Li^+ conductivity. Therefore, long-term air exposure exacerbates structural decomposition, leading to higher bulk resistance. Leng *et al.*[22] further studied the root cause of the instability of garnet-type SSEs and the characteristics of the air passivation layer (APL). They explored the cross-section of freshly sintered, unpolished $Li_{6.4}La_3Zr_{1.4}Ta_{0.6}O_{12}$ (LLZTO) ceramic pellets and found that LLZTO undergoes passivation when exposed to ambient air. X-ray photoelectron spectroscopy (XPS) depth profiling performed on cross-sections of freshly sintered LLZTO pellets, as shown in Fig. 2c, revealed impurity peaks of $LiOH\cdot H_2O$ and Li_2CO_3 in the Li 1s spectrum on the initial surface of LLZTO. As the etching depth increased, the intensity of Li_2CO_3 decreased. Correspondingly, $LiOH\cdot H_2O$ gradually moved toward the high-energy side and eventually evolved into larger peaks of the underlying LLZTO at the deepest etching levels. Fig. 2d demonstrates a rightward shift in the Zr 3d peak, primarily attributed to compositional changes in $LiOH\cdot H_2O$ and H-LLZTO during Li^+/H^+ exchange. Fig. 2e presents the most probable reaction pathway and formation mechanism of the APL. Fresh LLZTO absorbs water on its surface when exposed to air. Li^+/H^+ proton exchange then occurs, and specific Li^+ sites in LLZTO are replaced by H^+ to form H-LLZTO, eventually forming a $LiOH\cdot H_2O$ layer on the surface. Notably, the oxygen layer in surface $LiOH\cdot H_2O$ serves as a crucial intermediate and precursor for carbonation reactions, where it reacts with atmospheric CO_2 to form Li_2CO_3. To elucidate the Li_2CO_3 formation mechanism *via* Li^+/H^+ exchange,

Liu *et al.*[23] employed XPS and X-ray absorption spectroscopy (XAS) to investigate the APL evolution on garnet surfaces. They first obtained an ultra-clean LLZO surface through low-temperature vacuum annealing, then introduced H_2O into the LLZO surface and monitored surface composition using ambient pressure XPS (AP-XPS) and ambient pressure XAS (AP-XAS). As shown in Fig. 2f, no $O^{(2-x)-}$ and $O^{(2-x+y)-}$ signals around 530.8 eV were detected in the differential spectra of Auger electron yield (AEY) and total electron yield (TEY), indicating that the oxygen in the LLZO sublayer did not undergo a valence change after exposure to H_2O. These results confirm Li^+/H^+ ion exchange, wherein H^+ occupies vacancies created by Li^+ migration to the surface. Exposure to a mixed gas (0.5 mbar H_2O + 0.5 mbar CO_2) yielded distinct Li_2CO_3 peaks in both AEY and TEY spectra, confirming the surface reaction: $2LiOH + CO_2 \rightarrow Li_2CO_3 + H_2O$. These findings provide direct spectroscopic evidence for Li^+/H^+ exchange and elucidate the critical formation mechanism of the initial surface layer governing air stability.

2.1.2 Mechanism of the deleterious role of Li_2CO_3. A deeper understanding of the degradation mechanisms of Li_2CO_3 in batteries can help researchers take corresponding measures to mitigate its adverse effects. In 2017, Sharafi *et al.*[33] identified the contrasting interfacial properties between lithiophobic Li_2CO_3 and the intrinsically lithiophilic bulk garnet electrolyte. By comparing the garnet surface with and without Li_2CO_3, it was found that the Li–Li_2CO_3 interface contact angle was 146°, while the Li–LLZO interface contact angle was 95°. Further density functional theory (DFT) calculations predicted a Li–Li_2CO_3 interface contact angle of 142° (adhesion work W_{ad} = 0.1 J m^{-2}). By contrast, the Li–LLZTO interface had a W_{ad} of 0.67 J m^{-2}, indicating better interface contact between Li and LLZO, with a reduced contact angle (Fig. 3a and b). Clearly, the introduction of APL hinders the application of lithium anodes in SSLMBs. Furthermore, the low conductivity of Li_2CO_3 (with an electronic conductivity of approximately 10^{-8} S cm^{-1}) covering the garnet surface inhibits Li^+ migration, increasing the migration path and raising the activation energy from 0.5 eV to 0.8 eV (Fig. 3c).[34] The Li_2CO_3 layer is not static; its thickness and crystallinity increase with prolonged air exposure. Yang *et al.* observed that the Li_2CO_3 layer thickness grew from an initial 5 nm to 30 nm after 4 weeks of exposure, accompanied by the formation of secondary phases such as $La_2Zr_2O_7$.[37] Even nanoscale Li_2CO_3 can cause a significant, orders-of-magnitude increase in interfacial impedance. Zhang *et al.* reported a drop in the ionic conductivity of $Li_{6.5}La_3Zr_{1.5}Ta_{0.5}O_{12}$ from 3.54×10^{-5} S cm^{-1} to 1.42×10^{-5} S cm^{-1} after 4 weeks in humid air, severely degrading the battery performance.[38] This is due to the electrochemical potential difference between Li metal and Li_2CO_3, which triggers a space charge layer, further increasing the interface resistance. The formation of Li_2CO_3 also leads to changes in the interface structure. Its growth on the garnet surface can disrupt the intimate electrode–electrolyte contact, introducing pores and cracks. These defects increase the path length and resistance for Li^+ transport and compromise mechanical stability, promoting interfacial delamination and failure during cycling.[39] Kim *et al.*[35] used high-angle annular dark-field scanning transmission electron microscopy (HAADF-STEM) and electron energy loss spectroscopy (EELS) to observe carbon signals at the GBs of Li_2CO_3-contaminated LLZO (C-LLZO) (Fig. 3d), indicating that Li_2CO_3 can form and penetrate along GBs. This suggests that fabricating highly dense garnet pellets is effective in suppressing Li_2CO_3 ingress. However, Li^+/H^+ exchange may initiate during the cooling stage after sintering, and achieving full density requires meticulous control over various sintering parameters (*e.g.*, grain size, atmosphere, crucible material, temperature, and time). Guo *et al.*[40] demonstrated that optimized particle size distribution and a slow heating rate yielded a uniform, dense ceramic with only 1% open porosity. This pellet exhibited a high ionic conductivity of 7.3×10^{-4} S cm^{-1} at 303 K and a high CCD of 2.15 mA cm^{-2}, effectively mitigating the damage from Li_2CO_3.

The presence of Li_2CO_3 can undergo a series of detrimental chemical reactions with electrode or electrolyte materials, thus adversely affecting the structural integrity and electrochemical performance of SSBs. Under certain conditions, particularly at high voltages, Li_2CO_3 can decompose oxidatively, releasing species like CO_2 that may react with electrode materials, leading to structural degradation and performance fading.[41] Moreover, under low potential and lithium-rich conditions, Li_2CO_3 may also undergo reduction reactions, which should be of significant concern. Biao *et al.*[36] employed cryogenic transmission electron microscopy (cryo-TEM) to directly observe the chemical behavior of Li_2CO_3 at the GBs of LLZO during battery cycling, revealing the electrochemical reduction mechanism of Li_2CO_3 during lithium deposition (Fig. 3e). The study indicates that Li_2CO_3 located at GBs can be reduced during lithium plating ($Li_2CO_3 + 4Li \rightarrow 3Li_2O + C$). The resultant carbon further reacts with Li to form LiC_x. Compared to the intrinsically low electronic conductivity of LLZO (<10^{-10} S cm^{-1}), LiC_x exhibits a high electronic conductivity (~10^3 S cm^{-1}). This dramatic difference of several orders of magnitude implies that once LiC_x forms in the GB regions, it can substantially alter the local charge transport properties.

From the perspective of interface physics, garnet-type SSEs rely on their excellent electronic insulation to prevent electron migration within the electrolyte, thereby suppressing electrochemical lithium deposition at internal interfaces or GBs. However, when Li_2CO_3 at GBs is reduced and converted into an electronically conductive phase, the originally ion-conducting GB pathways can be activated as localized electron-conducting channels. This electronic percolation effect concentrates current at the GBs and disrupts the uniformity of lithium deposition. Consequently, it significantly lowers the energy barrier for lithium nucleation and growth at the interface, promoting the preferential propagation of lithium dendrites along these boundaries. Notably, this failure mechanism is intricately linked to the spatial distribution of Li_2CO_3 within the electrolyte, rather than being governed solely by the mere formation of a conductive phase. When Li_2CO_3 is present in isolated, discrete particles in surface regions, the impact of its reduction products may be locally constrained. In contrast, when Li_2CO_3 is continuously distributed along the GB network, the reduced LiC_x can progressively form interconnected,

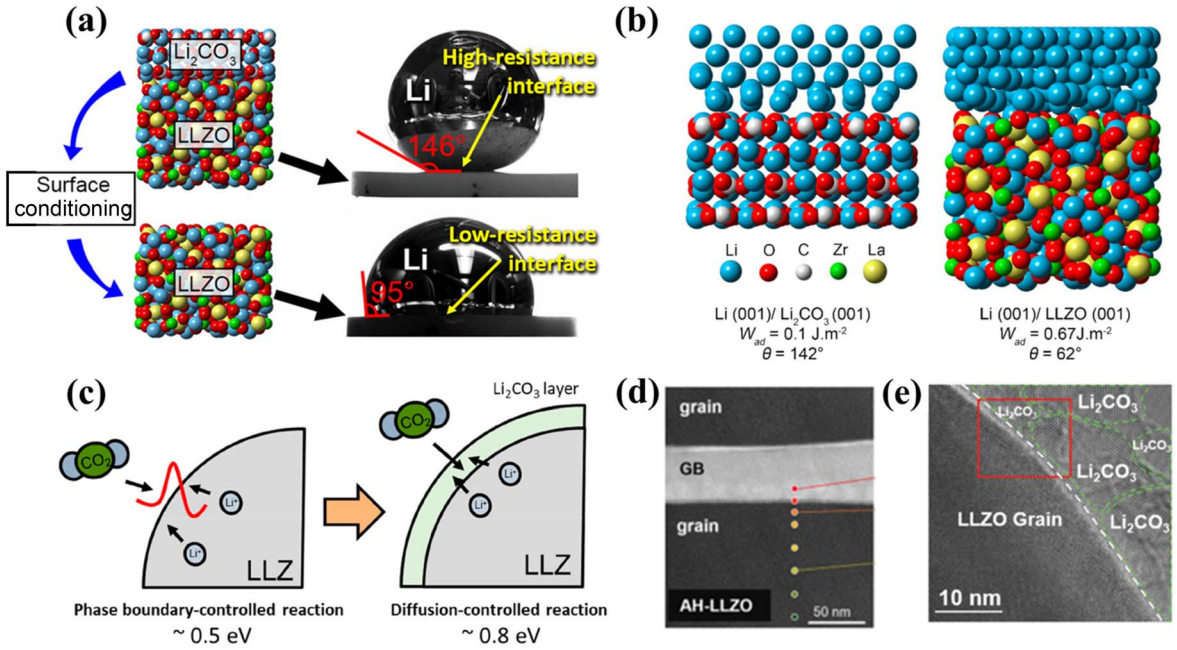

Fig. 3 (a) Contact angles of molten Li on LLZO@Li_2CO_3 *versus* pristine LLZO. (b) Calculated W_{ad}, contact angle (θ), and atomic structure at Li–Li_2CO_3 (left) and Li–LLZO (right) interfaces. Reproduced with permission from ref. 33. Copyright 2017, American Chemical Society. (c) Schematic of phase-controlled *versus* diffusion-controlled carbonation processes. Reproduced from ref. 34. Copyright 2023, American Chemical Society. (d) HAADF-STEM image of grains and GBs. Reproduced with permission from ref. 35. Copyright 2024, American Chemical Society. (e) Cryo-TEM Images of LLZO grains and GBs. Reproduced with permission from ref. 36. Copyright 2023, Wiley-VCH GmbH.

percolating electron-conducting pathways across GBs and potentially through the electrolyte thickness. Once such percolation paths are established, localized current leakage and rapid lithium penetration are significantly accelerated, ultimately leading to electrolyte piercing and internal short circuits.

In addition to electrochemical reduction, chemical reactions between Li_2CO_3 and LLZO may also occur at the interface, damaging the local structure of LLZO and impairing its ionic conductivity.[42,43] Furthermore, due to the significant mechanical property differences between Li_2CO_3 and LLZO, the deposition and dissolution of lithium during battery cycling can induce volume changes and stress evolution. The presence of Li_2CO_3 at the interface exacerbates stress concentration. Such stress concentration can induce interface cracking or delamination, which further compromises mechanical stability and ultimately accelerates structural degradation. During multiple charge–discharge cycles, the continuous generation and accumulation of Li_2CO_3 not only intensifies the chemical and mechanical mismatch at the interface but also accelerates the structural degradation of both the electrolyte and electrode through the aforementioned electrochemical and mechanical coupling mechanisms. Ultimately, this leads to interface failure and rapid capacity fading, making it difficult to meet the long-term stability requirements for practical applications.

Furthermore, the presence of Li_2CO_3 severely compromises the interfacial compatibility within the battery. In SSLMBs, optimal compatibility between the electrolyte and electrodes is crucial for achieving high performance. However, Li_2CO_3 disrupts this compatibility. Its lithiophobic nature results in poor affinity with lithium metal, leading to non-uniform contact, voids, and point contacts at the interface between the Li anode and the garnet-type SSEs. These imperfections cause uneven current distribution, creating localized areas of high current density that initiate the growth of lithium dendrites. The growth of lithium dendrites further compromises the interface stability, increases the interface resistance, and reduces the battery's cycle stability. During repeated cycling, propagating lithium dendrites may ultimately penetrate the SSE, causing an internal short circuit and battery failure.[44] The presence of Li_2CO_3 also adversely affects the long-term cycling stability of the battery. Throughout charge–discharge cycles, Li_2CO_3 contributes to gradual capacity fade. Its low ionic conductivity hinders Li^+ transport, preventing the full utilization of active materials and thereby reducing the achievable capacity. Chang *et al.*[45] proposed a novel and efficient TiO_2-induced conversion strategy designed to generate a lithium-ion-conducting phase. This approach simultaneously eliminates pre-existing pores/voids and Li_2CO_3 contaminants. SSLMBs constructed using $LiFePO_4$ cathodes treated with this strategy exhibited excellent cycling performance, delivering a reversible capacity of 152.9 mAh g^{-1} at 0.1C with a capacity retention of 96.7% after 100 cycles. In contrast, cells with pristine LLZTO suffered significant degradation, retaining only 127.9 mAh g^{-1} after 100 cycles.

From the above discussion, we can conclude that the Li_2CO_3 passivation layer forms on the exterior of LLZO particles, resembling a core–shell structure.[46] The formation of Li_2CO_3 reduces the structural stability and electrochemical

performance of the garnet, severely limiting its large-scale application and commercialization. Therefore, a deeper understanding of the mechanism behind the formation of Li_2CO_3 on the surface of LLZO and its detrimental effects on the interface is of great significance for optimizing the performance of garnet-type SSEs and advancing the development of SSLMBs.

2.2 Synergistic degradation mechanisms of Li_2CO_3 with other interfacial impurities

While the detrimental impact of the Li_2CO_3 APL itself on interfacial ion transport and contact has been widely recognized, its harm does not occur in isolation. In the realistic interfacial environment of SSBs, Li_2CO_3 often coexists with other interfacial impurities or incompatible components. Through coupled processes such as chemical reactions, interfacial transport imbalance, and mechanical mismatch, these factors produce a compounded detrimental effect, significantly exacerbating interfacial failure. Building upon the above-discussed failure mechanism of Li_2CO_3 in contact with lithium metal, this section further elaborates on the coupling mechanisms between Li_2CO_3 and other components or processes. Specifically, we analyze these interactions from three key dimensions: the cathode high-voltage environment, the coexistence with surface impurities, and material preparation stages. Finally, we examine their collective role in amplifying interfacial failure.

2.2.1 Cathode side: interaction with high-voltage decomposition products. On the cathode side, especially when high-nickel layered oxides (such as lithium nickel cobalt manganese oxide, NCM) or high-voltage lithium cobalt oxide ($LiCoO_2$) are used as cathode materials, the interface must withstand more stringent high-voltage environments. The conventional view holds that Li_2CO_3 is intrinsically unstable and prone to decomposition at high voltages. However, a deeper mechanism reveals that Li_2CO_3 reacts with residual lithium compounds (*e.g.*, LiOH) on the surface of cathode active materials and with decomposition products at the interface, forming a continuously thickening impedance layer.[47] For example, the coexistence of Li_2CO_3 and LiOH can promote side reactions at the interface, accompanied by gas generation. In the confined solid-state system, these gases are more likely to be trapped at the solid–solid interface, forming microscopic voids that further degrade contact and trigger a sharp increase in interfacial impedance. This chained process of decomposition, cross-reaction, gas evolution, and contact loss not only results in the persistent thickening of the interfacial impedance layer but also leads to the irreversible consumption of active lithium, ultimately degrading coulombic efficiency and cycle life.[48]

2.2.2 Coexistence and regeneration with other surface impurities (*e.g.*, LiOH). The formation of Li_2CO_3 often originates from Li^+/H^+ exchange, resulting in LiOH (eqn (2) and (3)). Therefore, in practical samples, LiOH and Li_2CO_3 typically coexist on the LLZO surface. LiOH is notably hygroscopic and readily adsorbs moisture from air, creating a localized high-humidity microenvironment at the interface. This not only provides a breeding ground for the continued formation of Li_2CO_3 but also allows the adsorbed water molecules to directly participate in interfacial side reactions, further degrading the interface stability. Furthermore, the differences in physical properties (*e.g.*, volume and elastic modulus) between LiOH and Li_2CO_3 introduce additional mechanical stress and stress concentration during volume changes induced by battery cycling. This can promote the initiation and propagation of interfacial microcracks, accelerating structural degradation at the interface and reducing long-term reliability.[49]

2.2.3 Material preparation stage: reaction/interdiffusion with cathode active materials and the electrolyte bulk. The hazard of Li_2CO_3 is not only evident during battery operation but also cannot be ignored during the material preparation stage before battery assembly. In particular, during the high-temperature co-sintering or heat treatment process of composite cathodes (typically within the 500–800 °C range), complex interface chemical reactions and diffusion may occur between LLZO and cathode materials (such as NCM). These reactions involve the migration of lithium and transition metals, potentially leading to interfacial structural reconstruction, the formation of new phases, or the emergence of secondary phases, thereby affecting interfacial contact, ion transport, and electrochemical performance.

For example, Demuth *et al.*[50] used high-resolution transmission electron microscopy (HRTEM) to study the interface structure evolution during the co-sintering of LLZO and NCM. The study found that even under sintering conditions around 500 °C, the layered structure of NCM near the interface can degrade into a rock-salt-like (NiO-like) structure, and a transition phase resembling $LaNiO_3$ forms in the contact region between LLZO and NCM. These newly formed interfacial phases significantly hinder Li^+ transport across the interface and increase interfacial impedance, indicating that unoptimized thermal treatment can induce irreversible chemical and structural changes at the interface, thereby degrading the performance of the electrode/electrolyte interface. Moreover, Li_2CO_3, acting as a lithium source and reaction medium, can accelerate the diffusion of transition metals (*e.g.*, Co and Ni) towards the LLZTO electrolyte side. This leads to interfacial phase transformations and defect generation, potentially forming ionically insulating phases (*e.g.*, $La_2Zr_2O_7$), thereby further exacerbating the risk of interfacial failure.[51,52] Therefore, during material design and process optimization, special attention must be paid to controlling the temperature and atmosphere during co-sintering. This control is crucial to avoid the formation of unfavorable side phases and to ensure controllable interfacial reactions. Ultimately, these measures are essential for enhancing the long-term stability and performance of the battery.

In conclusion, the hazards of Li_2CO_3 in garnet-based SSBs arise from the coupling of multiple factors during different stages: cathode high-voltage environments, surface impurity coexistence, and the material preparation stage. The synergistic effects amplify interfacial side reactions, impedance growth, and structural degradation. Consequently, interface optimization strategies should shift from merely removing Li_2CO_3 towards the systematic and synergistic regulation of interfacial

chemistry, transport, and structural stability to enhance long-term stability and application potential.

3 Mitigation of interfacial Li_2CO_3

3.1 Strategies for enhancing air stability

As detailed above, the formation mechanisms of Li_2CO_3 and its detrimental effects on electrochemical performance have been thoroughly discussed. This understanding provides critical guidance for developing strategies to enhance LLZO's air stability and prevent or mitigate the formation of the Li_2CO_3 passivation layer. It is important to note that not only the ambient atmosphere but also the elemental composition and microstructure of the garnet significantly influence its air stability, as the Li^+/H^+ exchange reaction is prevalent in these materials. In this section, we summarize three principal approaches for enhancing LLZO's air stability: (1) optimization of sintering techniques, (2) elemental doping, and (3) GB engineering.

3.1.1 Optimization of sintering techniques. The formation of Li_2CO_3 in garnet electrolytes is closely associated with lithium loss and the creation of surface defects during the sintering process. Traditional solid-state sintering at high temperatures (>1200 °C) often induces significant lithium volatilization (with loss rates >8%), increasing the concentration of surface lithium vacancies. These vacancies readily react with H_2O and CO_2 upon air exposure, forming LiOH and Li_2CO_3. Furthermore, the high interfacial energy and abundance of oxygen vacancies at GBs (*e.g.*, the oxygen vacancy concentration at GBs can be three times higher than within the grains) serve as preferential sites for Li^+ accumulation and CO_2 adsorption, further accelerating Li_2CO_3 nucleation.[56] To address the limitations of traditional solid-state reaction sintering, various strategies have been explored. Jonson *et al.*[57] found that high-energy ball milling (HEBM) provides a relatively simple method to reduce particle size, improve microstructural homogeneity, and lower the sintering temperature, thereby reducing the generation of Li_2CO_3 impurity phases. Feng *et al.* successfully prepared $Li_{6.4}Al_{0.1}La_3Zr_{1.7}Ta_{0.3}O_{12}$ using a graded sintering method (treating at 1200 °C for 2 h, followed by 10 h at 1100 °C), achieving full densification without excessive grain growth.[58] By precisely controlling the temperature profile to inhibit grain migration, the mechanical properties of the material were also enhanced. Traditional solid-state sintering typically requires high temperatures, and prolonged sintering can lead to the decomposition of the LLZO structure, generating impurities such as Li_2CO_3 and $La_2Zr_2O_7$. To improve process control and reduce impurity formation, researchers have utilized sintering aids to lower the ceramization temperature of LLZO. As shown in Fig. 4a, Zhou *et al.* reduced the sintering temperature in Ta-LLZO by adding Li_5AlO_4 as a sintering aid. Li_5AlO_4 melts at 950 °C and decomposes at 1000 °C to form Li_2O gas and Li–Al–O compounds.[53] The highly reactive Li_2O gas generated by *in situ* decomposition can replace traditional lithium compensation methods using LiOH that require high sintering temperatures. Additionally, the resulting Li–Al–O compounds alter the GB characteristics, favoring improved densification and effectively suppressing the issue of lithium dendrite growth. Zhang *et al.* introduced nano-sized Y_2O_3 (NYO) particles as sintering additives to prepare LLZTO ceramic electrolytes.[54] The LLZTO-5% NYO composite demonstrated optimal performance, exhibiting the highest ionic conductivity (7.39×10^{-4} S cm^{-1}) and lowest activation energy (0.17 eV) among the tested samples. Scanning electron microscope (SEM) characterization revealed a uniform, dense microstructure with nearly indistinguishable GBs and minimal porosity (Fig. 4b and c). Yang *et al.*[37] constructed a transition layer *via* a lithium donor reaction technique, employing a two-step sintering process to convert the Li_2CO_3 on the LLZTO surface into an active $LiCoO_2$ layer. During the first sintering step, Li_2CO_3 reacts with Co_3O_4 to form $LiCoO_2$. In the second sintering stage, Li_2O is added to compensate for the lithium loss, resulting in a phase-pure LLZTO@$LiCoO_2$ composite. X-ray diffraction (XRD) and Fourier transform infrared (FTIR) tests indicated that no Li_2CO_3 formation was detected after 4 months of air exposure for this material, and its ionic conductivity increased by 20% (Fig. 4d and e). Exploring novel sintering aids and additives to improve sintering outcomes and investigating their mechanisms of action during sintering are of significant importance for optimizing material properties and air stability. In general, traditional sintering processes often involve multi-step, repetitive heat treatments (*e.g.*, grinding–sintering cycles), which are not only energy-intensive and difficult to scale but also economically challenging due to the reliance on expensive equipment, such as hot presses in some cases.[62] In contrast, novel sintering techniques like microwave sintering have gained prominence since the 1990s owing to their environmental friendliness, low energy consumption, and high efficiency, and they are progressively moving towards industrialization.

Research indicates that LLZO SSEs prepared *via* microwave sintering possess more regular crystal structures, fewer internal defects, and reduced surface activation energy, collectively contributing to the effective suppression of Li_2CO_3 formation. Dabaki *et al.*[59] employed a reduced sintering temperature (1200 °C) and shorter duration (3 h) to limit lithium volatilization, yielding a high ionic conductivity of 4.58×10^{-4} S cm^{-1} and pellet density of 4.39 g cm^{-3}. Spark plasma sintering (SPS) substantially modifies garnet electrolyte microstructures. As shown in Fig. 4f, Kammampata *et al.* reported that, compared to traditional solid-state sintering, SPS utilizing lower temperatures and shorter holding times facilitates rapid densification *via* localized melting induced by electrical discharges between particles and simultaneously reduces active sites for CO_2 adsorption. In addition, the increased fine-grain structure provides additional ion transport channels, allowing for faster Li^+ hopping and improved ionic conductivity.[55] For instance, $Li_{6.5}La_{2.5}Sr_{0.5}TaZrO_{12}$ synthesized by SPS exhibited an ionic conductivity of 3.08×10^{-4} S cm^{-1}, superior to the 2.12×10^{-4} S cm^{-1} obtained *via* traditional solid-state sintering. With the advancement of flash sintering (FS) technology,[63,64] many ceramic materials have been sintered using this method. FS is known for its ability to operate at lower temperatures and achieve rapid densification, making it particularly suitable for LLZO materials, effectively reducing lithium evaporation during

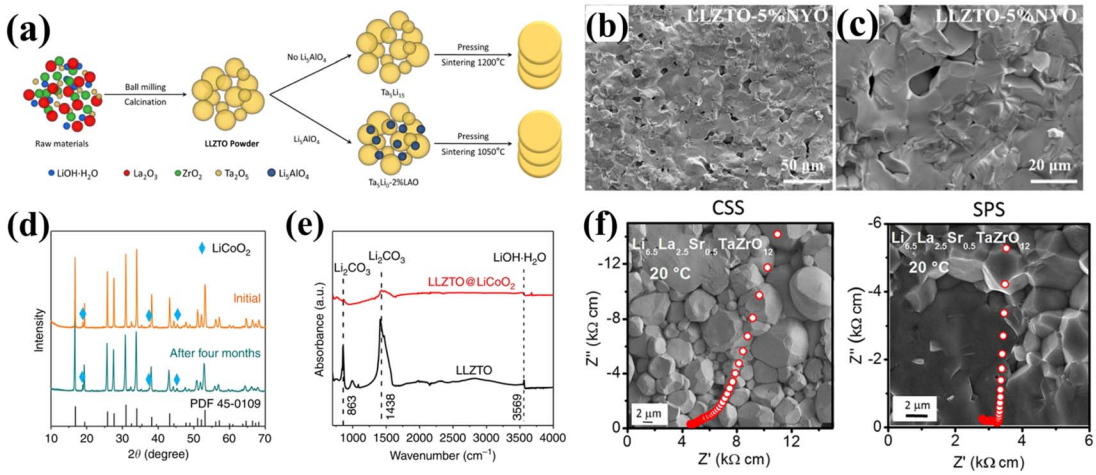

Fig. 4 (a) Schematic of Ta_5Li_{15}–Li_5AlO_4 and Ta_5Li_{15} ceramic sample preparation. Reproduced with permission from ref. 53. Copyright 2024, American Chemical Society. (b and c) Cross-sectional SEM images of LLZTO-5% NYO pellets. Reproduced with permission from ref. 54. Copyright 2024, Royal Society of Chemistry. (d) XRD patterns and (e) FTIR spectra comparing LLZTO@$LiCoO_2$ before and after 4-month air exposure, highlighting its enhanced stability. Reproduced from ref. 37. Copyright 2020, Springer Nature. (f) The SEM images of $Li_{6.5}La_{2.5}Sr_{0.5}$-$TaZrO_{12}$ in the CSS and SPS processes. Reproduced with permission from ref. 55. Copyright 2019, American Chemical Society.

Table 1 Comparison of different new sintering technologies

Technology	Temperature/ time	Relative d ensity	Ionic conductivity (S cm^{-1})	Advantages	Core challenges	Ref.
Microwave sintering	1200 °C/3 h	>97%	4.58×10^{-4}	Fast heating rate, short sintering time, high density	High equipment cost, sensitive process parameters	59
SPS	950 °C/10 min	>98.5%	3.08×10^{-4}	Low sintering temperature (<1000 °C), small grain size (1–2 μm) in preparation, optimized microstructure	Generation of hetero-phases in the high temperature region	55
FS	700 °C/5–10 s	94.72%	9.8×10^{-4}	Extremely short sintering time, low sintering temperature (<850 °C)	Mechanistic disputes, difficulty in large-scale production	60
CPS	350 °C/30–60 min	87.7%	$<1 \times 10^{-4}$	Extremely low sintering temperature (100–350 °C)	Grain-boundary phase is sensitive to air	61

prolonged high-temperature sintering. FS-prepared LLZO electrolytes exhibit significantly suppressed lithium loss associated with prolonged high-temperature exposure. Yang *et al.*[60] achieved densification by applying a direct current at 700 °C for 5 to 10 s, leveraging the interplay between Joule heating and defect migration, obtaining a garnet pellet with a relative density of 94.72%. More recently, the Randall team[70] developed a low-temperature sintering technique termed the cold sintering process (CSP), which can effectively densify various oxide ceramics within the temperature range of 100–350 °C.[71–73] Wang *et al.* demonstrated that CSP can achieve densities up to 87.7% at 350 °C.[61] However, CSP-sintered garnets showed increased sensitivity to air and reduced conductivity, attributed to an intergranular phase induced by preferential dissolution of Al and Li, necessitating post-sintering heat treatment to rectify these defects. Table 1 summarizes the characteristics of these four novel sintering techniques and provides a comparative analysis to guide the optimization of garnet-type SSE stability in air.

3.1.2 Elemental doping. In recent years, elemental doping has been employed to enhance the air stability of garnet-type SSEs. From the perspective of crystal structure, doped elements can induce lattice distortion, creating more Li^+ transport pathways or optimizing Li^+ migration routes, thereby potentially increasing ionic conductivity while simultaneously suppressing Li_2CO_3 formation.[74] Secondly, from an electronic structure standpoint, doping can alter the electron cloud density and energy level distribution of atoms, modulating the chemical reactivity with air constituents and inhibiting the chemical processes leading to Li_2CO_3 formation.[75] Following the 2011 discovery of Al incorporation into LLZO through reactions between molten precursors (Li_2CO_3 or LiOH) and

alumina crucibles during heat treatment, numerous M-doped LLZO variants (M = Fe^{3+}, Ga^{3+}, Nb^{4+}, Ta^{5+}, Te^{6+}, *etc.*) have been successfully synthesized.[76] Doping with high-valence cations (*e.g.*, Ta^{5+} and Nb^{5+}) can occupy lithium vacancies and increase the formation energy of new vacancies. Shiiba *et al.*, using DFT calculations, demonstrated that the formation energy for Li vacancies in Nb-doped LLZO increased from approximately 1.0 eV to about 1.7 eV, effectively suppressing Li^+ leaching and resulting in good ionic conductivity.[77] Al doping is also a common research strategy. The ionic radius of Al^{3+} (0.0535 nm) is smaller than that of Zr^{4+} (0.072 nm). When Al^{3+} substitutes for Zr^{4+} in the LLZO lattice, lattice defects are created. These defects can serve as fast Li^+ transport channels and inhibit the reactivity of LLZO with air. Experimental results confirm that the stability of Al-doped LLZO in humid air is improved.[78] However, the effectiveness of single-element doping is often limited, making it difficult to fully meet the requirements for enhanced air stability while maintaining other properties.

Double-element doping, leveraging the synergy between two elements, demonstrates more significant effects in suppressing Li_2CO_3 formation and improving air stability compared to single-element doping. Fig. 5a demonstrates that Bezabh *et al.* substantially improved LLZO's ionic conductivity *via* an optimized Al/Nb dual-doping strategy.[65] The substitution of Al^{3+} for Li^+ and Nb^{5+} for Zr^{4+}, along with the synergistic effect of Al and Nb, effectively minimized Li^+/H^+ exchange. The dual-doped LLZO particles maintained surface purity after 7-day air exposure, demonstrating exceptional air stability. Huang *et al.*[79] systematically examined dopant effects on moisture resistance in garnet-type SSEs. Relative to Al-LLZO, both Al-LLZTO and Al-LLZNO demonstrated superior air stability. DFT calculations revealed a higher decomposition energy barrier for Al-LLZTO, which effectively suppressed Li_2O formation and subsequent decomposition reactions: $Li_2O + H_2O \rightarrow 2LiOH$ and $2LiOH + CO_2 \rightarrow Li_2CO_3 + H_2O$. Concurrently, dual-doped LLZO also showed advantages in terms of interfacial compatibility with lithium metal anodes, exhibiting reduced interfacial impedance, suppressed lithium dendrite growth, and improved charge/discharge performance, indicating multi-scale performance optimization. Research by Kobi *et al.*[66] revealed that in the Al and Mg co-doped LLZO system, a clean, nearly perfect, and stable interface was formed, which was distinctly different from the material obtained with Al doping alone. Furthermore, studies found that lithium dendrite propagation primarily occurred through Al-LLZO, but not through Al/Mg-LLZO

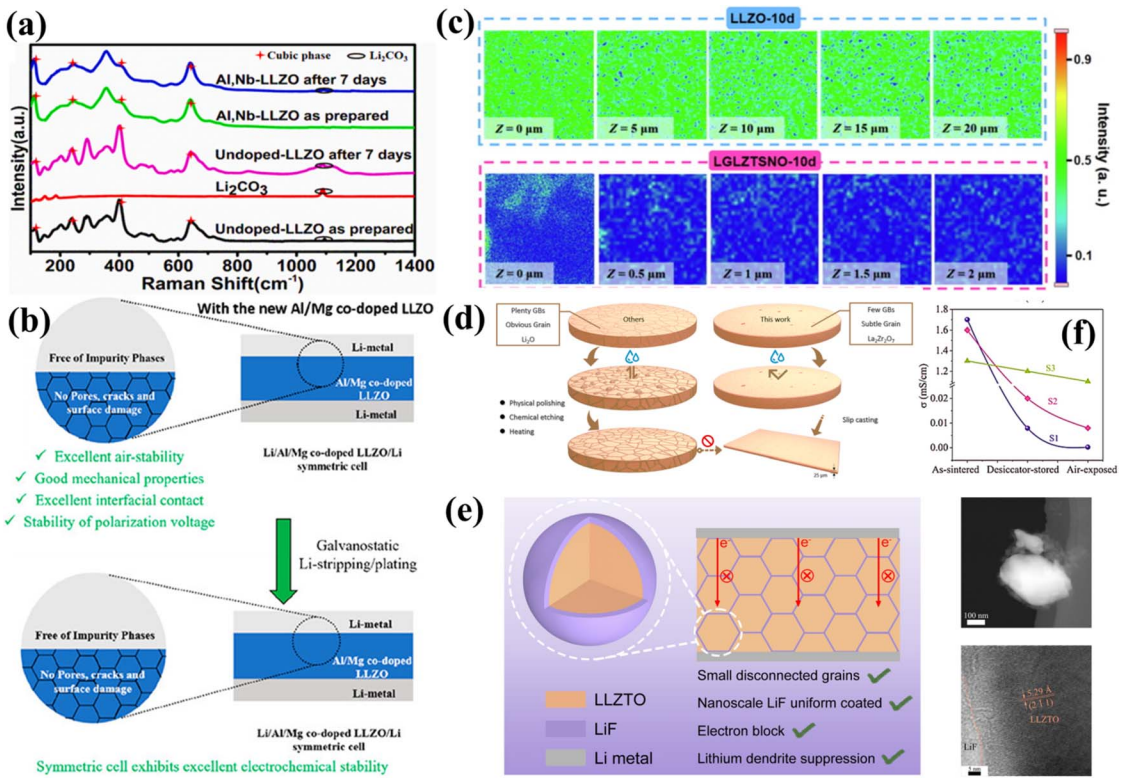

Fig. 5 (a) Raman spectra of pristine and (Al, Nb)-doped LLZO before and after 7-day air exposure. Reproduced with permission from ref. 65. Copyright 2024, Elsevier. (b) Mechanism of Al/Mg co-doping effects on LLZO performance. Reproduced with permission from ref. 66. Copyright 2023, American Chemical Society. (c) 3D Raman spectra of LLZO and LGLZTSNO electrolyte pellets following 10-day air exposure. Reproduced with permission from ref. 67. Copyright 2024, Elsevier. (d) Proposed water stabilization mechanism in LLZO pellets. Reproduced with permission from ref. 68. Copyright 2022, Elsevier. (e) Nanoscale LiF coating distribution on LLZTO grains. Reproduced with permission from ref. 56. Copyright 2024, Tsinghua University Press. (f) Variation in the Li-ion conductivities as a function of the aging behavior of samples. Reproduced with permission from ref. 69. Copyright 2023, Wiley-VCH GmbH.

(Fig. 5b). The cubic LLZO with a garnet structure possesses three-dimensional lithium channels and a sufficient amount of mobile Li^+ to meet high conductivity requirements.

Recent studies have shown that garnet structures synthesized using multi-element high-entropy strategies exhibit good tolerance to various species and demonstrate significantly enhanced ionic conductivity, leading to improved overall material performance.[80–82] Feng *et al.* developed an ultrafast synthesis method of high-entropy garnet-type SSEs with the composition $Li_{7+a-c-2d}La_3(A_a^{3+}B_b^{4+}C_c^{5+}D_d^{6+})O_{12}$ (A = Sc, Y, Bi; B = Zr, Mo, Sn, Te, Hf; C = Nb, Sb, Ta; D = W).[83] Among these compositions, the pentanary garnet $Li_{6.6}La_3Zr_{0.4}Sn_{0.4}Sc_{0.4}Ta_{0.4}$-$Nb_{0.4}O_{12}$ demonstrated optimal performance, achieving the highest ionic conductivity (3.57×10^{-3} S cm^{-1}) and the lowest electronic conductivity (5.26×10^{-9} S cm^{-1}). Fig. 5c illustrates that Yu *et al.* successfully synthesized a $Li_{5.75}Ga_{0.25}La_3Zr_{0.5}$-$Ti_{0.5}Sn_{0.5}Nb_{0.5}O_{12}$ (LGLZTSNO) garnet SSE *via* solid-state sintering.[67] After exposing both LLZO and LGLZTSNO to air for 10 days, the formation of Li_2CO_3 was detected using three-dimensional (3D) Raman mapping. The results indicated that the green areas in the 3D Raman map of LLZO-10d were associated with Li_2CO_3, whereas the blue areas in the map of LGLZTSNO-10d corresponded to the LLZO phase itself. The high-entropy LGLZTSNO exhibits substantially enhanced air stability compared to conventional LLZO. Thermogravimetric analysis (TGA) reveals that the weight loss between 380 and 710 °C predominantly results from Li^+/H^+ exchange, with the exchange extent quantifiable by the weight loss percentage. Notably, LGLZTSNO shows reduced weight loss relative to LLZO, demonstrating that the high-entropy effect effectively inhibits Li^+/H^+ exchange and consequently improves electrolyte stability. In summary, high-entropy doping or multi-element co-doping utilizes the complex interactions of various elements, demonstrating unique advantages in improving air stability and overall performance. The lattice distortion and atomic disorder induced by the high-entropy effect effectively suppress Li_2CO_3 formation while simultaneously improving ionic conductivity and battery cycling performance. However, high-entropy doping systems are more complex, requiring stricter control over synthesis parameters and elemental ratios, and related theoretical understanding is still inadequate. Future efforts need to overcome limitations in solid solubility and processing bottlenecks, combining multi-scale simulations and dynamic regulation techniques to facilitate the translation of doping strategies from laboratory research to large-scale application.[84,85]

3.1.3 Grain boundary engineering. In garnet-type SSEs, GBs serve as critical pathways for ion transport while also acting as highly reactive sites for interactions with the ambient environment. The structure, chemical composition, and electrical properties of GBs significantly influence the overall performance of garnet-type SSEs. GB engineering has recently emerged as a promising strategy for optimizing the electrochemical performance of garnet-type SSEs, yielding considerable progress in suppressing Li_2CO_3 formation and improving air stability. Fig. 5d schematically illustrates key features contributing to improved moisture stability in LLZO, including high relative density, limited GBs, the presence of a moisture-stable $La_2Zr_2O_7$ secondary phase, and the formation of lithium-deficient garnet phases.[68] Research indicates that lattice distortion and atomic mismatch at GBs lead to non-uniform local charge distribution, which enhances the adsorption ability for H_2O and CO_2 molecules, thereby accelerating Li^+/H^+ exchange and subsequent Li_2CO_3 formation. Biao *et al.*, using cryo-TEM and SEM, observed significant Li_2CO_3 accumulation at LLZO GBs, primarily attributed to the high concentration of defects such as vacancies and dislocations.[36] These defects provide fast diffusion channels for H_2O and CO_2, accelerating their reaction with LLZO at the GBs. Modifying the LLZO GB surface to form an *in situ* interface layer that conducts Li^+ while blocking electrons can effectively suppress the Li^+/H^+ exchange reaction. As shown in Fig. 5e, Xiang *et al.*[56] implanted F^- ions into LLZO GBs *via* ion implantation. The introduced F^- altered the electronic structure and chemical activity of the GBs, resulting in interfacial LiF nano-coating formation. The low electronic conductivity of LiF suppresses electron leakage and inhibits Li_2CO_3 generation. Furthermore, Sun *et al.* applied an Al_2O_3 coating onto LLZTO surfaces *via* atomic layer deposition (ALD).[90] Subsequent annealing formed a Li–Al–O interface layer, which effectively inhibited lithium dendrite nucleation and growth. Studies have shown that tailoring the preparation process to form a secondary phase with a specific structure and composition at the GBs, such as layered oxides, can effectively inhibit Li_2CO_3 formation. Jeong *et al.*[91] incorporated Ga to synthesize Ga-LLZTO, aiming to customize the GB structure. In accelerated durability tests (ADTs) under elevated CO_2 and H_2O concentrations, Ga-doped LLZTO demonstrated exceptional air stability. This is because the incorporation of Ga facilitated grain growth during sintering, reducing GB density and promoting the segregation of the H_2O and CO_2-resistant $LiGaO_2$ phase at GBs, which effectively suppressed the decrease in lithium conductivity. These results indicate that Ga doping not only modifies the lithium occupancy distribution within the garnet, enhancing ionic conductivity, but also accelerates the densification process of the garnet-type SSEs, thereby lowering the required sintering temperature.[92] The aforementioned results highlight the significance of elemental doping in GB phase design. The addition of appropriate GB phase additives during the preparation of garnet-type SSEs can modulate the structure and properties of GBs. Additives such as BN,[93] LiCl,[94] MgO,[95] and $LiAlO_2$ (ref. 96) have been utilized for this purpose. Qin *et al.*, using first-principles simulations, demonstrated that the high energy difference induced by Ta doping in LLZTO causes Ta to preferentially segregate along GBs as Ta_2O_5 precipitates.[97] They employed GB engineering to regulate Ta distribution by introducing a La_2O_3 additive. The excess La_2O_3 additives reacted with Ta_2O_5 precipitates, and the residual La_2O_3 nanoparticles filled void defects, promoting uniform distribution of Ta and increasing the relative density of LLZTO to ~98%. The CCD reached 2.12 mA cm^{-2}, indicating that the normal growth of high-density LLZTO particles and grains is beneficial for improving electrochemical performance. The influence of grain size in garnet ceramics on air stability remains debated. Several studies suggest that coarse-grained

garnet electrolytes exhibit superior air stability compared to their fine-grained counterparts. Zheng *et al.*[68] synthesized LLZTO with good particle connectivity and fewer GBs, achieving a high room-temperature ionic conductivity of 7.36×10^{-4} S cm^{-1}. Furthermore, the material exhibited exceptional moisture stability: after 24 h of steam testing in an atmosphere rich in H_2O and CO_2, its ionic conductivity only slightly decreased to 6.6×10^{-4} S cm^{-1}. During water immersion tests, the LLZTO raised the pH of deionized water from 6.0 to 7.7 during the first immersion, with negligible pH change in subsequent tests. Conversely, other researchers have reported that coarse-grained garnets are susceptible to oxidation in air, leading to more extensive Li_2CO_3 formation on the surface, which can induce spontaneous cracking and significantly reduce conductivity. For instance, Nasir *et al.*[69] developed a novel two-step sintering method to precisely control the microstructure of $Li_{6.25}Ga_{0.25}La_3Zr_2O_{12}$. Three electrolyte variants were synthesized: coarse-grained (S1), mixed grain (S2), and fine-grained (S3) microstructures, whose air stability was systematically investigated. As shown in Fig. 5f, after exposure to air, the S3 sample exhibited the least amount of Li_2CO_3 formation on its surface, and its ionic conductivity remained largely unchanged, suggesting that fine-grained pellets possess superior air stability. GB engineering must achieve the synergistic optimization of multiple properties, including suppressing Li_2CO_3 formation and enhancing air stability, while maintaining high ionic conductivity, good interfacial compatibility, and adequate mechanical properties. However, the effects of different GB engineering strategies on these various properties are complex and sometimes contradictory. For example, certain GB modification methods may improve air stability at the expense of ionic conductivity. Achieving synergistic optimization of these multifaceted properties remains a significant challenge in GB engineering.

3.2 Removal of Li_2CO_3 at the lithium anode interface

The Li_2CO_3 contamination layer on LLZO surfaces leads to poor anode/garnet interfacial contact, typically exhibiting impedance values >1000 Ω cm^2. As previously discussed, neither additives nor elemental doping can fully prevent Li_2CO_3 formation. Consequently, post-synthetic garnet interface treatment has emerged as a cost-effective approach for obtaining Li_2CO_3-free electrolytes. Current interface enhancement strategies primarily fall into three categories: (1) physical cleaning; (2) chemical treatment and conversion; (3) interface layer modification.

3.2.1 Physical cleaning. Physical cleaning to remove surface Li_2CO_3 and improve interfacial contact between the garnet-type SSEs and Li metal represents one of the simplest approaches, with polishing being a primary method. As shown in Fig. 6a, Ma *et al.* investigated the effect of surface treatment on the interfacial resistance with Li metal by polishing $Li_{6.25}Al_{0.2}La_3Zr_2O_{11.85}Br_{0.15}$ electrolyte surfaces with sandpapers of different grit sizes.[86] They found that surfaces treated with coarse grit paper exhibited irregular scratches that adversely affected Li metal wettability. Conversely, polishing with excessively fine grit paper resulted in an overly smooth surface that weakened lithium adhesion. Polishing with 600-grit sandpaper significantly reduced the interfacial impedance between the garnet and the Li anode to 20.9 Ω cm^2, ensuring intimate contact and further suppressing Li dendrite growth. Furthermore, the atmosphere during polishing also influences the residual Li_2CO_3 amount and interfacial side reactions. Zheng *et al.* compared polishing LLZO in air *versus* within a glovebox (Ar atmosphere) to study the wettability by molten Li.[42] The LLZTO polished in the glovebox was rapidly wetted by molten Li, forming a mirror-like Li coating. In contrast, LLZTO polished in air showed more significant contamination issues. When exposed to air, impurities rapidly formed on the LLZO surface, and the small amounts of H_2O and CO_2 adsorbed on the electrolyte surface severely polluted the molten Li, leading to interfacial side reactions. Thus, polishing the LLZO surface in an inert atmosphere significantly reduces the formation of Li_2CO_3 and interfacial side reactions. However, simple polishing is often ineffective at completely removing Li_2CO_3, and fine debris from the polishing paper can potentially contaminate the LLZO surface, further reducing wettability. Therefore, increasing the polishing speed and pressure is sometimes necessary for thorough impurity removal. Qin *et al.* employed a high-speed mechanical polishing (HMP) method for eco-friendly interface engineering, achieving an ultra-clean, lithium-free LLZTO surface and successfully removing Li_2CO_3 impurities.[87] As illustrated in Fig. 6b, this process utilized a wool brush tool for polishing. Fig. 6c illustrates the LLZTO interface morphology under varying rotational speeds. The as-received LLZTO-air surface exhibited uneven porosity and substantial impurity accumulation, significantly impeding Li^+ transport at the Li/LLZTO interface. Although low-speed mechanical polishing (500 rpm) partially removed surface contaminants, residual impurities persisted on the LLZTO-LMP surface. In contrast, the ultra-clean surface achieved by HMP at 5000 rpm completely removed impurities from the pores, attributed to the strong centrifugal force generated at high rotation speeds effectively washing away contaminants. After HMP treatment, the LLZTO surface transitioned from lithiophobic to lithiophilic, thereby promoting Li^+ transport at the Li/LLZTO–HMP interface. It should be noted that while HMP demonstrates clear benefits in removing Li_2CO_3 and improving interfacial wettability, the high-speed shear forces and localized friction introduced during the process may also affect the ceramic surface and its subsurface microstructure. At the microscopic scale, excessive mechanical action can induce nanoscale microcracks, local damage zones, or residual stress concentration within the surface or near-surface layer. Such subsurface structural alterations are often difficult to detect directly through conventional surface characterization techniques. Under long-term galvanostatic cycling, when an HMP-treated ceramic surface is in direct contact with lithium metal, the subsurface defects introduced by polishing may act as preferential nucleation sites for non-uniform lithium plating or dendrite growth. This risk is particularly pronounced under conditions of locally elevated current density, where electrochemical deposition couples with mechanical constraint at

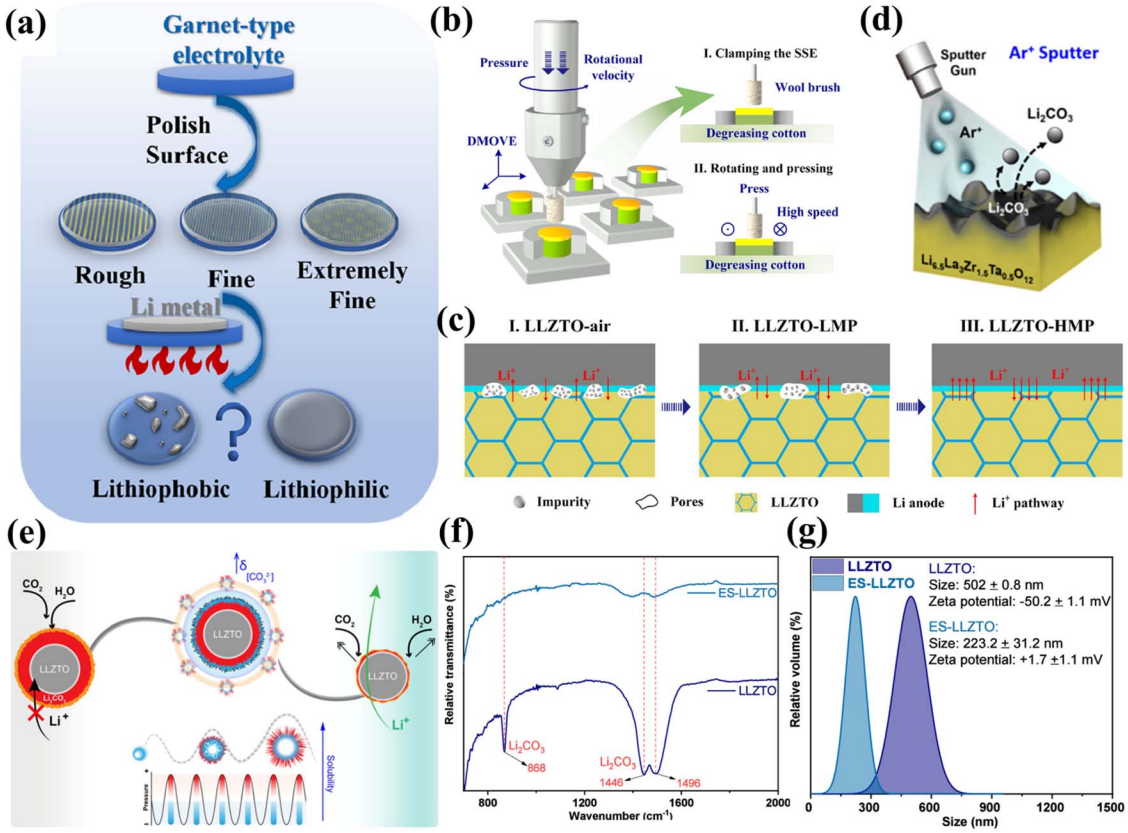

Fig. 6 (a) Schematic of garnet electrolyte surface polishing. Reproduced with permission from ref. 86. Copyright 2023, Elsevier. (b) Ultra-clean SSE surface obtained *via* HMP with a wool brush. (c) LLZTO interface evolution under varying rotation speeds. Reproduced with permission from ref. 87. Copyright 2022, Elsevier. (d) LLZTO surface cleaning mechanism using Ar^+ sputtering. Reproduced with permission from ref. 88. Copyright 2021, American Chemical Society. (e) Scalable sonication method for controlled Li_2CO_3 layer thickness (<10 nm) on LLZTO. (f) Comparative FTIR spectra of LLZTO and ES-LLZTO NPs. (g) DLS analysis of particle size and zeta potential changes of LLZTO NPs post-sonication. Reproduced with permission from ref. 89. Copyright 2025, American Chemical Society.

these flaw sites. Therefore, HMP should be regarded as an efficient yet parameter-sensitive physical cleaning strategy. Its processing parameters, such as polishing speed and treatment duration, must be carefully optimized to balance interfacial cleanliness with long-term cycling stability and to minimize mechanically induced damage to the ceramic subsurface.

In addition, vacuum heat treatment is another viable method for cleaning the LLZO surface, utilizing high temperature and vacuum to remove Li_2CO_3 at the lithium anode interface. This approach leverages the decomposition characteristics of Li_2CO_3 at elevated temperatures and the promoting effect of vacuum on the volatilization of decomposition products. Vema *et al.* found that LiOH and Li_2CO_3 begin to decompose at 500 °C and completely disappear by 800 °C under vacuum.[98] The decomposition reaction is $Li_2CO_3 \rightarrow Li_2O + CO_2\uparrow$. The resulting Li_2O and CO_2 can volatilize rapidly in the vacuum environment. However, excessively high temperatures can cause Li loss and the formation of $La_2Zr_2O_7$ impurity phases, disrupting the cubic LLZO structure and reducing ionic conductivity.

To lower the high treatment temperatures, plasma treatment has been explored as a physical cleaning method, utilizing the interaction between energetic particles in the plasma and Li_2CO_3. As shown in Fig. 6d, Li_2CO_3 and LiOH can be effectively removed under Ar^+ sputtering conditions at a relatively low temperature of 227 °C.[88] Energetic electrons collide with Li_2CO_3 molecules, inducing decomposition. Simultaneously, oxygen radicals ($O^\bullet$) react with carbon in Li_2CO_3, generating CO_2 and facilitating its breakdown. Furthermore, plasma treatment under different atmospheres can achieve surface doping effects. Chen *et al.*[99] proposed that N_2 plasma treatment effectively cleans and dopes the LLZTO electrolyte surface by etching away Li_2CO_3 and LiOH, while forming Ta–N bonds with surface/subsurface Ta atoms, significantly improving the ionic conductivity to 9.92×10^{-4} S cm^{-1}. The *in situ* formed Li_3N, upon contact with molten Li, drastically reduced the interfacial resistance from 125.8 Ω cm^2 to 3.50 Ω cm^2. Laser cleaning shares a similar principle with plasma etching. High-energy nanosecond laser scanning can effectively remove the surface impurity layer from air-exposed LLZTO electrolytes.[100]

Compared to other methods like heat treatment and mechanical polishing, laser cleaning requires significantly less time and energy. Additionally, Srivastava *et al.* developed a scalable, green, ultrasound-assisted technique for precisely controlling the thickness (<10 nm) of the Li_2CO_3 layer on LLZTO

Table 2 Comparison of the performance of different physical methods for removing Li_2CO_3

Chemical formula	Method	Ionic conductivity (S cm^{-1})	Interfacial resistance (Ω cm^2)	CCD (mA cm^{-2})	Ref.
$Li_{6.5}La_3Zr_{1.5}Ta_{0.5}O_{12}$	Polishing and spreading	—	17.5	2.8	42
$Li_{6.25}Al_{0.2}La_3Zr_2O_{11.85}Br_{0.15}$	Polish treatment	8.01×10^{-4}	20.9	1.1	86
$Li_{6.5}La_3Zr_{1.5}Ta_{0.5}O_{12}$	High-speed mechanical polishing	7.3×10^{-4}	28.15	1.91	87
$Al_{0.36}Li_{5.92}La_3Zr_2O_{12}$	Vacuum heat treatment	—	<10	>1	98
$Li_{6.5}La_3Zr_{1.5}Ta_{0.5}O_{12}$	Argon-ion sputtering	1.3×10^{-4}	18	0.9	88
$Li_{6.5}La_3Zr_{1.5}Ta_{0.5}O_{12}$	N_2 plasma	9.92×10^{-4}	3.5	1.6	99
$Li_{6.4}La_3Zr_{1.4}Ta_{0.6}O_{12}$	Laser cleaning	7.3×10^{-4}	76.4	—	100
$Li_{6.75}La_3Zr_{1.75}Ta_{0.25}O_{12}$	Sonication-assisted	$1.5 \times \mathbf{10^{-4}}$	—	1.5	89

nanoparticles (NPs).[89] As depicted in Fig. 6e, this method uses local mechanical energy generated by the ultrasonic cavitation effect to selectively peel off the Li_2CO_3 passivation layer from the surface of LLZTO NPs, creating an ultra-thin and structurally stable modified Li_2CO_3 interface, which significantly improves the air stability of LLZTO NPs. FTIR analysis confirmed the effectiveness of the ultrasound treatment: the characteristic Li_2CO_3 vibration peaks at 868, 1446, and 1496 cm^{-1} were significantly attenuated in the extensively sonicated LLZTO NPs (labeled ES-LLZTO), indicating a reduced Li_2CO_3 layer thickness (Fig. 6f). Dynamic light scattering (DLS) analysis revealed that sonication reduced the average hydrodynamic diameter of LLZTO NPs from 502 nm to 223 nm, accompanied by a zeta potential shift from -50.2 ± 1.1 mV to $+1.7 \pm 1.1$ mV (Fig. 6g). The initially negative zeta potential originated from the insulating Li_2CO_3 surface layer, which was substantially reduced in the ES-LLZTO. This direct, efficient *in situ* modulation strategy, free from chemical additives, effectively suppressed the ongoing passivation reaction of LLZTO in air. For practical applications, future efforts should focus on enhancing the feasibility of physical cleaning methods for large-scale production. Developing equipment and processes suitable for industrial manufacturing is crucial to ensure the stable and reliable removal of Li_2CO_3 from LLZO surfaces, thereby guaranteeing battery consistency and performance stability. Table 2 summarizes various physical methods for Li_2CO_3 removal and compares the performance of batteries assembled with the treated LLZTO.

3.2.2 *In situ* chemical surface conversion. Surface impurities, particularly Li_2CO_3 and LiOH, constitute the primary origin of interfacial challenges in garnet-type SSEs. *In situ* chemical conversion technology is an effective method for constructing a stable and lithiophilic interface layer on the garnet-type SSEs. This technique triggers specific chemical reactions on the electrolyte surface to form an interface layer with special properties, which transforms harmful surface impurities into beneficial interface components. This process suppresses the formation of Li_2CO_3, enhances the air stability of garnet-type SSEs, and improves battery performance.

Researchers have been actively seeking effective methods to remove Li_2CO_3 from the surface of garnet-type SSEs to improve their stability in air. A promising approach involves the chemical reaction-based removal of Li_2CO_3. Given the alkaline nature of Li_2CO_3, treatment with acidic compounds offers a straightforward and effective solution. Ruan *et al.*[108] developed a facile phosphoric acid (H_3PO_4) treatment to convert detrimental Li_2CO_3/LiOH passivation layers on LLZTO surfaces into a lithiophilic Li_3PO_4 modification layer. This *in situ* formed Li_3PO_4 layer simultaneously (1) reduces the Li/LLZTO interfacial energy to enhance contact and (2) establishes a robust solid electrolyte interphase (SEI) that effectively blocks Li dendrite penetration. The treated interfaces achieved an ultra-low resistance of 7 Ω cm^2, enabling stable cycling of Li symmetric cells for >1600 h at 0.1 mA cm^{-2}. Beyond H_3PO_4, alternative precursors can generate similar Li_3PO_4 protective layers, as demonstrated by Liu *et al.* who employed molten NaH_2PO_2 salts to drive the Li_2CO_3-to-Li_3PO_4 conversion reaction on garnet surfaces.[101] As shown in Fig. 7a, the Li_2CO_3 passivation layer was converted to ion-conductive Li_3PO_4 under mild conditions (200 °C) using a simple gas molecule release and cleaning strategy. The reaction process is as follows:

$$2NaH_2PO_2 \rightarrow Na_2HPO_4 + PH_3\ (g) \quad (4)$$

$$2PH_3 + 3Li_2CO_3 \rightarrow 2Li_3PO_4 + 2C + CH_4\ (g) + H_2O\ (g) \quad (5)$$

Furthermore, DFT calculations were performed to evaluate the adhesion work (W_{ad}) of different interfaces and assess the adhesion strength of the interfaces. W_{ad} refers to the energy required to separate two components at the interface, where a higher W_{ad} value corresponds to stronger interface adhesion. As shown in Fig. 7b, the W_{ad} of the Li_3PO_4 (001)/Li (001) interface is significantly higher than that of the Li_2CO_3 (001)/Li (001) interface, with values of 2.452 and 0.183 J m^{-2}, respectively.[102] This suggests that the *in situ* chemical transformation of the Li_2CO_3 layer on the LLZTO and Li metal surface strengthens the interface contact. Based on both experimental and theoretical research, the Li_3PO_4 protective layer demonstrates potential advantages in optimizing the interfacial performance of SSLMBs. Similarly, Wang *et al.* utilized acid vapor to remove Li_2CO_3 impurities from the surface of $Li_{6.4}La_3Zr_{1.4}Ta_{0.6}O_{12}$ (LLZT).[103] The surface alkali species readily react with volatile HI gas, simultaneously generating a protective LiI layer (Fig. 7c). Due to its low electronic conductivity, the LiI buffer layer effectively prevents electron tunneling and attack on LLZT. The

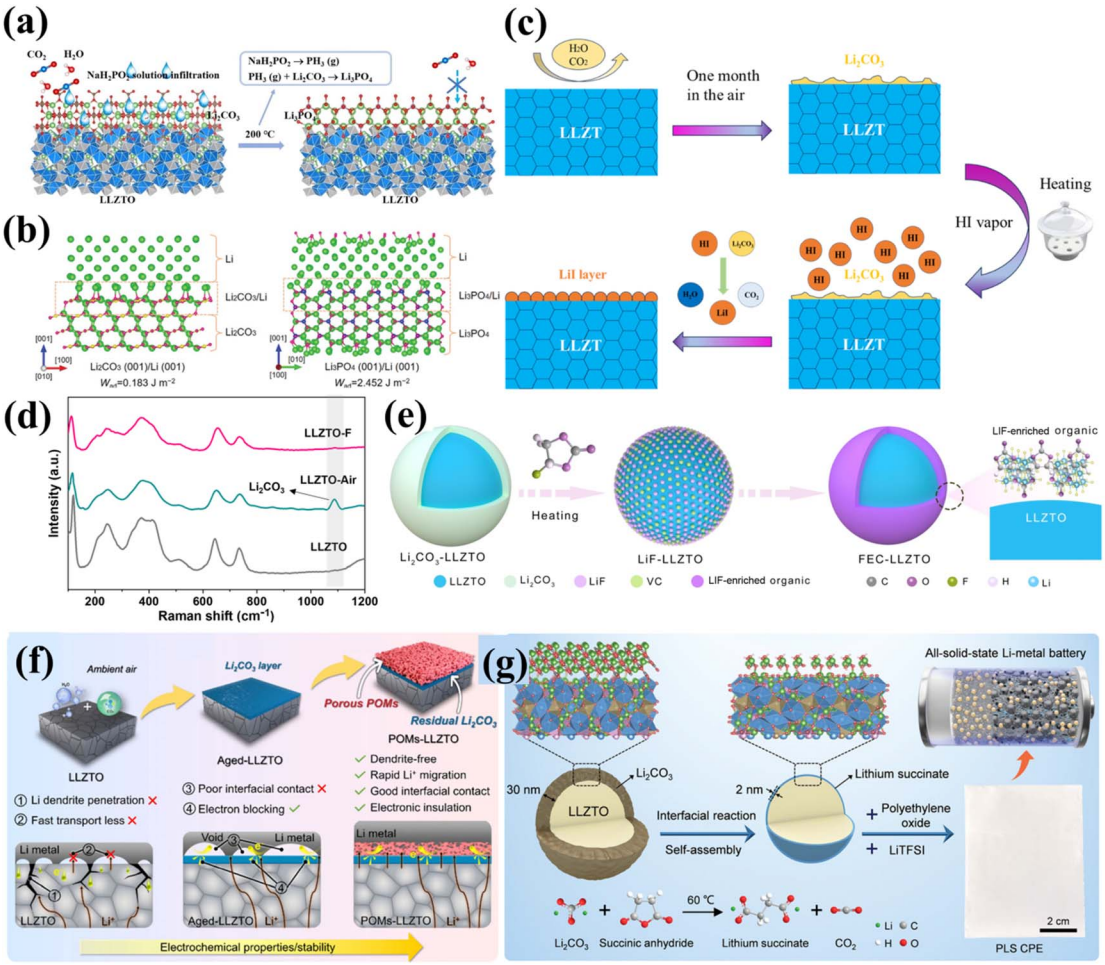

Fig. 7 (a) Schematic diagram of the conversion of the Li_2CO_3 passivation layer on LLZTO into a Li_3PO_4 layer through the thermal decomposition of the infiltrated NaH_2PO_2 salt. Reproduced with permission from ref. 101. Copyright 2022, Elsevier. (b) Atomic configurations of fully relaxed supercells of Li_2CO_3 (001)/Li (001) and Li_3PO_4 (001)/Li (001) interfaces. Reproduced with permission from ref. 102. Copyright 2022, Wiley-VCH GmbH. (c) Li_2CO_3 removal from LLZT surfaces using HI vapor. Reproduced with permission from ref. 103. Copyright 2024, Elsevier. (d) Comparative Raman spectra of pristine LLZTO, LLZTO-air and LLZTO-F pellets. Reproduced with permission from ref. 104. Copyright 2024, Royal Society of Chemistry. (e) Synthesis mechanism of FEC-LLZTO. Reproduced with permission from ref. 105. Copyright 2025, Elsevier. (f) Schematic illustration and interfacial characteristics of the Li/LLZTO, Li/Aged-LLZTO, and Li|POMs-LLZTO interfaces. Reproduced with permission from ref. 106. Copyright 2025, American Chemical Society. (g) Schematic diagram of interfacial reconstruction of LLZTO through mild liquid-phase reaction and its further application in SSBs. Reproduced with permission from ref. 107. Copyright 2024, Wiley-VCH GmbH.

LiI layer also mitigates side decomposition reactions between the lithium metal and the electrolyte. In traditional LIBs, gas–solid reactions involving iodine and lithium metal have been used to create LiI interface layers, proven to enhance electrochemical performance. In SSLMBs, LiI demonstrates exceptional interfacial stability between the Li anode and SSE. This additive reduces the LLZT/Li interfacial resistance from 6160 Ω cm^2 to 30 Ω cm^2 while enabling a CCD of 1.5 mA cm^{-2} at room temperature (RT). Moreover, Li symmetric cells maintained stable cycling for >1000 h at 0.6 mA cm^{-2}. In a similar approach, Chen *et al.* treated Li_2CO_3 impurities on the LLZTO surface with a $LiPF_6$ solution at 60 °C.[109] The Li_2CO_3 impurities *in situ* converted to Li_3PO_4 and LiF, achieving good interfacial contact. The presence of Li_3PO_4 effectively enhanced the ionic conductivity at the interface, improving battery performance, while the protective nature of the LiF layer safeguarded the underlying LLZTO from solvent decomposition. Both LiI and LiF, as primary components of lithium halides, exhibit excellent characteristics in SSLMBs.

Additionally, Cai *et al.*[142] used an aqueous H_3BO_3 solution and HF vapor to form a nanoporous interlayer *in situ* on the LLZTO surface. The vigorous chemical reaction between the lithium salt and lithium, characterized by a relatively small Gibbs free energy ($\Delta G = -208.84$ kcal mol^{-1}), combined with the capillary force of the nanoporous layer, resulted in excellent lithiophilicity. The high surface energy and electronic insulation suppress dendrite formation.

Regarding chemical treatment methods, surface coating can effectively inhibit the formation of Li_2CO_3. Hu *et al.* proposed an unconventional interface reaction strategy where the typically undesirable Li_2CO_3 is intentionally retained and cleverly utilized.[104] A solvent-free trifluoroacetic acid (TFA) treatment

strategy was employed to successfully construct a LiF-rich interlayer on the LLZTO surface. This process achieves *in situ* conversion of the Li_2CO_3 contaminant without damaging the structural integrity of the LLZTO bulk. The introduction of the solvent-free system effectively avoids parasitic reactions between organic media and LLZTO, preventing the generation of secondary impurities. Raman spectroscopy confirmed the presence of Li_2CO_3 in LLZTO exposed to air (LLZTO-air) through characteristic peaks at 158 cm^{-1} (weak peak, assigned to CO_3^{2-} ν_1 symmetric stretching vibration) and 1090 cm^{-1} (strong peak, assigned to CO_3^{2-} ν_4 out-of-plane bending vibration). In contrast, these carbonate signals completely disappeared in fluorinated LLZTO (LLZTO-F), indicating the complete conversion of harmful Li_2CO_3 without detectable byproducts (Fig. 7d). Similarly, as shown in Fig. 7f, a multi-metallic polyoxometalate (POM) layer, $Li_3PW_{12}O_{40}$, was constructed on the LLZTO surface through the controlled reaction of phosphotungstic acid (PTA) with Li_2CO_3.[106] This design selectively retains an appropriate thickness of the Li_2CO_3 layer through precise control of the reaction process, forming a unique LLZTO/Li_2CO_3/POMs sandwich structure. The POMs layer significantly enhances the lithium metal wettability and constructs a 3D ionic diffusion channel, while the residual Li_2CO_3, with its intrinsic low electronic conductivity, serves as an effective electronic barrier to prevent interface electron leakage. This strategy transforms the traditional harmful phase into a functional interface component, offering a new path for the large-scale development of garnet-type SSLMBs.

By combining chemical treatment and transformation methods, the advantages of both can be leveraged to generate a synergistic effect, more effectively suppressing the formation of Li_2CO_3 and improving the performance of garnet-type SSEs. Lu *et al.*[110] designed a surface layer on LLZTO using ultrathin, super-lithiophilic but hydrophobic AlF_3. Through reactive modification using LiOH, $Al(NO_3)_3$, and HF, the LLZTO surface acquired excellent hydrophobicity, effectively inhibiting Li_2CO_3 formation and significantly improving air durability even under humid conditions (25 °C, 60% humidity). Reaction with molten Li yielded a composite interfacial layer comprising Li–Al alloy, Li, and LiF species, demonstrating superior interfacial compatibility. The Li–Al alloy promotes homogeneous distribution of both electrons and Li^+, while the LiF phase serves as an electron-blocking barrier due to its high ionic diffusivity and low electronic conductivity. This dual mechanism effectively suppresses Li dendrite formation at both LLZTO GBs and interfaces. As shown in Fig. 7e, Li *et al.* achieved multifunctional interfacial modification of LLZTO through a surface conversion reaction between fluoroethylene carbonate (FEC) and LLZTO, constructing an organic layer rich in lithiophilic LiF *in situ* on the LLZTO surface.[105] FEC undergoes defluorination at high temperatures, generating HF and vinylene carbonate (VC). The HF then eliminates Li_2CO_3 impurities on the LLZTO surface *via* an acid–base neutralization reaction, producing lithiophilic LiF. VC undergoes polymerization catalyzed by Lewis acids and bases, forming a LiF-rich organic layer that enhances both the air stability and lithiophilicity of LLZTO. Symmetric cells incorporating this modified interface demonstrated exceptional cycling stability, maintaining operation for >2000 h at 0.1 mA cm^{-2}.

Surface coating technology can form a physical barrier on garnet-type SSEs, preventing direct contact between air (H_2O and CO_2) and the electrolyte, thereby reducing Li_2CO_3 generation. *In situ* chemical conversion technology, on the other hand, can construct a stable and lithiophilic interface layer, further improving the surface properties of the electrolyte, reducing interfacial impedance, and enhancing battery stability. Similarly, Zhan *et al.*[107] developed an interface reconstruction approach utilizing mild liquid-phase chemistry and self-assembly processes (Fig. 7g). This strategy utilizes a controlled chemical reaction between succinic anhydride (SA) and Li_2CO_3 on the LLZTO surface to synchronously construct an ultrathin, nanoscale lithium succinate (SALi) ion conductor interface layer. The *in situ* generated SALi layer serves a dual function: effectively isolating the LLZTO from gas–solid reactions with environmental components and maintaining excellent lithium-ion transport kinetics. More importantly, the SALi-modified LLZTO (LLZTO-SALi) composite with polyethylene oxide (PEO) as the SSE (PEO/LLZTO-SALi, PLS) exhibits outstanding compatibility with lithium metal interfaces. The assembled Li/PLS/$LiFePO_4$ all-solid-state battery demonstrated 84.3% capacity retention after 1400 cycles at 1C and room temperature. Table 3 compares recent chemical treatment approaches for Li_2CO_3 surface conversion, highlighting their substantial improvements in interfacial stability and electrochemical performance.

Although the above *in situ* chemical conversion strategies effectively transform Li_2CO_3 into functional interfacial phases like Li_3PO_4, LiF, and LiI, representing a promising approach for interface engineering, the chemical-potential stability of these newly formed interlayers under extreme electrochemical conditions requires a more comprehensive understanding. This is particularly crucial when assessing their compatibility with Li metal anodes and diverse cathode chemistries. Taking phosphate-based interphases as an example, Li_3PO_4 is thermodynamically susceptible to reduction toward phosphides like Li_3P under extremely low lithium chemical potentials. However, both theoretical and experimental studies indicate that this deep reduction process is typically subject to significant kinetic limitations. On one hand, Li_3PO_4 itself possesses strong ionic bonding and low electronic conductivity, necessitating electron transport across the dense interphase to drive the reduction reaction. On the other hand, once localized reduction occurs at the interface, the resulting reaction products establish a new electron-ion transport boundary, thereby suppressing further progression of the reaction and resulting in a self-limiting rather than complete conversion process (*e.g.*, Li_3PO_4 → Li_3P).[143]

This self-limiting conversion can exert dual effects on the long-term evolution of interfacial impedance. On the positive side, when the reaction-derived interphase formed upon contact between Li_3PO_4 and lithium metal is dense and exhibits moderate Li^+ conductivity, it can rapidly passivate the interface, forming a composite interfacial structure reminiscent of LiPON-like layers. This stabilizes the interfacial impedance and

Table 3 Comparison of interfacial resistance with different surface chemical treatments

Driver reagent	Conversion product	Interfacial resistance (Ω cm^2)	CCD (mA cm^{-2})	Cycling performance	Ref.
H_3PO_4	Li_3PO_4	7	0.8	1600 h (J = 0.1 mA cm^{-2}, 25 °C)	108
NaH_2PO_2	Li_3PO_4	2	2.6	1500 h (J = 0.1 mA cm^{-2}, 25 °C)	101
HI	LiI	30	1.5	1050 h (J = 0.5 mA cm^{-2})	103
$LiPF_6$	LiF/Li_3PO_4	32.4	1.1	700 h (J = 0.2 mA cm^{-2}, 60 °C)	109
TFA	LiF	—	2.0	10 000 h (J = 0.1 mA cm^{-2}, RT)	104
PTA	$Li_3PW_{12}O_{40}$	5.8	1.5	3000 h (J = 0.5 mA cm^{-2})	106
HF	Li–Al/LiF	1.3	1.2	3000 h (J = 0.3 mA cm^{-2}, 25 °C)	110
FEC	LiF	75.8	—	2500 h (J = 0.1 mA cm^{-2}, 25 °C)	105
SA	SALi	40	0.7	2000 h (J = 0.2 mA cm^{-2}, RT)	107
HCOOH	HCOOLi	3	1.7	1000 h (J = 0.5 mA cm^{-2})	111
HCl–HF	LiF–LiCl	11.6	1.8	1000 h (J = 0.5 mA cm^{-2}, 25 °C)	112
$NaBF_4$	$LiF/LiBO_2$/NaF	6	2.0	3000 h (J = 0.3 mA cm^{-2}, RT)	113

promotes Li^+ transport across the interface.[102] In fact, components such as Li_3P and Li_2O, which may be present within the interphase layer, are known to exhibit good ionic conductivity and can remain stable within the SEI/interphase. In conventional ionic battery systems, they can also facilitate Li^+ desolvation and interfacial migration, thereby positively contributing to reduced interfacial polarization and enhanced cycling performance.[144,145] Conversely, if the reaction-formed interphase layer is thick, porous, or accompanied by significant volume changes and microstructural damage, it may lead to a gradual increase in interfacial impedance and reduced interfacial stability over long-term cycling. Therefore, the evolution of interfacial impedance depends not merely on whether reduction occurs, but also on the depth of the reduction, the structural compactness of the interphase layer, and its conductive properties.

Furthermore, the electrochemical stability windows of different cathode materials impose distinct requirements on the applicability of these *in situ* formed interphases. For high-voltage cathode systems, such as high-nickel NCM series materials, the interphase layer must possess sufficient oxidative stability to withstand high potentials while maintaining ionic conductivity and suppressing detrimental side reactions.[146] Generally, LiF-rich interphases exhibit a wider oxidative stability window under high-voltage conditions owing to their excellent chemical inertness and electronic insulation. However, their limited ionic conductivity may introduce additional polarization if the layer is overly thick. In contrast, phosphate-based interphases offer favorable ion transport and film-forming properties, though their composition and stability may adjust according to the interfacial chemical environment. Accordingly, rational interphase design should integrate considerations of electrochemical stability, transport properties, and structural integrity to realize persistently stable interfacial impedance and robust long-term cycling performance.

3.2.3 Interfacial interlayer modification. The high interfacial resistance at the Li/garnet-type SSE interface and the phenomenon of non-uniform lithium deposition primarily stem from poor interfacial contact and the presence of lithium-deficient contaminant layers on the garnet electrolyte. Recent computational modeling reveals that the CCD for dendrite formation at Li anode interfaces is substantially lower than at GBs, indicating preferential dendrite nucleation at electrode–electrolyte interfaces.[147] Consequently, during electrochemical stripping/plating, lithium dendrites propagate uncontrollably at the interface. This underscores the necessity of removing Li_2CO_3 from the garnet surface for a stable Li/garnet interface. The most extensively researched strategy involves constructing a stable and reliable interface through the implementation of an interfacial interlayer. As summarized in Table 4, various reported interfacial modification strategies demonstrate that these methods not only remove Li_2CO_3 and improve contact but also significantly reduce interfacial impedance. Furthermore, they effectively suppress lithium dendrite growth, greatly enhancing the durability of SSLMBs.

3.2.3.1 Construction of inorganic interlayers. Introducing an inorganic interfacial interlayer between the Li anode and the garnet-type SSE is an effective strategy for inhibiting Li_2CO_3 formation and improving air stability. The inorganic interlayer can enhance the interfacial stability by modifying the physicochemical properties of the interface, indirectly suppressing Li_2CO_3 formation.[148,149] Ji *et al.* employed a solid-state polishing technique, rubbing Bi_2Te_3 powder (particle size ~1 μm) between two sandpapers to polish LLZTO ceramic pellets.[114] This process yielded a uniform, dense Bi_2Te_3 coating on LLZTO surfaces (Fig. 8a). The modified interface demonstrated enhanced lithiophilicity upon molten Li contact while preventing electron accumulation at surface defects, thereby achieving optimal Li/LLZTO interfacial contact with superior dendrite suppression. The solid-state polishing approach completely filled surface cracks and pores, outperforming wet-chemical methods in preventing interfacial Li dendrite growth. Zhang *et al.*[115] employed vacuum thermal evaporation to deposit a 50-nm KF layer on LLZTO. The excellent Li/KF wettability enabled effective void repair at the Li/LLZTO interface, achieving an interfacial impedance of 5.9 Ω cm^2. As illustrated in Fig. 8b, the resulting dense LiF/KF layer completely coated the LLZTO surface, functioning as: (1) an electron-blocking barrier to minimize leakage currents and (2) an electronic conductivity suppressor. This dual functionality

Table 4 Comparison of the modification effects of different interface modification strategies

Categorization	Materials	Method	Interfacial resistance (Ω cm^2)	CCD (mA cm^{-2})	Cycling performance	Ref.
Inorganic composite interlayers	Bi_2Te_3	Solid-state polishing	2.0	5.2	1500 h (J = 0.5 mA cm^{-2})	114
	KF	Vacuum thermal evaporation	5.9	1.0	3000 h (J = 0.2 mA cm^{-2}, 25 °C)	115
	Te/Se	Chemical vapor deposition	2.5/3.3	0.6/1.3	500 h (J = 0.2 mA cm^{-2}, 25 °C) 1200 h (J = 0.3 mA cm^{-2}, 25 °C)	116
	SbI_3	Drop-casting	139	0.8	5000 h (J = 0.1 mA cm^{-2})	117
	HI	Facile liquid phase	10.3	2.3	800 h (J = 1 mA cm^{-2})	118
	Urea	Drop-casting	85	1.7	600 h (J = 0.5 mA cm^{-2})	119
	$BiCl_3$	Facile liquid phase	7.46	2.9	>10 000 h (J = 0.3 mA cm^{-2}, RT)	120
	ZnO	Ultrasonic spraying	36	2.15	600 h (J = 2 mA cm^{-2})	121
	$SnCl_2$	Facile liquid phase	9.4	0.8	6000 h (J = 0.2 mA cm^{-2})	122
	Ag	Magnetron sputtering	2	5.1	300 h (J = 0.1 mA cm^{-2})	123
	SnO_2-Al	Direct-current/radio-frequency plasma magnetron co-sputtering	9	5.4	8700 h (J = 0.2 mA cm^{-2}, 30 °C)	124
	Ga_2O_3	Liquid metal painting	5	1.7	10 000 h (J = 0.2 mA cm^{-2}, 60 °C)	125
	GaIn	Liquid metal painting	52.5	2.7	1400 h (J = 1 mA cm^{-2}, 25 °C)	126
	SiO_2	Ultrasonic spraying	24.2	1.2	1000 h (J = 0.2 mA cm^{-2})	127
	$InCl_3$	Facile liquid phase	10	1.4	4000 h (J = 0.2 mA cm^{-2}, 25 °C)	128
Organic compound interlayers	A solid polymer electrolyte (SPE)	Drop-casting	—	0.3	700 h (J = 0.2 mA cm^{-2}, 90 °C)	129
	PEO	Spin-coating	177	—	200 h (J = 0.2 mA cm^{-2})	130
	ETPTA	*In situ* thermal polymerizing	88	1.1	400 h (J = 0.1 mA cm^{-2}, 30 °C)	131
	PDA and PEO	Solution oxidation method and spin-coating	218	1.1	800 h (J = 0.15 mA cm^{-2}, 80 °C)	132
	Azo compound	Acid–base neutralization	—	1.4	>1500 h (J = 0.1 mA cm^{-2}, 50 °C)	133
	PLSS	Spin-coating	9	1.1	400 h (J = 0.5 mA cm^{-2}, 25 °C)	134
	PEGMEMA and PVDF-HFP with PFPE additive	Electrostatic spinning and UV-irradiation methods	142.1	3.6	400 h (J = 1.0 mA cm^{-2}, 25 °C)	135
	poly(MAAc-*co*-MMA-*co*-NMMAm) in G4/LITFSI	UV-irradiation method	38	1.58	1500 h (J = 0.2 mA cm^{-2}, 25 °C)	136
	$P_{1444}FSI$	Spin-coating	120	0.15	—	137
Inorganic–organic composite interlayers	COMF	Spin-coating	—	>1	1000 h (J = 0.1 mA cm^{-2})	138
	PVDF-HFP and $BaTi_2O_5$	Pasting	—	0.678	0.05 h (J = 0.1 mA cm^{-2})	139
	$(C_6H_5)_3Sb$	Liquid metal painting	6	1.3	500 h (J = 0.1 mA cm^{-2}, 60 °C)	140
	MMA/EGDMA/AIBN + LLZTO + $LiPF_6$-LE	*in situ* thermal polymerization	—	1.9	600 h (J = 1.5 mA cm^{-2})	141

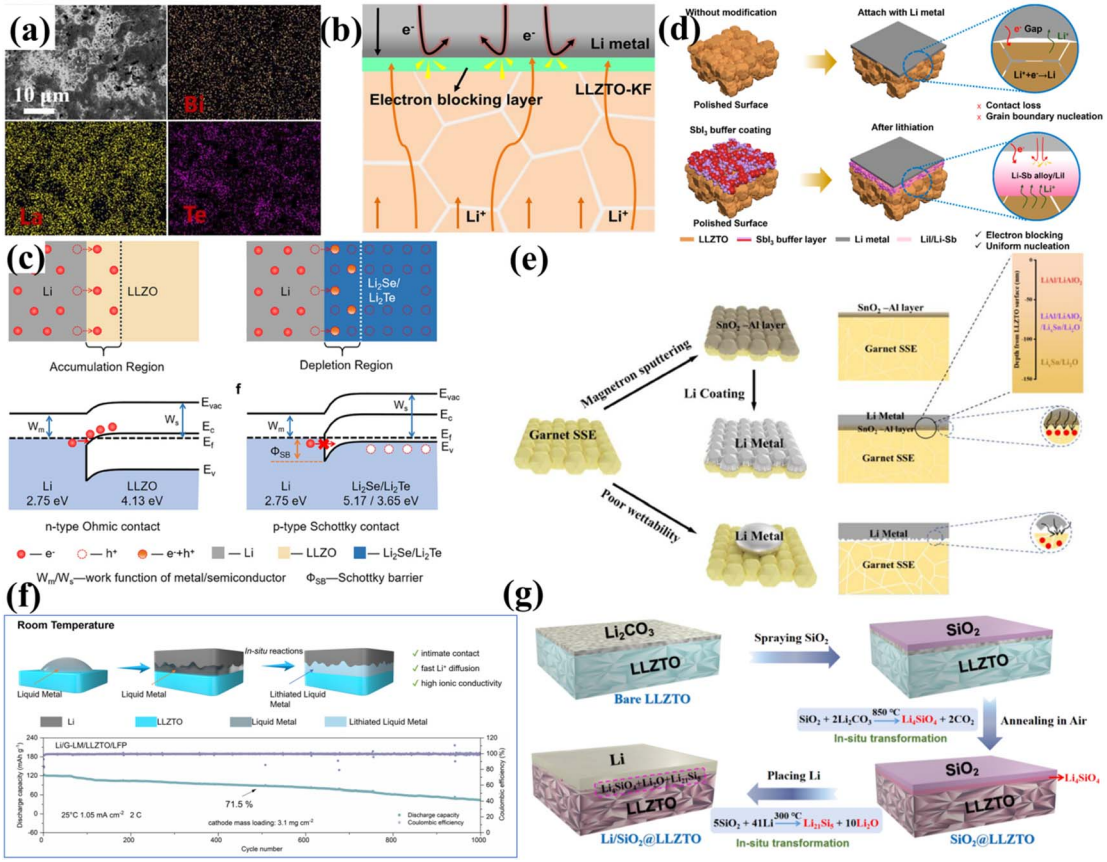

Fig. 8 (a) Top-view SEM and energy dispersive X-ray spectroscopy (EDS) elemental mapping (Bi, Te, and La) of LLZTO@Bi_2Te_3. Reproduced with permission from ref. 114. Copyright 2025, Elsevier. (b) Li|LLZTO-KF interface demonstrating dendrite-free cycling enabled by an electron-blocking interlayer. Reproduced with permission from ref. 115. Copyright 2024, Springer Nature. (c) Formation mechanisms of n-type ohmic and p-type Schottky contacts. Reproduced with permission from ref. 116. Copyright 2025, Wiley-VCH GmbH. (d) Ion-electron composite layer enhancing Li/LLZTO interfacial contact while suppressing Li penetration. Reproduced with permission from ref. 117. Copyright 2025, American Chemical Society. (e) Lithium wettability characteristics on garnet SSE surfaces. Reproduced with permission from ref. 124. Copyright 2025, Wiley-VCH GmbH. (f) Fabrication process of Li/G-LM/LLZTO and cycling performance of Li/G-LM/LLZTO/LFP cells at 1.05 mA cm^{-2}. Reproduced with permission from ref. 126. Copyright 2025, Elsevier. (g) *In situ* SiO_2-mediated Li_2CO_3 elimination creating a stabilized multifunctional interlayer. Reproduced with permission from ref. 127. Copyright 2025, Elsevier.

effectively prevented Li dendrite propagation along GBs and pores while eliminating current hotspots, thereby enhancing the CCD. Liu *et al.*[116] proposed an innovative strategy to suppress dendrite penetration by depositing Se/Te nanofilms on the LLZTO surface *via* chemical vapor deposition, followed by an *in situ* reaction with molten lithium to form a tightly bonded interface with highly ion-conductive Li_2Se/Li_2Te interlayers. As illustrated in Fig. 8c, the core mechanism lies in a solid-state physical effect: the Li_2Se/Li_2Te semiconductor layers (with high work function characteristics) form a p-type Schottky contact with lithium metal. The resulting Schottky barrier effectively blocks electron migration towards the LLZTO electrolyte. Theoretical analysis revealed that without an interlayer, the Fermi level difference between Li and LLZTO drives spontaneous electron injection, forming a highly conductive inversion layer (n-type ohmic contact) on the LLZTO surface that promotes Li penetration. In contrast, the Schottky barrier significantly inhibits electron leakage, fundamentally suppressing dendrite growth. Furthermore, some materials can effectively wet molten lithium *via* conversion reactions with low ΔG. Liu *et al.*[117] successfully introduced a dense LiI/Li–Sb layer through a conversion reaction between SbI_3 and Li to construct ionically and electronically conductive layers. This led to a more uniform distribution of electric field and current density on the surface, effectively regulating Li deposition (Fig. 8d). Additionally, various materials such as LiI/$ZnLi_x$,[118] Li–N,[119] $BiCl_3$,[120] ZnO,[121] and $SnCl_2$ (ref. 122) have been prepared as lithiophilic interfacial layers. Wu *et al.* deposited a 20 nm Ag layer on the LLZTO surface *via* magnetron sputtering.[123] The subsequent *in situ* electrochemical reaction formed a Li–Ag alloy that filled interfacial voids and defects, achieving intimate contact between the electrolyte and lithium metal. This resulted in a significant reduction in interfacial impedance, effectively preventing the deposition of Li atoms and dendrite formation on the metal surface. Hao *et al.*[124] proposed a multi-target co-sputtering strategy, which allows for more precise control over the interfacial composition compared to single-target deposition. Using direct-current/radio-frequency magnetron co-

sputtering, they deposited a nanoscale SnO_2/Al (SA) multilayer interlayer on the LLZTO surface. Reaction with molten lithium formed a gradient artificial SEI structure with a triple-functional design (Fig. 8e): (1) surface interface layer: highly ion-conductive $LiAlO_2$ ensures efficient Li^+ transport; (2) middle regulation layer: lithiophilic Li_9Al_4 alloy induces uniform Li deposition, suppressing dendrite nucleation; (3) substrate bonding layer: a mixed conductive phase of Li_2O/Li_xSn balances ion/electron transport. This spatially graded structure reduced the interfacial impedance from 764.5 Ω cm^2 to 9 Ω cm^2, and the synergistic effect increased the CCD to 5.4 mA cm^{-2}. The Li/SA-LLZTO-SA/Li symmetric cell exhibited dendrite-free cycling for >8700 h at 0.1–0.2 mA cm^{-2}, providing a new paradigm for SSB interface engineering.

In contrast to methods involving additional artificial lithiophilic layers or removal of lithium contaminants, Meng *et al.*[125] applied a simple functional liquid metal (FLM) coating on the LLZTO surface. This process allowed the FLM droplets to fully wet Li_2CO_3, reducing its size and tearing it into Li_2CO_3 nanodomains surrounded by FLM nanoparticles. The dissipation effect enabled the lithiated FLM nanodomains to act as alternative lithium flux carriers at the Li/garnet interface. This simple method requires no additional deposition equipment or precise control of alloy composition. Meanwhile, the native oxide layer of the FLM allows for smooth coating on the solid electrolyte surface, preventing further exposure of the garnet to H_2O and CO_2. Similarly, Ji *et al.*[126] proposed an innovative interface engineering strategy based on GaIn liquid metal (G-LM), constructing a multifunctional gradient interface through an electrochemically driven *in situ* lithiation process. This strategy transformed G-LM into $LiGaO_2$/$LiInO_2$ compounds with high dielectric constants during the initial lithiation stage, while retaining an electronically conductive phase. The unique structure achieved a triple synergistic effect: (1) the adaptive deformation capability of the liquid metal ensured intimate interfacial contact; (2) the high-dielectric $LiGaO_2$/$LiInO_2$ layer homogenized the electric field distribution; (3) the *in situ* formed electronically conductive phase created selective ion/electron transport channels. This design simultaneously addressed issues of interfacial resistance, dendrite growth, and side reactions, enabling stable cycling of SSLMBs for 1000 cycles at 1.05 mA cm^{-2}, breaking the performance limits of existing liquid metal interface designs (Fig. 8f). Furthermore, Yu *et al.* sprayed SiO_2 material onto the LLZTO surface.[127] A high-temperature reaction with the surface Li_2CO_3 generated Li_4SiO_4, which subsequently underwent a conversion reaction with Li to form a multi-component buffer layer comprising Li_4SiO_4, Li_2O, and $Li_{21}Si_5$. This approach successfully transformed the detrimental Li_2CO_3 passivation layer into a beneficial lithiophilic layer, achieving a waste-to-wealth valorization (Fig. 8g). The introduced Li_4SiO_4/Li_2O/$Li_{21}Si_5$ nano-multifunctional interlayer significantly improved the air stability and interfacial contact of LLZTO/Li, reducing the interfacial impedance to 24.2 Ω cm^2 and enabling stable operation for 2400 h and 1000 h at current densities of 0.05 mA cm^{-2} and 0.2 mA cm^{-2}, respectively. From the perspective of physical isolation, the inorganic interlayer can form an effective physical barrier between the Li anode and garnet-type SSEs, preventing direct contact with H_2O and CO_2 in air. From a chemical adsorption and reaction perspective, inorganic interfacial materials can passivate the impurity passivation layer on the garnet surface through specific chemical reactions, converting it into harmless substances or immobilizing them within the interlayer, thereby reducing their impact on the garnet-type SSEs.

3.2.3.2 Construction of organic interlayers. Modification with organic interfacial interlayers involves introducing a layer of organic material between the Li anode and the garnet-type SSEs, forming a dual physical and chemical barrier. This approach effectively inhibits Li_2CO_3 formation and improves contact with the Li anode. An effective method involves depositing a soft solid polymer electrolyte (SPE) interfacial layer onto solid electrolytes like LLZTO, significantly reducing interfacial resistance and enhancing air stability. For instance, Chi *et al.* proposed a strategy of depositing an SPE interfacial layer on the LLZTO surface.[129] This SPE layer, based on a poly(ethylene oxide) (PEO) polymer, was achieved by directly drop-casting an SPE solution onto the solid electrolyte to ensure uniform coverage. The soft SPE layer forms a continuous contact interface between LLZTO and the Li metal, effectively resolving interfacial issues (Fig. 9a). Similarly, as shown in Fig. 9c, Bi *et al.*[131] employed an *in situ* thermal polymerization method, combining ethoxylated trimethylolpropane triacrylate (ETPTA) monomer with a lithium salt ($LiPF_6$) to prepare a multifunctional gel polymer electrolyte (GPE). This GPE not only served as an interfacial interlayer to address the interface problem between the Li anode and LLZTO but also acted as a binder to connect garnet pellets, enabling the construction of flexible and large-scale SSBs. In terms of interface engineering, the liquid electrolyte precursor effectively wets the Li/LLZTO interface and penetrates into the bulk of the electrolyte before polymerization. After thermal polymerization, the precursor conformally solidifies at the Li/LLZTO interface, forming uniform Li/LLZTO contact. Furthermore, the GPE with uniform Li distribution ensures uniform lithium deposition and stripping, leading to the formation of a stable SEI layer and effectively suppressing lithium dendrite formation. In inhibiting Li_2CO_3 formation and improving air stability, polydopamine (PDA) coatings have shown exceptional effectiveness. Chen *et al.* demonstrated the introduction of a dual interfacial layer at the electrode/garnet interface, consisting of a PDA film and a PEO-based composite electrolyte layer.[132] The adhesive nature of the PDA film facilitates intimate interfacial bonding and improves the interfacial wettability between the PEO layer and the garnet-type SSE. Research indicates that PDA molecules contain numerous polar groups, such as amino and hydroxyl groups, which can interact with water and CO_2 molecules, hindering their diffusion towards the garnet solid electrolyte surface. The introduction of the PEO layer helps establish continuous interfacial contact and regulates uniform Li transport and current distribution at the Li/garnet interface. Additionally, the dual interfacial layer effectively isolates GBs from the Li metal, suppressing Li dendrite nucleation. Whether using soft SPEs, GPEs, or dual interfacial layers, these organic interlayers exhibit good compactness and continuity, tightly covering the garnet

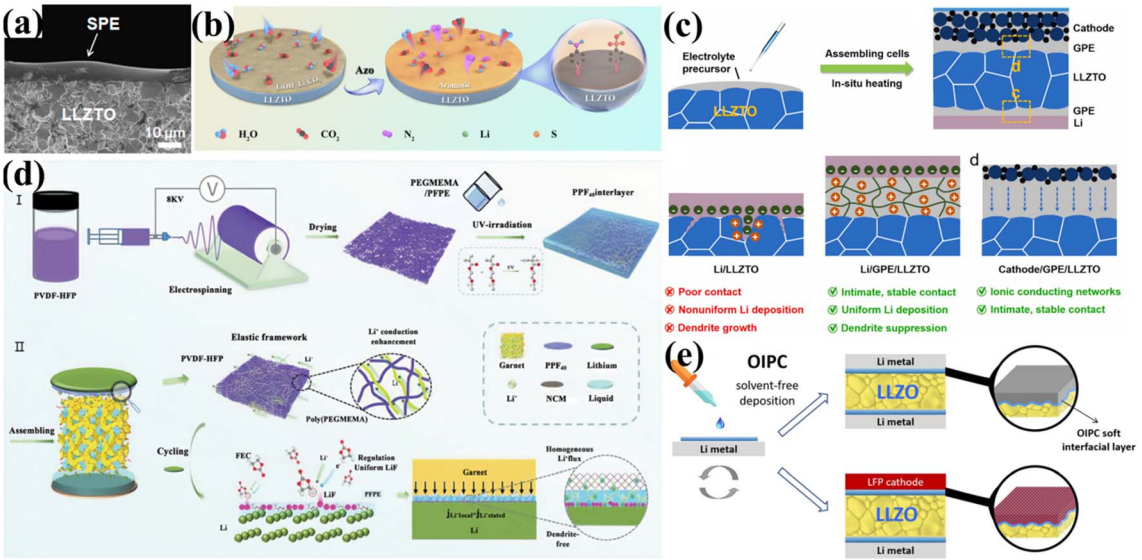

Fig. 9 (a) Cross-sectional SEM images demonstrating intimate interfacial contact *via* SPE deposition on LLZTO. Reproduced with permission from ref. 129. Copyright 2018, Elsevier. (b) Azo-compound conversion mechanism transforming Li-contaminated LLZTO to aromatic-coated surfaces. Reproduced with permission from ref. 133. Copyright 2022, Elsevier. (c) *In situ* formed GPE interfacial modification layer on garnet electrolytes. Reproduced with permission from ref. 131. Copyright 2021, Elsevier. (d) Polymer interlayer synthesis and interfacial interactions. Reproduced with permission from ref. 135. Copyright 2023, Wiley-VCH GmbH. (e) OIPC layer deposition process and surface characteristics. Reproduced with permission from ref. 137. Copyright 2021, American Chemical Society.

solid electrolyte surface. When exposed to air, they effectively prevent direct contact between H_2O/CO_2 and the electrolyte. During diffusion, water and CO_2 molecules are blocked by the organic layer, cutting off the source of reactants needed for Li_2CO_3 formation.

Organic substances can also react with Li_2CO_3 on the LLZO surface, converting it into a lithiophilic interlayer. Li *et al.*[133] proposed a mechanism where azo compounds, under certain conditions, remove contaminants from the LLZTO surface and form a high-coverage aromatic layer (Fig. 9b). The azo compounds undergo acid–base neutralization reactions with LiOH and Li_2CO_3, generating aromatic radicals that improve the garnet/lithium interface properties. Furthermore, through the *in situ* construction of a high-coverage organic layer, these radicals can transfer to the LLZTO surface, reducing the resistance to lithium-ion transport. After exposing the treated LLZTO sample to air for one week, no Li_2CO_3 formation was detected by XRD and FTIR spectroscopy, further indicating the significant positive role of azo compounds in suppressing Li_2CO_3 formation on the LLZTO surface and improving air stability.

Studies have found that organic interlayers can also improve interfacial compatibility by interacting with active sites on the garnet-type SSE surface. Research by Yang *et al.*[134] confirmed the ability of poly(lithium 4-styrenesulfonate) (PLSS) introduced between LLZTO and the lithium metal to improve interfacial performance. PLSS contains abundant lithium sulfonate groups ($-SO_3Li$), which form strong coordination interactions with metal atoms (*e.g.*, La, Zr, Ta, and Li) exposed on the LLZTO surface. This atomic-level interaction successfully builds an efficient Li^+ migration channel, exhibiting low energy barriers and high Li^+ diffusion coefficients at the LLZTO/PLSS interface. This transport mechanism not only enhances Li^+ transport efficiency but also reduces Li^+ accumulation and uneven distribution at the interface, thereby lowering the possibility of Li_2CO_3 formation. It is precisely this atomic-level interaction that maintains a robust and seamless interface contact between LLZTO and the Li anode during long-term cycling. The interfacial resistance dropped to 9 Ω cm^2 at 25 °C, and the prepared symmetric cell stably cycled for 4800 h at 0.1 mA cm^{-2}. As shown in Fig. 9d, Zheng *et al.*[135] developed a novel elastic conductive interlayer. This interlayer was formed by UV-curing of poly(ethylene glycol) methyl ether methacrylate (PEGMEMA) and poly(vinylidene fluoride-*co*-hexafluoropropylene) (PVDF-HFP), creating an elastic skeleton, with perfluoropolyether (PFPE) added to form an interlayer structure. The elastic skeleton provides effective transport paths for Li^+ and enhances deformation resistance and interfacial contact quality through its unique viscoelastic properties. Furthermore, the ether oxygen atoms in PEGMEMA can coordinate with lithium ions, promoting Li^+ migration. Simultaneously, fluoroethylene carbonate (FEC) molecules can be reduced by acquiring Li^+ and electrons, forming an LiF-rich SEI layer. This multifunctional organic interlayer helps improve interfacial contact and significantly enhances air stability. Furthermore, Zhao *et al.* designed a multifunctional interlayer with both ionic conductivity and self-healing capabilities (ICSHI).[136] This layer is based on a copolymer network of methacrylic acid (MAAc), *N*-methyl methacrylamide (NMMAm), and methyl methacrylate (MMA), whose abundant hydrogen bonds confer excellent self-healing properties and flexibility. Tetraethylene glycol dimethyl ether (G4) containing dissolved lithium bis(fluorosulfonyl)imide (LiTFSI) was used to ensure ion

transport. Placed between LLZTO and the lithium anode, the ICSHI utilizes its flexibility to conform tightly to the interface, repairing mechanical damage during cycling in real-time and improving interfacial contact. *In situ* observation directly confirmed that without ICSHI, LLZTO cracked rapidly at high current and was penetrated by lithium dendrites, whereas the ICSHI-protected interface significantly suppressed dendrite growth, maintaining the structural integrity of LLZTO for over 50 min and achieving uniform and stable lithium deposition. Given that most organic solvents, even in trace residues, readily undergo side reactions with lithium metal, significantly deteriorating interfacial Li^+ transport kinetics and overall battery performance, a solvent-free deposition technique was used to construct a flexible interfacial layer of triisobutylmethylphosphonium bis(trifluoromethane)sulfonimide (P_{1444}TFSI) organic ionic plastic crystals (OIPCs) on the surface of the lithium metal and LLZO solid electrolyte (Fig. 9e). This flexible OIPC layer effectively enhanced Li^+ conduction at the interface, increasing the room-temperature ionic conductivity of the composite OIPC-LLZO solid electrolyte to 1.1×10^{-3} S cm^{-1} and reducing the interfacial impedance by five times compared to the untreated interface.[137]

Regarding the enhancement of air stability, traditional physical and chemical methods often only address already formed Li_2CO_3 and have limited effectiveness in preventing its regeneration. After mechanical or chemical treatments, Li_2CO_3 can rapidly regenerate when the garnet-type SSE is re-exposed to air. In contrast, the stable interfacial layer formed by organic interlayer modification can effectively maintain the interfacial stability between the Li anode and the garnet SSE, even under prolonged air exposure, thereby significantly improving the storage and operational stability of the battery in air. Although traditional methods can mitigate the impact of Li_2CO_3 on battery performance to some extent, their ability to comprehensively enhance overall battery performance is limited. Mechanical treatments may introduce new interfacial issues that impede Li^+ transport, while chemical treatment may alter the chemical composition and structure of materials, adversely impacting the long-term stability of the battery. In comparison, organic interlayer modification not only suppresses the formation of Li_2CO_3 but also improves the interfacial compatibility between the Li anode and the garnet-type SSE, optimizes Li^+ transport kinetics, and thus holistically enhances battery performance. The organic interlayer can effectively reduce interfacial resistance, improve charge/discharge efficiency, regulate Li^+ distribution, inhibit the growth of lithium dendrites, and enhance cycling stability and safety.

3.2.3.3 Construction of organic/inorganic composite interlayers. Polymeric interlayers are increasingly emerging as a promising solution to address the interfacial challenges between lithium anodes and electrolytes in advanced battery systems, improving interfacial stability by effectively suppressing Li_2CO_3 formation. On one hand, flexible polymer interlayers can form composite layers with good flexibility and denseness, combined with the lithium anode, thereby mitigating the accumulation of interfacial voids during lithium deposition and subsequently reducing the growth of lithium dendrites near the interface. On the other hand, polymer interlayers also face numerous challenges, such as low ionic conductivity and weak mechanical properties, which may lead to aggravated interfacial decomposition and side reactions during battery cycling, ultimately resulting in battery failure. Therefore, achieving high ionic conductivity, excellent mechanical strength, superior electrochemical performance, and effective suppression of interfacial Li_2CO_3 formation remain significant challenges in the design of polymer interlayers.

As shown in Fig. 10a, Wang *et al.* coated a carbonized metal–organic framework (CMOF) interlayer on the LLZTO surface to ensure good interfacial contact between Li metal and LLZTO.[138] The abundant zinc clusters within the CMOF layer interact with molten lithium metal (forming Li-CMOF), creating an intimate contact interface between the lithium metal and LLZTO. The CMOF interfacial layer serves as a lithiophilic nucleation template, directing uniform Li deposition by regulating both electric field distribution and Li^+ flux, thereby effectively suppressing dendrite formation. Consequently, the Li-CMOF/LLZTO/Li-CMOF symmetric cell could cycle stably for over 1000 h at a current density of 0.1 mA cm^{-2} without short-circuiting. Furthermore, Li *et al.*[139] proposed incorporating the ferroelectric material barium titanate $BaTi_2O_5$ (BT) nanorods into a PVDF-HFP matrix, successfully preparing an inorganic-modified polymer composite (CPE-BT). The ferroelectric additive simultaneously enhanced polymer electrolyte performance through two mechanisms: (1) plasticization effects increasing chain mobility and (2) spontaneous polarization facilitating Li^+ transport, yielding significantly improved ionic conductivity and transference numbers (Fig. 10b). Complementary studies have demonstrated that NP incorporation or high-valence cation doping can further strengthen mechanical properties while maintaining electrochemical stability in polymer interlayers. In an innovative study, Liu *et al.*[140] developed an alloyable viscous interfacial wetting layer for garnet electrolytes to enable highly reversible SSBs. Upon contact with lithium, triphenyl antimony (TPA, $(C_6H_5)_3Sb$) self-assembled into a fluid, liquid-metal-like interlayer. The *in situ* process generated a mixed-conducting interphase comprising Sb, Li_3Sb, $LiSbO_3$, and Li_2C_2, which stabilized the Li/LLZTO interface during cycling (Fig. 10c). This modification reduced the interfacial impedance to 6 Ω cm^2 and enabled stable symmetric cell operation for >500 h at 0.1 mA cm^{-2}, with a maximum current density tolerance of 1.3 mA cm^{-2}. Separately, Zhang *et al.* demonstrated a scalable thermal polymerization approach to fabricate an organic–inorganic gel interlayer (GI) at the LLZTO/Li interface (Fig. 10d).[141] The GI forms *via in situ* polymerization of LLZTO particles with methyl methacrylate (MMA) and ethylene glycol dimethacrylate (EGDMA) monomers, initiated by 2,2′-azobisisobutyronitrile (AIBN) in a $LiPF_6$-containing liquid electrolyte ($LiPF_6$-LE). The design leverages the intrinsic lithiophilicity of LLZTO particles to significantly optimize interfacial physical contact and electrochemical compatibility. The 3D cross-linked network within the GI, synergizing with the LLZTO particles, constructs continuous lithium-ion channels, achieving uniform ion flux distribution at the interface. Its innovative rigid–flexible coupled structure is characterized by a rigid inorganic-rich

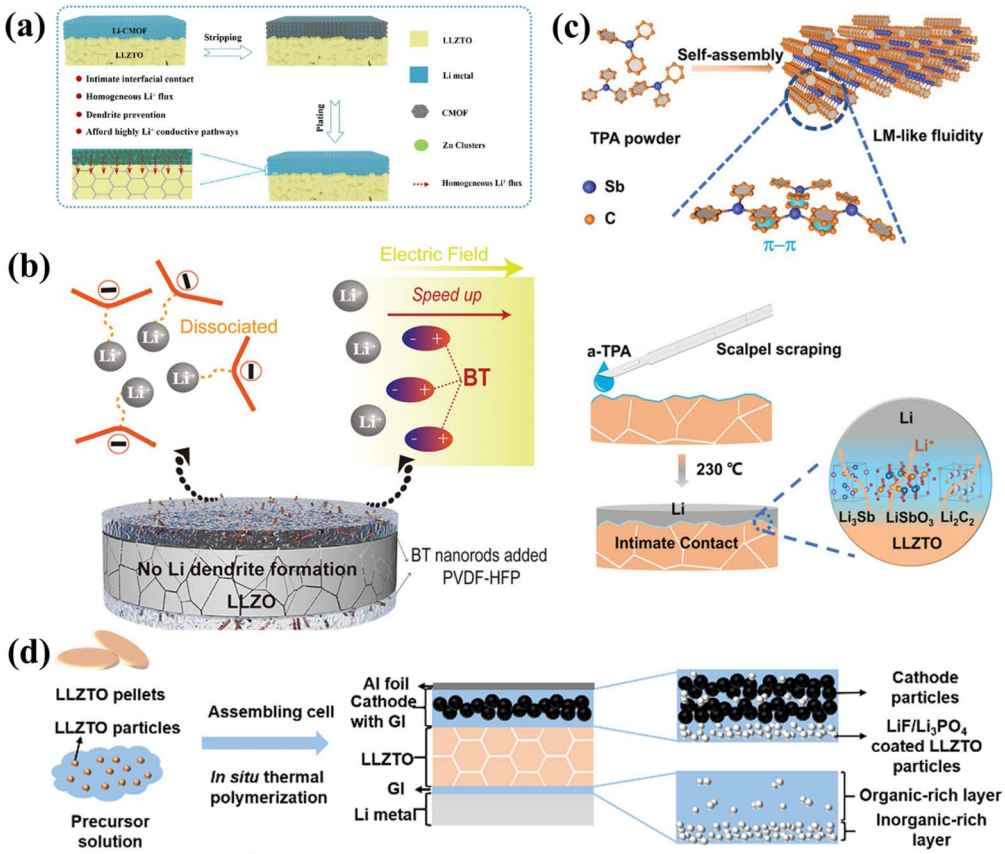

Fig. 10 (a) Casting process of pure Li and Li-CMOF on LLZTO. Reproduced with permission from ref. 138. Copyright 2024, American Chemical Society. (b) Electrochemical behavior of the CPE-BT modified Li/LLZO interface. Reproduced with permission from ref. 139. Copyright 2023, American Chemical Society. (c) Blade-coating and thermal lithiation of a-TPA on LLZTO. Reproduced with permission from ref. 140. Copyright 2022, Wiley-VCH GmbH. (d) *In situ* thermal polymerization for GI-modified SSLMB fabrication. Reproduced with permission from ref. 141. Copyright 2025, Elsevier.

composition near the lithium side to suppress dendrites and a flexible organic-rich composition near the LLZTO side to accommodate volume fluctuations. The GI enhanced the CCD to 1.9 mA cm^{-2} while demonstrating exceptional cycling stability (>2000 h at 0.1 mA cm^{-2} and >600 h at 1.5 mA cm^{-2}), confirming its superior dendrite suppression capability. Research has also found that charge transfer and interdiffusion at the interface significantly influence the modification by organic–inorganic interlayers.[150] When organic and inorganic materials contact, charge transfer may occur due to differences in their electron cloud distributions. This charge transfer can alter the electronic structure at the interface, thereby affecting the electrical properties and chemical reactivity of the materials. Simultaneously, interdiffusion of molecules may occur at the interface between the organic and inorganic materials. Under specific conditions, segments of organic molecular chains might diffuse into the lattice interstices of the inorganic material, or atoms/ions from the inorganic material might diffuse between the molecular chains of the organic material. This interdiffusion can enhance the bonding between organic and inorganic materials, improving interfacial compatibility.[141,151] The preparation of unique organic/inorganic composite interlayers demonstrates multifaceted advantages, particularly at high current densities and during long-term battery cycling, fully proving their potential benefits in improving interfacial contact, suppressing dendrite growth, and enhancing air stability.

In summary, the organic/inorganic composite interlayer not only improves the chemical interfacial contact between LLZO and electrodes, but also regulates the modulus gradient and mitigates local stress concentration. This dual functionality opens up new avenues for designing and fabricating stable ultrathin garnet-type SSEs.

3.3 Coupling of the surface state and mechanical reliability in roll-to-roll LLZO membrane manufacturing

Garnet-type SSEs feature high elastic and shear moduli, yet their intrinsically low fracture toughness renders them highly sensitive to surface and near-surface flaws under tensile or bending loads.[152] When LLZO is transitioned from bulk or thick-sheet forms to ultrathin ceramic membranes or free-standing composite films, this flaw sensitivity is markedly amplified during roll-to-roll (R2R) processing. As illustrated by the process-evolution model in Fig. 11, membrane transport along an R2R line is not merely physical conveyance, but rather

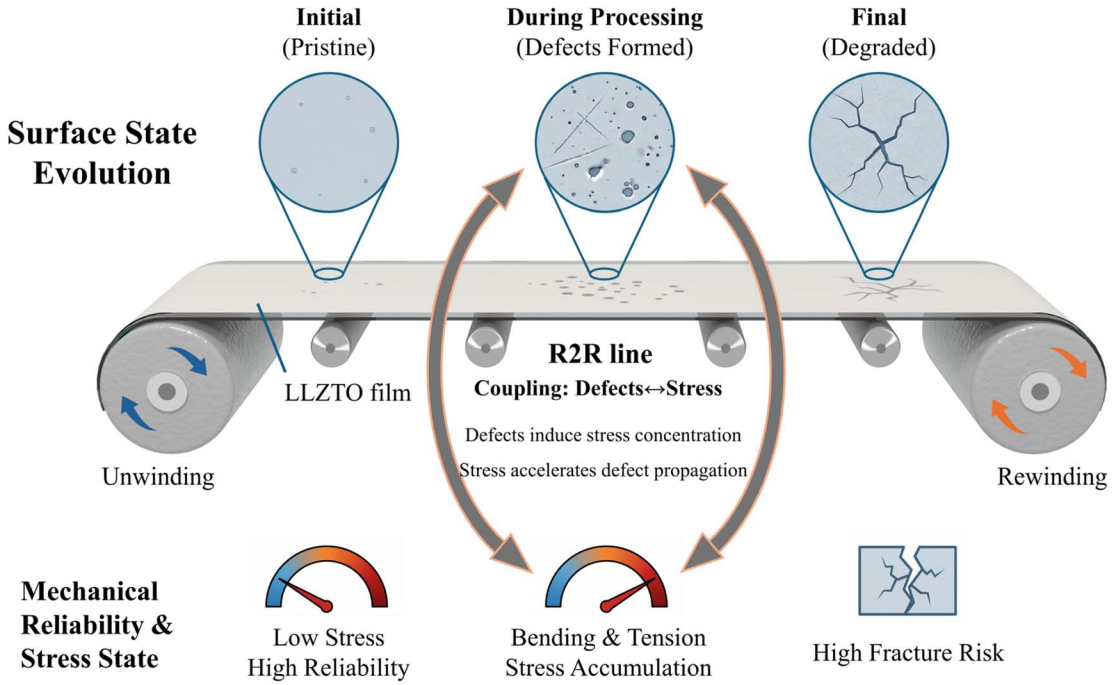

Fig. 11 Schematic illustration of the coupling between the surface state and mechanical reliability for an ultrathin LLZO membrane during roll-to-roll (R2R) processing. The membrane transitions from an initial pristine state to a degraded state containing processing-induced defects, while bending and tensile stresses gradually accumulate, leading to a decline in mechanical reliability. The central circular arrow emphasizes the vicious cycle of coupling between surface defects and mechanical stress.

a process accompanied by dynamic evolution of mechanical reliability. During this process, the membrane is no longer a static elastic body but a dynamic system defined jointly by its surface state and external stress. Under bending conditions, the outer surface of the membrane experiences tensile stress, while the inner surface is under compression, causing surface defects to become primary sites for stress concentration. Consequently, the effective bending reliability of the membrane is governed not by its bulk mechanical properties but by defect-controlled fracture behavior.[156,157]

Surface post-treatments used to remove Li_2CO_3 or improve interfacial wettability (*e.g.*, chemical etching, halogenation reactions, plasma treatment, and mechanical polishing) can optimize interfacial chemistry, but they often inevitably modify the surface topography and near-surface microstructure. Non-uniform chemical etching may introduce micron-scale pits, plasma or ion treatments can create amorphous damaged layers or residual stress fields in the subsurface region, and improper mechanical polishing can easily produce directional scratches. This progression corresponds to the surface-state evolution depicted at the top of Fig. 11, where the membrane surface accumulates damage as processing proceeds, transitioning from a pristine state to a degraded state containing microcracks and defects. While such defects may not be prominent in static characterization, they can substantially reduce the effective fracture resistance under bending or cyclic loading, serving as critical triggers for crack initiation and propagation.

As the LLZO thickness is reduced to tens of micrometers or below, the tensile strain at the outer surface can become significant even at relatively large bending radii, allowing micron-scale surface flaws to trigger catastrophic fracture. Moreover, the coupling of web tension and bending in R2R manufacturing, repetitive low-strain cycling, and modulus mismatch within composite architectures may further accelerate subcritical crack growth and amplify failure risk.[158–160] This underpins the defect–stress coupling mechanism highlighted in Fig. 11: surface defects induce local stress concentration, while the tensile and bending moments imposed by R2R processing, in turn, promote defect growth. This adverse feedback loop leads to a rapid deterioration of mechanical reliability along the processing line (as schematically shown by the dashboard at the bottom of Fig. 11), ultimately resulting in a sharply increased fracture risk. In this context, organic/inorganic composite interlayers serve a dual purpose. They improve electrochemical performance by enhancing interfacial contact. Simultaneously, the compliant organic phase helps redistribute tensile stress and blunts crack tips. These combined effects thereby improve the processing tolerance and structural robustness of ultrathin LLZO membranes during practical manufacturing.

In this section, we have systematically summarized a range of interfacial and surface engineering techniques. These strategies primarily aim to reduce the interfacial impedance between LLZO and Li and suppress the formation of Li_2CO_3, thereby enhancing interfacial stability and electrochemical performance. Meanwhile, with the development of garnet electrolytes toward ultrathin ceramic membranes and free-standing composite films, manufacturing-induced surface-

state changes and their impacts on mechanical reliability have become increasingly important. Different technical approaches possess distinct advantages and limitations regarding interfacial chemistry regulation, structural integrity, and manufacturing compatibility. Therefore, rational selection for specific application scenarios is particularly crucial. Based on available studies, the following principles may serve as practical guidance for researchers:

(1) Technical effectiveness: priority should be given to technologies that have been experimentally validated to significantly reduce interfacial impedance and efficiently remove or convert Li_2CO_3. For instance, attention should be paid to quantitative metrics such as the actual reduction magnitude of interfacial resistance and the residual amount of Li_2CO_3 after implementing the technology. A technology demonstrating a consistent reduction of interfacial impedance by more than 50% across multiple experimental sets, coupled with minimal residual Li_2CO_3, can be considered highly effective.

(2) Compatibility considerations: the selected technology must exhibit good chemical and physical compatibility with both the LLZO electrolyte and the Li electrode. On one hand, the technology itself should not undergo chemical reactions with LLZO or Li that could damage their structure and electrochemical properties. On the other hand, any newly introduced materials should coexist stably with these two components. For example, when selecting a coating material, its coefficient of thermal expansion should be matched with those of LLZO and Li to avoid interfacial failure or delamination induced by temperature fluctuations.

(3) Alignment with application scenario requirements: the choice of technology should be tailored to the specific operating conditions of the battery, such as temperature, voltage, and humidity. In high-temperature or high-pressure environments, priority should be given to inorganic interlayers or high-entropy doped materials with good thermal stability. For flexible or wearable devices, organic interlayers designed for enhanced flexibility to accommodate mechanical deformation are preferable. In high-humidity environments, hydrophobic interlayers with a contact angle greater than 110° should be used to block moisture infiltration, thereby preventing the formation of Li_2CO_3.

(4) Cost-effectiveness and resource constraints: a balance between performance enhancement and cost input is necessary, prioritizing cost-effective solutions. For applications where performance requirements are not stringent, low-cost chemical treatment strategies may be more suitable. In scenarios demanding high performance, although techniques like plasma cleaning or composite interlayer design involve higher costs, they can effectively achieve a Li_2CO_3-free interface, significantly mitigate interfacial issues, and markedly improve battery cycle life.

(5) Manufacturing compatibility and mechanical reliability: for ultrathin LLZO membranes or self-supporting composite electrolytes, the selection of interface engineering strategies requires careful prioritization. Strategies should be chosen primarily for their ability to enhance interfacial electrochemical performance. Crucially, they must also avoid introducing significant surface damage or stress concentration risks. Particularly under R2R processing conditions, their impact on bending stability and fracture tolerance must be thoroughly evaluated.

By comprehensively weighing the above principles, researchers can make more informed decisions when choosing suitable interface engineering strategies, thereby accelerating the development of high-performance garnet-based SSLMBs.

3.4 Mitigation of Li_2CO_3 at the cathode interface

In garnet-type SSLMBs, the stability and ion transport efficiency of the cathode/LLZO interface are critical factors determining the energy density, rate performance, and long-term reliability of the battery. Among these, the formation, evolution, and high-voltage reactivity of Li_2CO_3 at the cathode interface have increasingly been recognized as key scientific and engineering bottlenecks affecting the intrinsic properties, electrochemical stability, and even device lifetime. Li_2CO_3 primarily originates from the unavoidable surface chemical reactions of the garnet electrolyte in air, and its presence at the cathode interface exerts multidimensional and multiscale effects on the interface. From a relatively static physicochemical perspective, Li_2CO_3 is an electronic insulator with extremely low ionic conductivity. When it exists as a continuous or discontinuous thin layer between the cathode active material (*e.g.*, high-nickel NCM, $LiCoO_2$) and the LLZO electrolyte, it introduces a significant energy barrier for Li^+ migration from the electrolyte bulk into the cathode interior. This leads to a marked increase in interfacial ion transport resistance, manifesting as elevated initial polarization and poor first-cycle efficiency.

Under high-voltage charge/discharge conditions, the electrochemical instability of Li_2CO_3 exacerbates the above issues. When the cell operating voltage exceeds its stability window (generally considered to start around 3.8–4.0 V *vs.* Li^+/Li), Li_2CO_3 at the interface undergoes oxidative decomposition, releasing O_2 and CO_2. In solid-state systems lacking the re-wetting capability of liquid electrolytes, these gases accumulate within the cathode composite layer, at GBs, and at solid–solid interfaces, forming microscopic gas cavities. This physically disrupts the initially intimate contact between cathode active particles and LLZO particles, blocking ion transport pathways. The contact failure caused by gas generation in solid-state systems is highly irreversible and is a more destructive degradation mechanism compared to traditional liquid cells. Moreover, the decomposition of Li_2CO_3 generates active oxygen species. These species further oxidize and erode the cathode material surface, triggering the continuous growth of a thicker and higher-impedance cathode electrolyte interphase (CEI) layer.[161] Concurrently, they promote the leaching and migration of transition metal ions, collectively establishing a vicious cycle of continuous interface degradation. By using cycling and potential-resolved electrochemical impedance spectroscopy (PR-EIS), measurements clearly demonstrate that the abrupt increase in interfacial impedance is strongly correlated with gas evolution during the operation of $LiMn_2O_4$ (LMO)/LLZO/Li batteries within the 4–4.6 V range. This correlation confirms

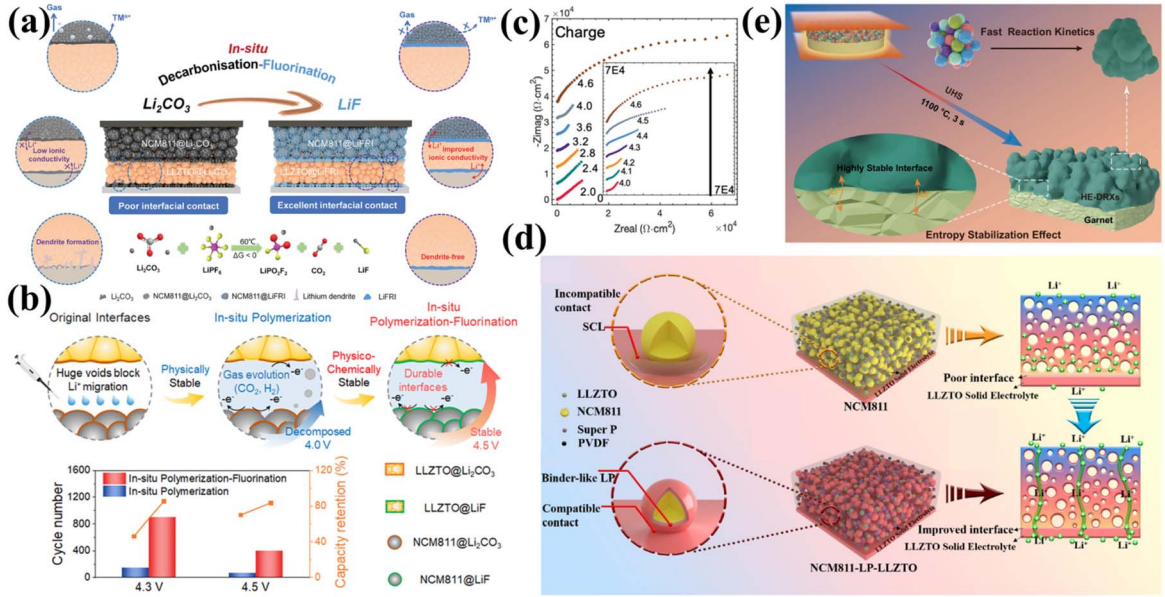

Fig. 12 (a) *In situ* Li_2CO_3-to-LiF conversion at cathode/LLZTO interfaces. Reproduced with permission from ref. 153. Copyright 2023, Wiley-VCH GmbH. (b) Comparative electrode/LLZTO interface engineering for high-voltage SSBs. Reproduced with permission from ref. 154. Copyright 2025, American Chemical Society. (c) Potential-resolved impedance spectra of LMO/LLZO/Li cells (4.6 V cutoff), with the inset showing 100 mV interval data from 4.0–4.6 V. Reproduced with permission from ref. 48. Copyright 2021, Wiley-VCH GmbH. (d) *In situ* engineered NCM811/LLZTO interface. Reproduced with permission from ref. 155. Copyright 2020, Elsevier. (e) UHS-processed HE-DRX|LLZTO interface stabilization. Reproduced with permission from ref. 81. Copyright 2024, Springer Nature.

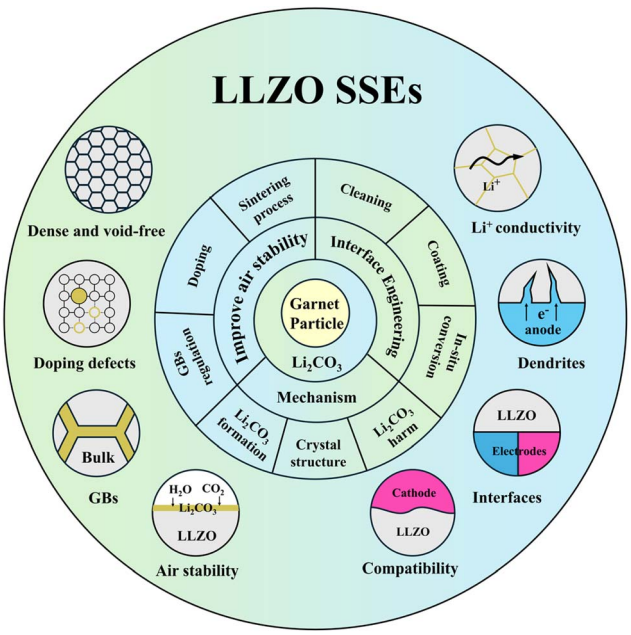

Fig. 13 Schematic diagram of the content structure of this review.

the central role of Li_2CO_3 decomposition in cathode interface degradation, as illustrated in Fig. 12c.[48]

During the material preparation stage, Li_2CO_3 can also have a profound impact on the compatibility of the cathode/LLZO interface. During the high-temperature co-sintering of composite cathodes, Li_2CO_3 on the LLZO surface can react with the cathode material. This reaction may lead to the formation of electrochemically inert impurity phases, such as $La_2Zr_2O_7$, or promote the diffusion of transition metals like Co and Ni into the electrolyte. These processes compromise the structural integrity of both the cathode and the electrolyte. Traditional long-duration high-temperature sintering processes often exacerbate these side reactions.[47,50]

Faced with the systematic challenges posed by Li_2CO_3 at the cathode interface, current research has shifted from passively avoiding its formation to actively utilizing and engineering its conversion, developing multi-level and multi-approach interface regulation strategies.

3.4.1 *In situ* conversion to build functional interface layers. Through carefully designed chemical reactions, *in situ* conversion of Li_2CO_3 to interface phases with ionic conductivity or electrochemical activity is an effective way to turn waste into treasure. For example, Yang *et al.*[37] introduced Co_3O_4 during the preparation of LLZTO-based composite cathodes, enabling a solid-state reaction with Li_2CO_3 on the LLZTO surface to form $LiCoO_2$. This process effectively eliminates the insulating Li_2CO_3 layer at the interface while simultaneously enabling the in-suit construction of an ionically conductive $LiCoO_2$ coating. This significantly improves the interfacial compatibility and contact tightness between LLZTO and the $LiCoO_2$ active particles within the composite cathode. Consequently, the cycle stability of the battery is enhanced. Additionally, Liu *et al.*[162] found that introducing 3% $LiCoO_2$ as a sintering aid into the garnet electrolyte helped avoid cross-diffusion and improved the cathode/LLZO interface contact.

For interface failure issues under high-voltage conditions, constructing an artificial LiF-rich interface layer is considered a more targeted solution. Guo *et al.*[153] developed a $LiPF_6$-mediated decarbonization–fluorination reaction at 60 °C (Li_2CO_3 → LiF), constructing a crystalline LiF-rich cathode electrolyte interphase at the interface. This stable layer effectively suppresses the high-voltage decomposition and gas generation problems of Li_2CO_3 (Fig. 12a). Similarly, as shown in Fig. 12b, Yin *et al.*[154] proposed a synergistic *in situ* polymerization–fluorination strategy (Poly-FR), using a bifunctional initiator to simultaneously trigger polymer matrix formation and the LiF interface. Both strategies, by converting detrimental Li_2CO_3 into a stable LiF layer, fundamentally circumvent the regeneration limitations of traditional calcination methods, offering universal solutions for high-voltage SSB interface engineering.

3.4.2 Introduction of functional additives or coating layers to optimize the interface microenvironment. In the preparation or sintering process of composite cathodes, introducing low-melting-point additives with certain lithium-ion conductivity can melt during heat treatment and fill the gaps between particles, forming a more dense and continuous ion conduction network. For instance, Zhao *et al.*[155] introduced a binder-like Li_3PO_4 precursor *in situ* during a one-step calcination process, constructing a Li^+-conductive layer (LLZTO–Li_3PO_4) on the NCM811 surface. This effectively reduced interfacial impedance and weakened the space-charge layer effect (Fig. 12d). Based on this design, the initial discharge capacity at 1C was 153.4 mAh g^{-1} at 55 °C and 149.6 mAh g^{-1} at 80 °C. After 100 cycles, it remained at 117.5 mAh g^{-1} and 115.2 mAh g^{-1}, respectively. In the annealing process of composite cathodes, *in situ* coating can be achieved by introducing low-melting-point sintering additives. The molten additives form conformal coatings on the cathode active material particles and LLZTO-based ion conductors. Han *et al.*[163] used a pre-existing Li_2CO_3 and borate precursor ($Li_{2.3-x}Co_{0.7+x}B_{0.3-x}O_3$) reaction to *in situ* generate highly conductive lithium borate oxide (LCBO) matrices, achieving tight integration between the cathode and LLZTO interfaces. However, the ionic conductivity of currently reported sintering additives is generally lower than that of the electrolyte, underscoring the urgent need to develop additives with both low melting points and high ionic conductivity to facilitate composite cathode sintering.[164,165]

3.4.3 Innovating preparation processes to construct clean interfaces from the source. On the process level, ultrafast high-temperature sintering (UHS) employs extremely high heating rates and very short dwell times, enabling densification and interface bonding between the cathode material and LLZO under conditions far from thermodynamic equilibrium. This significantly suppresses Li_2CO_3 formation, interfacial side reactions, and element interdiffusion. As shown in Fig. 12e, Kong *et al.*[81] utilized UHS technology to co-sinter high-entropy disordered rock-salt (HE-DRX) cathodes and LLZTO in approximately 3 s, achieving a low interface impedance of 31.6 Ω cm^2, which is 700 times lower than that of traditional sintering methods. This demonstrates the great potential of addressing interface contamination at its source. The rapid heating and cooling process effectively inhibited elemental cross-diffusion and increased the interface stability temperature of HE-DRXs/LLZTO to 1100 °C. The integration of entropy-stabilized effects and rapid reaction kinetics achieved a good combination of chemical stability and wettability, promoting the development of durable, conformal interfaces. The assembled cell delivered 239.7 ± 2 mAh g^{-1} at 25 mA g^{-1} with 95% capacity retention after 100 cycles (150 °C).

In summary, suppressing the formation of Li_2CO_3 and reducing ion transport resistance at the interface are crucial for maintaining the structural stability and electrochemical compatibility of the cathode/LLZO interface. The synergistic application of interface wetting, *in situ* chemical conversion, and advanced preparation processes can alleviate Li_2CO_3-induced interface failure issues across different scales, providing a reliable interfacial foundation for the stable operation of high-voltage, high-energy-density SSLMBs. Furthermore, starting from the perspective of stabilizing the interface and near-interface transport structure, Fan *et al.* regulated ion migration and interfacial compatibility through confined interaction networks, offering new ideas and directions for interface design under high-voltage conditions.[166] Notably, the high-voltage stability of LiF-rich interfaces has gradually become a common recognition across different systems. Recent research on high-voltage electrolyte design also emphasizes achieving more stable interface structures through fluorine-containing chemistry, which indirectly confirms the universal value of LiF-rich interlayers in high-voltage stabilization.[167]

4 Conclusion and perspective

Garnet-type SSEs, particularly LLZO, exhibit exceptional promise for all-solid-state batteries owing to their high ionic conductivity, superior chemical stability, and broad electrochemical window. However, air exposure induces the formation of insulating Li_2CO_3/LiOH passivation layers on particle surfaces, as confirmed by both experimental and computational studies. These surface layers not only create resistive core–shell architectures but also promote deleterious phase transformations during synthesis, generating impurity phases (*e.g.*, $La_2Zr_2O_7$) that degrade bulk ionic conductivity by up to 2–3 orders of magnitude. More critically, the surface Li_2CO_3 layer severely deteriorates the electrochemical performance of SSLMBs. Its detrimental effects are primarily manifested in a dramatic increase in interfacial resistance, hindered lithium-ion transport, and accelerated lithium dendrite growth. Furthermore, within composite cathodes, Li_2CO_3 contaminants impede effective contact between active materials and LLZO electrolyte particles, leading to diminished capacity retention. The ultra-low ionic conductivity and lithiophobic nature of these contaminants exert a profoundly negative impact on Li^+ migration and solid–solid interfacial contact, posing a significant bottleneck for the commercialization of garnet-type SSBs. Therefore, achieving the scalable production, storage, and application of LLZO electrolytes without reaction with ambient air remains a critical challenge to be addressed. This paper systematically reviews the inherent causes of the instability of garnet electrolytes in air, summarizes recent strategies to

improve their air stability (including controlling external environments and regulating internal microstructures), and delves into interfacial engineering methods to solve the electrode/garnet electrolyte interface issues. These strategies aim to collaboratively enhance the ionic conductivity, air stability, dendrite suppression ability, and interfacial compatibility of garnet electrolytes (Fig. 13). By offering profound insights into the Li_2CO_3 contamination problem, this review is intended to facilitate the development of high-performance and highly stable garnet-type SSLMBs.

4.1 Enhancing air stability and suppressing Li_2CO_3 formation

While sulfide-type SSEs generally exhibit higher sensitivity to air compared to garnet electrolytes, relatively mature strategies have been established to enhance their air stability, notably through rational elemental doping. Inspired by this, utilizing elemental doping to improve the air stability of garnet-type SSEs and inhibit Li_2CO_3 formation has become a prominent research avenue. However, a deep understanding of the reaction mechanisms of dopant elements is crucial for their rational selection. Current research hotspots focus on high-entropy doping strategies, which aim to enhance the thermodynamic stability of the electrolyte by introducing multi-component elements to lower the system's ΔG. Looking ahead, the combination of machine learning (ML) and automated reaction screening holds promise as a novel approach for guiding element selection prior to experimental doping, enabling rapid screening of target products. ML can not only analyze the effects of different dopants but also integrate electrochemical data and structural characterization results. Subsequently, artificial intelligence (AI) could be leveraged to predict the formation mechanisms of Li_2CO_3. Building on this, inverse materials design can be further explored: intelligently designing novel high-entropy doped garnet electrolyte materials based on predefined target performance parameters (*e.g.*, ionic conductivity and interfacial stability).

4.2 Developing multifunctional composite interface modification strategies

Current mainstream interface modification methods primarily focus on introducing single protective layers (*e.g.*, AlF_3, Zn, and Ag). However, such single-layer structures struggle to effectively address the multiple complex challenges at solid–solid interfaces. Therefore, there is an urgent need to develop multifunctional composite interface modification strategies. Examples include synergistically constructing interface layers with mixed ionic/electronic conductive properties and designing composite anode structures, aiming to achieve more stable and efficient interfacial ion transport kinetics and mechanical stability. A core future research direction will be to intensively investigate how such composite strategies effectively suppress lithium dendrite growth and increase the CCD, ultimately constructing an optimal Li/LLZO interface.

4.3 Optimizing the cathode/electrolyte interface

Compared to the electrolyte/lithium metal anode interface, optimizing the cathode/electrolyte interface requires greater emphasis. Current research often relies on introducing liquid electrolytes to address challenges like poor solid–solid interfacial compatibility and limited ion transport on the cathode side, which deviates from the fundamental goal of an all-solid-state solution. Although introducing sintering aids can effectively improve the contact and stability at the cathode/garnet electrolyte interface, systematic studies in this area remain limited. Optimizing the composite cathode interface requires a multi-dimensional collaborative effort, including but not limited to increasing the effective solid–solid contact area, maintaining interfacial structural/chemical stability, and constructing a continuous and efficient mixed ionic/electronic conductive network. Therefore, deeply analyzing the internal hierarchical structure and key interfacial issues of LLZO-based composite cathodes is a decisive factor for achieving the large-scale application of high-performance garnet-type SSBs, holding significant fundamental research value and practical guidance.

4.4 Reconsidering the role of Li_2CO_3

Currently, numerous studies report comprehensive strategies to inhibit Li_2CO_3 formation, such as optimizing sintering processes and tailoring microstructures or using physical/chemical methods to remove Li_2CO_3 contaminants after air exposure. However, these strategies often struggle to effectively improve interfacial wettability or require expensive equipment, presenting significant limitations. In light of this, rather than focusing solely on the complete eradication of Li_2CO_3 from garnet particle interfaces, it is worthwhile to shift perspective and explore the possibility of its rational utilization. Li_2CO_3 at the interface can provide an alkaline environment, and its properties could be harnessed to construct lithiophilic, hydrophobic, or wetting layers between phases. Furthermore, the inherent chemical inertness of Li_2CO_3 allows it to potentially serve as a stable interfacial layer. Under proper storage conditions, its negative impact on the structure and electrochemical performance of the electrolyte material can be effectively controlled. From this viewpoint, the traditionally perceived Li_2CO_3 layer as an insulating barrier might instead offer new opportunities and possibilities for achieving intimate solid–solid interfacial contact, enhancing material air stability, and optimizing battery electrochemical performance.

4.5 Advanced characterization for interface evolution

Building on a deep understanding of the formation mechanisms of Li_2CO_3 on the LLZO surface and multi-scale interface regulation strategies, research finds that breakthroughs in core issues like tracing the origin of contaminants and interface engineering optimization highly depend on the precise analysis of material dynamic evolution processes. The current research frontier is undergoing a crucial shift from static component analysis to the visual tracking of dynamic processes. There is an urgent need to develop advanced characterization techniques

with spatiotemporal resolution capabilities to enable the full-cycle dynamic monitoring of ion transport, stress distribution, and chemical reconstruction behaviors at solid–solid interfaces. Representative techniques include: synchrotron-based *in situ* XAS, which can resolve the real-time evolution of the local electronic structure and coordination environment of transition metal elements (*e.g.*, Ni, Co, and Mn) in electrode materials; three-dimensional layer-by-layer analysis using Time-of-Flight Secondary Ion Mass Spectrometry (ToF-SIMS), capable of precisely revealing the gradient distribution characteristics of elements in the interface region; and the combination of atomic-level interface imaging *via* cryo-TEM with chemical fingerprint identification by Raman spectroscopy, which can construct quantitative correlation models between interfacial reaction kinetics and macroscopic electrochemical performance at the mesoscale. The synergistic application and innovation of these multi-dimensional, high-resolution characterization techniques not only provide critical experimental criteria for evaluating the effectiveness of interface modification strategies but also reveal the complex mechanisms behind interface modifications at a deeper level. This promotes a paradigm shift in solid electrolyte research from empirical optimization to mechanism-driven design, laying a scientific foundation for the multi-scale, dynamic, and precise regulation of SSB interfaces.

4.6 From lab to fab: the scalability and manufacturability of Li_2CO_3 mitigation strategies

While significant progress has been made at the laboratory scale in understanding the formation mechanisms, interfacial degradation, and mitigation strategies for Li_2CO_3, its translation into practical applications hinges critically on manufacturability and cost control during the industrial-scale production process. Unlike processing single pellet samples under controlled lab conditions, mass production emphasizes process consistency, continuity, and robustness against environmental fluctuations. Therefore, future developments in Li_2CO_3-related interface engineering need to shift from performance optimization to design for manufacturability.

At the scale-up preparation level, garnet-type SSEs are highly sensitive to exposure to H_2O/CO_2, making atmosphere control and process integration critical challenges. Post-treatment steps such as polishing, chemical conversion, or surface modification risk having their effectiveness rapidly diminished during transfer and storage if they cannot be integrated *in situ* or in a closed-loop manner with subsequent manufacturing steps. Furthermore, many laboratory techniques, such as acid treatment, fluorination, or phosphate conversion strategies, require comprehensive evaluation for their safety, solvent recovery, by-product management, and large-area uniformity control when scaled up. In contrast, physical processes such as plasma, laser, or ultrasound could potentially offer advantages in process controllability if they can be adapted to online, continuous operation. However, these processes still require careful consideration of equipment costs and energy consumption per unit output.

On the other hand, industrialization demands that interface performance enhancement be translated into actionable quality control (QC) metrics. For example, the residual levels of Li_2CO_3/LiOH, interface roughness, defect density, and the statistical distribution of key interface impedance need to be characterized using rapid, low-cost, online or spot-checking methods to ensure consistency and yield in mass production. Interface engineering strategies without clear process windows and quality thresholds will struggle to be reliably reproduced in actual production lines. From a cost and system integration perspective, more practical Li_2CO_3 control strategies typically feature low temperature, short time, and low environmental sensitivity, while being compatible with existing slurry coating, roll-to-roll lamination, co-sintering, or rapid sintering processes. Future research should place greater emphasis on establishing quantifiable trade-offs between interface stability improvements and manufacturing complexity, energy consumption, and unit kWh costs.

Overall, solving the Li_2CO_3 issue is not only a material or interface chemistry problem but also a systemic engineering challenge that spans material synthesis, interface engineering, and process scaling. Only through the collaborative optimization of mechanistic understanding and manufacturability design can the interface control strategies for Li_2CO_3 in garnet-type LMBs be truly scaled for practical applications.

In conclusion, garnet-type SSEs show considerable promise for enabling high-energy-density and high safety in SSLMBs. However, the interface chemical, electrochemical, and mechanical failure issues caused by Li_2CO_3 are not isolated phenomena but represent a systemic challenge that spans material synthesis, interface construction, and device manufacturing. In recent years, significant progress has been made in understanding the formation mechanisms of Li_2CO_3, its high-voltage failure behavior, and interface control strategies. The research focus has gradually expanded from material optimization to the synergistic design of interface engineering and process strategies. Looking to the future, the scalability of garnet-type SSLMBs will not only depend on further improvements in interface performance but also on the comprehensive balance of manufacturability, consistency, and cost controllability of the related strategies. With the deepening understanding of interfacial evolution mechanisms and the introduction of advanced preparation and engineering approaches, garnet-type SSLMBs are poised to overcome existing bottlenecks and advance steadily toward practical application and commercialization.

Author contributions

B. Hao: investigation, writing – original draft and format analysis; Q. Wang: investigation; F. Zhao: formal analysis; J. Wu: formal analysis; W. Chen: formal analysis; Z.-J. Jiang: supervision and writing – review & editing; Z. Jiang: resources, writing – review & editing, and supervision.

Conflicts of interest

There are no conflicts to declare.

Data availability

No primary research results, software or code have been included and no new data were generated or analysed as part of this review.

Acknowledgements

The authors acknowledge support from the Zhejiang Provincial Natural Science Foundation (No. LRG26E070001 and LR22E070001), the National Natural Science Foundation of China (No. 12275239), and the Guangdong Basic and Applied Basic Research Foundation (No. 2025A1515010349).

Notes and references

1 Z. Deng, Y. Liu, L. Wang, N. Fu, Y. Li, Y. Luo, J. Wang, X. Xiao, X. Wang, X. Yang, X. He and H. Zhang, Challenges of Thermal Stability of High-Energy Layered Oxide Cathode Materials for Lithium-Ion Batteries: A Review, *Mater. Today*, 2023, **69**, 236–261.

2 J. Biao, C. Bai, J. Ma, M. Liu, F. Kang, Y. Cao and Y.-B. He, Perspectives on Li Dendrite Penetration in $Li_7La_3Zr_2O_{12}$-Based Solid-State Electrolytes and Batteries: Materials, Interfaces, and Charge Transfer, *Adv. Energy Mater.*, 2024, **14**, 2303128.

3 H. Wan, J. Xu and C. Wang, Designing Electrolytes and Interphases for High-Energy Lithium Batteries, *Nat. Rev. Chem.*, 2024, **8**, 30–44.

4 C. Bai, Y. Li, G. Xiao, J. Chen, S. Tan, P. Shi, T. Hou, M. Liu, Y.-B. He and F. Kang, Understanding the Electrochemical Window of Solid-State Electrolyte in Full Battery Application, *Chem. Rev.*, 2025, **125**, 6541–6608.

5 J. Lee, S. Zhou, V. C. Ferrari, C. Zhao, A. Sun, S. Nicholas, Y. Liu, C. Sun, D. Wierzbicki, D. Y. Parkinson, J. Bai, W. Xu, Y. Du, K. Amine and G.-L. Xu, Halide Segregation to Boost All-Solid-State Lithium-Chalcogen Batteries, *Science*, 2025, **388**, 724–729.

6 S. C. Kim, J. Wang, R. Xu, P. Zhang, Y. Chen, Z. Huang, Y. Yang, Z. Yu, S. T. Oyakhire, W. Zhang, L. C. Greenburg, M. S. Kim, D. T. Boyle, P. Sayavong, Y. Ye, J. Qin, Z. Bao and Y. Cui, High-Entropy Electrolytes for Practical Lithium Metal Batteries, *Nat. Energy*, 2023, **8**, 814–826.

7 L. Chen, P. Shi, T. Gu, J. Mi, K. Yang, L. Zhao, J. Lv, M. Liu, Y.-B. He and F. Kang, Strategies of Constructing Highly Stable Interfaces with Low Resistance in Inorganic Oxide-Based Solid-State Lithium Batteries, *eScience*, 2025, **5**, 100277.

8 P. López-Aranguren, M. Reynaud, P. Głuchowski, A. Bustinza, M. Galceran, J. M. López del Amo, M. Armand and M. Casas-Cabanas, Crystalline LiPON as a Bulk-Type Solid Electrolyte, *ACS Energy Lett.*, 2021, **6**, 445–450.

9 Z. Jian, Y.-S. Hu, X. Ji and W. Chen, NASICON-Structured Materials for Energy Storage, *Adv. Mater.*, 2017, **29**, 1601925.

10 S. Woo and B. Kang, Superior Compatibilities of a LISICON-Type Oxide Solid Electrolyte Enable High Energy Density All-Solid-State Batteries, *J. Mater. Chem. A*, 2022, **10**, 23185–23194.

11 D. Zeng, J. Yao, L. Zhang, R. Xu, S. Wang, X. Yan, C. Yu and L. Wang, Promoting Favorable Interfacial Properties in Lithium-Based Batteries using Chlorine-Rich Sulfide Inorganic Solid-State Electrolytes, *Nat. Commun.*, 2022, **13**, 1909.

12 X. Zhou, C. Gao, D. Wang, S. Peng, L. Huang, W. Yang, W.-H. Zhang and X. Gao, Revealing the Dominant Factor of Domain Boundary Resistance on Bulk Conductivity in Lanthanum Lithium Titanates, *J. Energy Chem.*, 2022, **73**, 354–359.

13 Z. Jin, X. Kong, H. Huang, Y. Jiang, W. Xiang, Y. Xu, L. Zhang, R. Peng and C. Wang, Garnet-Type Solid-State Mixed Ionic and Electronic Conductor, *Energy Storage Mater.*, 2023, **59**, 102788.

14 C. Wang, K. Fu, S. P. Kammampata, D. W. McOwen, A. J. Samson, L. Zhang, G. T. Hitz, A. M. Nolan, E. D. Wachsman, Y. Mo, V. Thangadurai and L. Hu, Garnet-Type Solid-State Electrolytes: Materials, Interfaces, and Batteries, *Chem. Rev.*, 2020, **120**, 4257–4300.

15 X. He, F. Yan, M. Gao, Y. Shi, G. Ge, B. Shen and J. Zhai, Cu-Doped Alloy Layer Guiding Uniform Li Deposition on a Li-LLZO Interface under High Current Density, *ACS Appl. Mater. Interfaces*, 2021, **13**, 42212–42219.

16 J.-F. Wu, B.-W. Pu, D. Wang, S.-Q. Shi, N. Zhao, X. Guo and X. Guo, In Situ Formed Shields Enabling Li_2CO_3-Free Solid Electrolytes: A New Route to Uncover the Intrinsic Lithiophilicity of Garnet Electrolytes for Dendrite-Free Li-Metal Batteries, *ACS Appl. Mater. Interfaces*, 2019, **11**, 898–905.

17 B. Chen, J. Zhang, T. Zhang, R. Wang, J. Zheng, C. Liu and X. Liu, Directly Using Li_2CO_3 as a Lithiophobic Interlayer to Inhibit Li Dendrites for High-Performance Solid-State Batteries, *ACS Energy Lett.*, 2023, **8**, 2221–2231.

18 A. Sharafi, S. Yu, M. Naguib, M. Lee, C. Ma, H. M. Meyer, J. Nanda, M. Chi, D. J. Siegel and J. Sakamoto, Impact of Air Exposure and Surface Chemistry on Li-$Li_7La_3Zr_2O_{12}$ Interfacial Resistance, *J. Mater. Chem. A*, 2017, **5**, 13475–13487.

19 C. Cao, L. Zhao, Y. Zhong, J. Simi and Z. Shao, Optimization of Garnet-Type Solid-State Lithium Batteries via Synergistic Integration of an Advanced Composite Interface for Elevated Performance, *Chem. Eng. J.*, 2024, **495**, 153649.

20 Y. Wang, Z. Chen, K. Jiang, Z. Shen, S. Passerini and M. Chen, Accelerating the Development of LLZO in Solid-State Batteries Toward Commercialization: A Comprehensive Review, *Small*, 2024, **20**, 2402035.

21 G. J. Redhammer, P. Badami, M. Meven, S. Ganschow, S. Berendts, G. Tippelt and D. Rettenwander, Wet-Environment-Induced Structural Alterations in Single- and Polycrystalline LLZTO Solid Electrolytes Studied by Diffraction Techniques, *ACS Appl. Mater. Interfaces*, 2021, **13**, 350–359.

22 J. Leng, H. Wang, H. Liang, Z. Xiao, S. Wang, Z. Zhang and Z. Tang, Storage of Garnet Solid Electrolytes: Insights into

Air Stability and Surface Chemistry, *ACS Appl. Energy Mater.*, 2022, **5**, 5108–5116.

23 N. Zhang, G. Ren, L. Li, Z. Wang, P. Yu, X. Li, J. Zhou, H. Zhang, L. Zhang, Z. Liu and X. Liu, Dynamical Evolution of CO_2 and H_2O on Garnet Electrolyte Elucidated by Ambient Pressure X-ray Spectroscopies, *Nat. Commun.*, 2024, **15**, 2777.

24 Q. Zhao, S. Stalin, C.-Z. Zhao and L. A. Archer, Designing Solid-State Electrolytes for Safe, Energy-Dense Batteries, *Nat. Rev. Mater.*, 2020, **5**, 229–252.

25 M. Du, Y. Sun, B. Liu, B. Chen, K. Liao, R. Ran, R. Cai, W. Zhou and Z. Shao, Smart Construction of an Intimate Lithium | Garnet Interface for All-Solid-State Batteries by Tuning the Tension of Molten Lithium, *Adv. Funct. Mater.*, 2021, **31**, 2101556.

26 K. Yoon, S. Lee, K. Oh and K. Kang, Challenges and Strategies towards Practically Feasible Solid-State Lithium Metal Batteries, *Adv. Mater.*, 2022, **34**, 2104666.

27 L. Zhang, Q. Meng, Y. Dai, X. Feng, M. Shen, Q. Zhuang, Z. Ju, R. Zheng, Z. Wang, Y. Cui, H. Sun and Y. Liu, Ion/Electron Conductive Layer with Double-Layer-Like Structure for Dendrite-Free Solid-State Lithium Metal Batteries, *Nano Energy*, 2023, **113**, 108573.

28 F. Wang, Z. Jiang, Y. Zhang, Y. Zhang, J. Li, H. Wang, Y. Jiang, G. Xing, H. Liu and Y. Tang, Revitalizing Sodium-Ion Batteries Via Controllable Microstructures and Advanced Electrolytes for Hard Carbon, *eScience*, 2024, **4**, 100181.

29 L. Cheng, E. J. Crumlin, W. Chen, R. Qiao, H. Hou, S. Franz Lux, V. Zorba, R. Russo, R. Kostecki, Z. Liu, K. Persson, W. Yang, J. Cabana, T. Richardson, G. Chen and M. Doeff, The Origin of High Electrolyte-Electrode Interfacial Resistances in Lithium Cells Containing Garnet Type Solid Electrolytes, *Phys. Chem. Chem. Phys.*, 2014, **16**, 18294–18300.

30 W. Xia, B. Xu, H. Duan, X. Tang, Y. Guo, H. Kang, H. Li and H. Liu, Reaction Mechanisms of Lithium Garnet Pellets in Ambient Air: The Effect of Humidity and CO_2, *J. Am. Ceram. Soc.*, 2017, **100**, 2832–2839.

31 W. Lu, T. Wang, M. Xue and C. Zhang, Improved $Li_{6.5}La_3Zr_{1.5}Nb_{0.5}O_{12}$ Electrolyte and Effects of Atmosphere Exposure on Conductivities, *J. Power Sources*, 2021, **497**, 229845.

32 Z. Zhang, E. Zhao, W. Yin, B. Wang, Y. Li and F. Wang, Visualization and Quantification of Li Distribution in Garnet Solid Electrolytes $Li_{6.25}La_3Zr_2Al_{0.25}O_{12}$, *Appl. Phys. Lett.*, 2024, **125**, 243903.

33 A. Sharafi, E. Kazyak, A. L. Davis, S. Yu, T. Thompson, D. J. Siegel, N. P. Dasgupta and J. Sakamoto, Surface Chemistry Mechanism of Ultra-Low Interfacial Resistance in the Solid-State Electrolyte $Li_7La_3Zr_2O_{12}$, *Chem. Mater.*, 2017, **29**, 7961–7968.

34 M. Nakayama, T. Horie, R. Natsume, S. Hashimura, N. Tanibata, H. Takeda, H. Maeda and M. Kotobuki, Reaction Kinetics of Carbonation at the Surface of Garnet-Type $Li_7La_3Zr_2O_{12}$ as Solid Electrolytes for All-Solid-State Li Ion Batteries, *J. Phys. Chem. C*, 2023, **127**, 7595–7601.

35 A. Kim, K. Song, M. Avdeev and B. Kang, High Energy Density Ultra-thin Li Metal Solid-State Battery Enabled by a Li_2CO_3-Proof Garnet-Type Solid Electrolyte, *ACS Energy Lett.*, 2024, **9**, 1976–1983.

36 J. Biao, B. Han, Y. Cao, Q. Li, G. Zhong, J. Ma, L. Chen, K. Yang, J. Mi, Y. Deng, M. Liu, W. Lv, F. Kang and Y.-B. He, Inhibiting Formation and Reduction of Li_2CO_3 to LiC_x at Grain Boundaries in Garnet Electrolytes to Prevent Li Penetration, *Adv. Mater.*, 2023, **35**, 2208951.

37 Y.-N. Yang, Y.-X. Li, Y.-Q. Li and T. Zhang, On-Surface Lithium Donor Reaction Enables Decarbonated Lithium Garnets and Compatible Interfaces within Cathodes, *Nat. Commun.*, 2020, **11**, 5519.

38 T. Zhang, T. D. Christopher, S. Huang, Y. g. Liu, W. Gao, T. Söhnel and P. Cao, Pressureless Sintering of Al-free Ta-Doped Lithium Garnets $Li_{7-x}La_3Zr_{2-x}Ta_xO_{12}$ and the Degradation Mechanism in Humid Air, *Ceram. Int.*, 2019, **45**, 20954–20960.

39 M. W. Swift, J. W. Swift and Y. Qi, Modeling the Electrical Double Layer at Solid-State Electrochemical Interfaces, *Nat. Comput. Sci.*, 2021, **1**, 212–220.

40 Z. Guo, Q. Li, X. Li, Z. Wang, H. Guo, W. Peng, G. Li, G. Yan and J. Wang, Uniform Densification of Garnet Electrolyte for Solid-State Lithium Batteries, *Small Methods*, 2023, **7**, 2300232.

41 D. Cao, C. Tan and Y. Chen, Oxidative Decomposition Mechanisms of Lithium Carbonate on Carbon Substrates in Lithium Battery Chemistries, *Nat. Commun.*, 2022, **13**, 4908.

42 H. Zheng, G. Li, R. Ouyang, Y. Han, H. Zhu, Y. Wu, X. Huang, H. Liu and H. Duan, Origin of Lithiophilicity of Lithium Garnets: Compositing or Cleaning?, *Adv. Funct. Mater.*, 2022, **32**, 2205778.

43 D. Wang, H. Shi, S. Liang, R. Shao, S. Wang, W. Cui, W. Wang and Z. Xu, Evolution of the Cell Structure, Ionic Conductivity, and Elastic Modulus of the γ-Irradiated LLZTO Electrolyte via Neutron Diffraction and Nanoindentation, *J. Phys. Chem. C*, 2024, **128**, 1911–1920.

44 P. Chen, P. Guo, W. Guo, B. Ding, H. Dou and X. Zhang, Identifying Interface Evolutions for Achieving Stable Solid-State Li Metal Batteries, *J. Energy Chem.*, 2025, **110**, 363–371.

45 C.-Y. Chang, C.-C. Wang, C.-H. Cheng, Y.-L. Lu, S.-H. Lin, J. Granwehr, A. Windmüller, C.-L. Tsai, R.-A. Eichel and K.-F. Chiu, Enhanced Stability and High Rate Capability of Garnet Solid-State Electrolyte Interface through Integration of Nanoscale $Li_4Ti_5O_{12}$ for Li Battery Applications, *J. Power Sources*, 2025, **652**, 237593.

46 C. Tang, Z. Fan, B. Ding, C. Xu, H. Wu, H. Dou and X. Zhang, Functional Separator with Poly(Acrylic Acid)-Enabled Li_2CO_3-Free Garnet Coating for Long-Cycling Lithium Metal Batteries, *Small*, 2025, **21**, 2407558.

47 S. Weinmann, H. Gobena, L. Quincke, J. J. Hinricher, S. Merk, H. Chu, T. Prein, J. L. M. Rupp and K. J. Kim, Stabilizing Interfaces of All-Ceramic Composite Cathodes for Li-Garnet Batteries, *Adv. Energy Mater.*, 2025, **15**, 2502280.

48 A. A. Delluva, J. Kulberg-Savercool and A. Holewinski, Decomposition of Trace Li_2CO_3 During Charging Leads to Cathode Interface Degradation with the Solid Electrolyte LLZO, *Adv. Funct. Mater.*, 2021, **31**, 2103716.

49 Q. Gan, N. Qin, H. Yuan, L. Lu, Z. Xu and Z. Lu, Critical review on the degradation mechanisms and recent progress of Ni-rich layered oxide cathodes for lithium-ion batteries, *EnergyChem*, 2023, **5**, 100103.

50 T. Demuth, T. Fuchs, F. Walther, A. Pokle, S. Ahmed, M. Malaki, A. Beyer, J. Janek and K. Volz, Influence of the sintering temperature on LLZO-NCM cathode composites for solid-state batteries studied by transmission electron microscopy, *Matter*, 2023, **6**, 2324–2339.

51 Y. Kim, I. Waluyo, A. Hunt and B. Yildiz, Avoiding CO_2 Improves Thermal Stability at the Interface of $Li_7La_3Zr_2O_{12}$ Electrolyte with Layered Oxide Cathodes, *Adv. Energy Mater.*, 2022, **12**, 2102741.

52 W. S. Scheld, K. Kim, C. Schwab, A. C. Moy, S.-K. Jiang, M. Mann, C. Dellen, Y. J. Sohn, S. Lobe, M. Ihrig, M. G. Danner, C.-Y. Chang, S. Uhlenbruck, E. D. Wachsman, B. J. Hwang, J. Sakamoto, L. F. Wan, B. C. Wood, M. Finsterbusch and D. Fattakhova-Rohlfing, The Riddle of Dark LLZO: Cobalt Diffusion in Garnet Separators of Solid-State Lithium Batteries, *Adv. Funct. Mater.*, 2023, **33**, 2302939.

53 H. Zhou, Y. Zhou, X. Li, X. Huang and B. Tian, Li_5AlO_4-Assisted Low-Temperature Sintering of Dense $Li_7La_3Zr_2O_{12}$ Solid Electrolyte with High Critical Current Density, *ACS Appl. Mater. Interfaces*, 2024, **16**, 5989–5998.

54 H. Zhang, Y. Wu, J. Zhu, X. Xie, Z. Liu, Z. Zhang, Y. Ma, T. Huang, L. Wang, J. Lin, Q. Xie and D.-L. Peng, Fusing Ta-Doped $Li_7La_3Zr_2O_{12}$ Grains Using Nanoscale Y_2O_3 Sintering Aids for High-Performance Solid-State Lithium Batteries, *Nanoscale*, 2024, **16**, 14871–14878.

55 S. P. Kammampata, R. H. Basappa, T. Ito, H. Yamada and V. Thangadurai, Microstructural and Electrochemical Properties of Alkaline Earth Metal-Doped Li Garnet-Type Solid Electrolytes Prepared by Solid-State Sintering and Spark Plasma Sintering Methods, *ACS Appl. Energy Mater.*, 2019, **2**, 1765–1773.

56 X. Xiang, Z. Fang, C. Du, Z. Zhao, J. Chen, Y. Zhang, H. Wang, C. Wei, F. Chen and Q. Shen, Constructing Electron-Blocking Grain Boundaries in Garnet to Suppress Lithium Dendrite Growth, *J. Adv. Ceram.*, 2024, **13**, 166–175.

57 R. A. Jonson and P. J. McGinn, Effects of High Energy Ball Milling on Phase Stability of $Li_7La_3Zr_2O_{12}$, *ECS Meet. Abstr.*, 2016, **MA2016-03**, 673.

58 X. Feng, L. Zhang, C. Li, M. Shen, R. Zheng, Z. Wang, H. Sun and Y. Liu, Al-Ta Dual-Substituted $Li_7La_3Zr_2O_{12}$ Ceramic Electrolytes with Two-Step Sintering for Stable All-Solid-State Lithium Batteries, *Ceram. Int.*, 2024, **50**, 38999–39009.

59 Y. Dabaki, M. Kassem, A. Sammoury, M. Bokova, M. Fourmentin, O. El-Kedim and E. Bychkov, Influence of Microwave Sintering and Pellet Pressure on the Phase Formation, Microstructure and Lithium-Ion Conductivity of the $Li_{6.28}Al_{0.24}La_3Zr_2O_{12}$ Solid Electrolyte, *J. Mater. Eng. Perform.*, 2025, **34**, 6733–6742.

60 Y. Yang, Z. Zhang, T. Ma, S. Jia and C. Huang, Low-Temperature Flash Sintering of Dense Ta-Doped $Li_7La_3Zr_2O_{12}$ Solid Electrolyte for Solid-State Lithium Batteries, *Ionics*, 2025, **31**, 1341–1350.

61 X. Wang, J. Wang, F. Li, F. Zhu and C. Ma, Influence of Cold Sintering Process on the Structure and Properties of Garnet-Type Solid Electrolytes, *Ceram. Int.*, 2020, **46**, 18544–18550.

62 A. C. Moy, G. Häuschen, D. Fattakhova-Rohlfing, J. B. Wolfenstine, M. Finsterbusch and J. Sakamoto, The Effects of Aluminum Concentration on the Microstructural and Electrochemical Properties of Lithium Lanthanum Zirconium Oxide, *J. Mater. Chem. A*, 2022, **10**, 21955–21972.

63 R. Shi, Y. Pu, W. Wang, Y. Shi, J. Li, X. Guo and M. Yang, Flash Sintering of Barium Titanate, *Ceram. Int.*, 2019, **45**, 7085–7089.

64 M. Biesuz and V. M. Sglavo, Flash Sintering of Ceramics, *J. Eur. Ceram. Soc.*, 2019, **39**, 115–143.

65 H. K. Bezabh, L. H. Abrha, S.-F. Chiu, Y. Nikodimos, T. M. Hagos, M.-C. Tsai, W.-N. Su and B. J. Hwang, Enhancing Ionic Conductivity and Air Stability of $Li_7La_3Zr_2O_{12}$ Garnet-Based Electrolyte through Dual-Dopant Strategy, *J. Alloys Compd.*, 2025, **1010**, 177277.

66 S. Kobi, A. Sharma and A. Mukhopadhyay, Low Interfacial Resistance and Superior Suppression to Li-Dendrite Penetration Facilitated by Air-Stable and Mechanically Robust Al/Mg-Co-Doped Li-La-Zirconate as Electrolyte for Li-Based Solid-State Cells, *ACS Appl. Mater. Interfaces*, 2023, **15**, 39276–39290.

67 S. Yu, Y. Li, J. Luo, D. Chen, L. Yang, Y. Wei, D. Li, Y. Li and Y. Chen, Reasonable Design a High-Entropy Garnet-Type Solid Electrolyte for All-Solid-State Lithium Batteries, *J. Energy Chem.*, 2024, **96**, 414–423.

68 H. Zheng, G. Li, J. Liu, S. Wu, X. Zhang, Y. Wu, H. Zhu, X. Huang, H. Liu and H. Duan, A rational Design of Garnet-Type $Li_7La_3Zr_2O_{12}$ with Ultrahigh Moisture Stability, *Energy Storage Mater.*, 2022, **49**, 278–290.

69 M. Nasir, J. Y. Park, P. Heo, K. H. Choi and H. J. Park, Li-La-Zr-O Garnets with High Li-Ion Conductivity and Air-Stability by Microstructure-Engineering, *Adv. Funct. Mater.*, 2023, **33**, 2303397.

70 J. Guo, H. Guo, A. L. Baker, M. T. Lanagan, E. R. Kupp, G. L. Messing and C. A. Randall, Cold Sintering: A Paradigm Shift for Processing and Integration of Ceramics, *Angew. Chem., Int. Ed.*, 2016, **55**, 11457–11461.

71 B. Nie, T.-W. Wang, S. W. Lee, J. Zhang and H. Sun, Probing Cold Sintering-Regulated Interfaces and Integration of Polymer-in-Ceramic Solid-State Electrolytes, *Mater. Today Energy*, 2025, **49**, 101829.

72 H. Salazar, B. F. Gonçalves, A. Valverde, R. Gonçalves, C. M. Costa, L. P. Cavalcanti, J. M. Porro, V. Petrenko, S. Lanceros-Mendez and Q. Zhang, High-Performance Composite Solid-State Electrolyte Combining NASICON-Type $Li_{1.5}Al_{0.5}Ti_{1.5}(PO4)_3$ with Ionic Liquid and Polymeric Binders, *Electrochim. Acta*, 2025, **509**, 145299.

73 H. Leng, J. Huang, J. Nie and J. Luo, Cold Sintering and Ionic Conductivities of $Na_{3.256}Mg_{0.128}Zr_{1.872}Si_2PO_{12}$ Solid Electrolytes, *J. Power Sources*, 2018, **391**, 170–179.

74 Y. Chen, T. Wang, H. Chen, W. H. Kan, W. Yin, Z. Song, C. Wang, J. Ma, W. Luo and Y. Huang, Local Structural Features of Medium-Entropy Garnet with Ultra-Long Cycle Life, *Matter*, 2023, **6**, 1530–1541.

75 R. Jalem, Y. Morishita, T. Okajima, H. Takeda, Y. Kondo, M. Nakayama and T. Kasuga, Experimental and First-Principles DFT Study on the Electrochemical Reactivity of Garnet-Type Solid Electrolytes with Carbon, *J. Mater. Chem. A*, 2016, **4**, 14371–14379.

76 D. Rettenwander, C. A. Geiger, M. Tribus, P. Tropper and G. Amthauer, A Synthesis and Crystal Chemical Study of the Fast Ion Conductor $Li_{7-3x}Ga_xLa_3Zr_2O_{12}$ with x = 0.08 to 0.84, *Inorg. Chem.*, 2014, **53**, 6264–6269.

77 H. Shiiba, M. Koyama, N. Zettsu and K. Teshima, Li-Ion Conduction Characteristics at Grain Boundaries in Garnet $Li_{7-x}La_3Zr_{2-x}Nb_xO_{12}$ $(0 \leq x \leq 2)$, *Chem. Mater.*, 2024, **36**, 6370–6380.

78 A. Kim, J.-H. Kang, K. Song and B. Kang, Simultaneously Improved Cubic Phase Stability and Li-Ion Conductivity in Garnet-Type Solid Electrolytes Enabled by Controlling the Al Occupation Sites, *ACS Appl. Mater. Interfaces*, 2022, **14**, 12331–12339.

79 L. Huang, J. Gao, Z. Bi, N. Zhao, J. Wu, Q. Fang, X. Wang, Y. Wan and X. Guo, Comparative Study of Stability against Moisture for Solid Garnet Electrolytes with Different Dopants, *Energies*, 2022, **15**, 3206.

80 S. Wang, X. Wen, Z. Huang, H. Xu, F. Fan, X. Wang, G. Tian, S. Liu, P. Liu, C. Wang, C. Zeng, C. Shu and Z. Liang, High-Entropy Strategy Flattening Lithium Ion Migration Energy Landscape to Enhance the Conductivity of Garnet-Type Solid-State Electrolytes, *Adv. Funct. Mater.*, 2025, **35**, 2416389.

81 X. Kong, R. Gu, Z. Jin, L. Zhang, C. Zhang, W. Xiang, C. Li, K. Zhu, Y. Xu, H. Huang, X. Liu, R. Peng and C. Wang, Maximizing Interface Stability in All-Solid-State Lithium Batteries through Entropy Stabilization and Fast Kinetics, *Nat. Commun.*, 2024, **15**, 7247.

82 Y. Zeng, B. Ouyang, J. Liu, Y.-W. Byeon, Z. Cai, L. J. Miara, Y. Wang and G. Ceder, High-Entropy Mechanism to Boost Ionic Conductivity, *Science*, 2022, **378**, 1320–1324.

83 Y. Feng, L. Yang, Z. Yan, D. Zuo, Z. Zhu, L. Zeng, Y. Zhu and J. Wan, Discovery of High Entropy Garnet Solid-State Electrolytes via Ultrafast Synthesis, *Energy Storage Mater.*, 2023, **63**, 103053.

84 E. Anderson, E. Zolfaghar, A. Jonderian, R. Z. Khaliullin and E. McCalla, Comprehensive Dopant Screening in $Li_7La_3Zr_2O_{12}$ Garnet Solid Electrolyte, *Adv. Energy Mater.*, 2024, **14**, 2304025.

85 M. Ali, M. Saleem, T. Sattar, M. Z. Khan, J. H. Koh, O. Gohar, I. Hussain, Y. Zhang, M. B. Hanif, G. Ali and M. F. Khan, High-Entropy Battery Materials: Revolutionizing Energy Storage with Structural Complexity and Entropy-Driven Stabilization, *Mater. Sci. Eng., R*, 2025, **163**, 100921.

86 X. Ma and Y. Xu, Effects of Polishing Treatments on the Interface Between Garnet Solid Electrolyte and Lithium Metal, *Electrochim. Acta*, 2023, **441**, 141789.

87 Z. Qin, Y. Xie, X. Meng, D. Qian, C. Shan, D. Mao, G. He, Z. Zheng, L. Wan and Y. Huang, Interface Engineering for Garnet-Type Electrolyte Enables Low Interfacial Resistance in Solid-State Lithium Batteries, *Chem. Eng. J.*, 2022, **447**, 137538.

88 S. Rajendran, A. Pilli, O. Omolere, J. Kelber and L. M. R. Arava, An All-Solid-State Battery with a Tailored Electrode-Electrolyte Interface Using Surface Chemistry and Interlayer-Based Approaches, *Chem. Mater.*, 2021, **33**, 3401–3412.

89 P. Srivastava, B. Bazri, D. K. Maurya, Y.-T. Hung, D.-H. Wei and R.-S. Liu, Green Strategy for Li_2CO_3 Regulation in Garnet-Type Solid-State Electrolytes via Acoustic Cavitation, *ACS Energy Lett.*, 2025, **10**, 1725–1732.

90 T. Sun, X. Cheng, T. Cao, M. Wang, J. Tian, T. Yan, D. Qin, X. Liu, J. Lu and Y. Zhang, Optimizing Li Ion Transport in a Garnet-Type Solid Electrolyte via a Grain Boundary Design, *Batteries*, 2023, **9**, 526.

91 W. Jeong, S. S. Park, J. Yun, H. R. Shin, J. Moon and J.-W. Lee, Tailoring Grain Boundary Structures and Chemistry of $Li_7La_3Zr_2O_{12}$ Solid Electrolytes for Enhanced Air Stability, *Energy Storage Mater.*, 2023, **54**, 543–552.

92 K. Ma, B. Chen, C.-X. Li and V. Thangadurai, Improvement of the Li-Ion Conductivity and Air Stability of the Ta-doped $Li_7La_3Zr_2O_{12}$ Electrolyte via Ga Co-Doping and Its Application in Li–S batteries, *J. Mater. Chem. A*, 2024, **12**, 3601–3615.

93 G. Zhao, C. Luo and Q. Hua, Enhanced Comprehensive Performance of the LLZO Series Solid Electrolyte via Multifunctional Additive, *J. Eur. Ceram. Soc.*, 2024, **44**, 2251–2260.

94 Y. Luo, J. Dong, Y. Wang, Z. Wang, Z. a. Chen and H. Zhang, Enhanced Electrochemical Performance of Garnet $Li_7La_3Zr_2O_{12}$ Electrolyte by Efficient Incorporation of LiCl, *Ceram. Int.*, 2024, **50**, 51055–51064.

95 X. Huang, C. Liu, Y. Lu, T. Xiu, J. Jin, M. E. Badding and Z. Wen, A Li-Garnet composite ceramic electrolyte and its solid-state Li-S battery, *J. Power Sources*, 2018, **382**, 190–197.

96 Y.-G. Lee, S. Hong, B. Pan, X. Wu, E. C. Dickey and J. F. Whitacre, Improving Bulk and Interfacial Lithium Transport in Garnet-Type Solid Electrolytes through Microstructure Optimization for High-Performance All-Solid-State Batteries, *ACS Appl. Mater. Interfaces*, 2024, **16**, 60340–60347.

97 Z. Qin, Y. Xie, X. Meng, D. Qian, D. Mao, Z. Zheng, L. Wan and Y. Huang, Grain Boundary Engineering in Ta-Doped Garnet-Type Electrolyte for Lithium Dendrite Suppression, *ACS Appl. Mater. Interfaces*, 2022, **14**, 40959–40966.

98 S. Vema, F. N. Sayed, S. Nagendran, B. Karagoz, C. Sternemann, M. Paulus, G. Held and C. P. Grey, Understanding the Surface Regeneration and Reactivity of Garnet Solid-State Electrolytes, *ACS Energy Lett.*, 2023, **8**, 3476–3484.

99 Y. Chen, B. Ouyang, X. Li, W. Liu, B. Yang, P. Ning, Q. Xia, F. Zan, E. Kan, J. Xu and H. Xia, Gradient Nitrogen Doping in the Garnet Electrolyte for Highly Efficient Solid-State-Electrolyte/Li Interface by N_2 Plasma, *ACS Appl. Mater. Interfaces*, 2023, **15**, 44962–44973.

100 L. Chen, Y. Su, J. Zhang, H. Zhang, B. Fan, G. Shao, M. Zhong and C.-A. Wang, Nanosecond Laser Cleaning Method to Reduce the Surface Inert Layer and Activate the Garnet Electrolyte for a Solid-State Li Metal Battery, *ACS Appl. Mater. Interfaces*, 2021, **13**, 37082–37090.

101 Y. Liu, M. Lei, C. Lai, J. Meng, X. Wu, Y. Yu, Y. Zhang and C. Li, Enable High Reversibility of Fe/Cu Based Fluoride Conversion Batteries via Interfacial Gas Release and Detergency of Garnet Electrolytes, *Mater. Today*, 2022, **61**, 65–77.

102 Z. Bi, Q. Sun, M. Jia, M. Zuo, N. Zhao and X. Guo, Molten Salt Driven Conversion Reaction Enabling Lithiophilic and Air-Stable Garnet Surface for Solid-State Lithium Batteries, *Adv. Funct. Mater.*, 2022, **32**, 2208751.

103 Z. Wang, W. Li, S. Jiao, J. Zhu, Z. Wang, J. Peng, W. Gong, J. Wang, H. Huang, H. Song and M. Yu, An in Situ-Formed LiI Interface Layer for Garnet-Based Lithium Metal Batteries, *Electrochim. Acta*, 2024, **488**, 144242.

104 X. Hu, Y. Wang, W. Guo, Y. Tian, X. Zhang, F. Kang, D. Zhou and B. Li, Garnet-Based Solid Lithium Metal Batteries with Ultralong Lifespan Enabled by Solvent-Free Trifluoroacetic Acid-Induced Interfacial Engineering, *J. Mater. Chem. A*, 2024, **12**, 13830–13840.

105 Q. Li, Z. Xiao, K. Pu, Y. Ma, C. Xian, W. Sun, M. Xu and S.-J. Bao, FEC-Driven Surface Conversion Reaction to Construct Lithiophilic and Air-Stabilized LLZTO for Durable Lithium Battery, *Chem. Eng. J.*, 2025, **507**, 160413.

106 W. Liu, B. Zhang, Q. Zhu, H. Qin, Z. Xiao, X. He, F. Zheng and X. Ou, Contradictory Structure Design with Li_2CO_3 Retention for Garnet-Based Solid-State Lithium Metal Batteries, *Nano Lett.*, 2025, **25**, 7818–7825.

107 X. Zhan, X. Pang, F. Mao, J. Lin, M. Li, Y. Zhao, P. Xu, Z. Xu, K. Liao, Q. Zhang and L. Zhang, Interfacial Reconstruction Unlocks Inherent Ionic Conductivity of Li-La-Zr-Ta-O Garnet in Organic Polymer Electrolyte for Durable Room-Temperature All-Solid-State Batteries, *Adv. Energy Mater.*, 2024, **14**, 2402509.

108 Y. Ruan, Y. Lu, X. Huang, J. Su, C. Sun, J. Jin and Z. Wen, Acid Induced Conversion Towards a Robust and Lithiophilic Interface for Li-$Li_7La_3Zr_2O_{12}$ Solid-State Batteries, *J. Mater. Chem. A*, 2019, **7**, 14565–14574.

109 N. Chen, B. Gui, B. Yang, C. Deng, Y. Liang, F. Zhang, B. Li, W. Sun, F. Wu and R. Chen, $LiPF_6$ Induces Phosphorization of Garnet-Type Solid-State Electrolyte for Stable Lithium Metal Batteries, *Small*, 2024, **20**, 2305576.

110 G. Lu, W. Liu, Z. Yang, Y. Wang, W. Zheng, R. Deng, R. Wang, L. Lu and C. Xu, Superlithiophilic, Ultrastable, and Ionic-Conductive Interface Enabled Long Lifespan All-Solid-State Lithium-Metal Batteries under High Mass Loading, *Adv. Funct. Mater.*, 2023, **33**, 2304407.

111 H. Zhao, M. Du, H. Mo, C. Wang, W. Zhou, K. Liao and Z. Shao, Garnet-Based Solid Li-Metal Batteries Operable under High External Pressure with HCOOH-Induced Electron-Blocking and Lithiophilic Interlayer, *ACS Appl. Mater. Interfaces*, 2024, **16**, 44997–45005.

112 Y. Ruan, Y. Lu, Y. Li, C. Zheng, J. Su, J. Jin, T. Xiu, Z. Song, M. E. Badding and Z. Wen, A 3D Cross-Linking Lithiophilic and Electronically Insulating Interfacial Engineering for Garnet-Type Solid-State Lithium Batteries, *Adv. Funct. Mater.*, 2021, **31**, 2007815.

113 L. Wang, Y. Lu, C. Zheng, M. Cai, F. Xu and Z. Wen, In Situ Construction of a Lithiophilic and Electronically Insulating Multifunctional Hybrid Layer Based on the Principle of Hydrolysis for a Stable Garnet/Li Interface, *Adv. Funct. Mater.*, 2024, **34**, 2402971.

114 C. Ji, S. Zhou, L. Cai, Y. Yuan, X. Liu, P. Huang and X. Xiong, Minimizing Surface Defects for High-Performance Garnet-Based Solid-State Li Metal Batteries, *Chem. Eng. J.*, 2025, **506**, 160161.

115 C. Zhang, J. Yu, Y. Cui, Y. Lv, Y. Zhang, T. Gao, Y. He, X. Chen, T. Li, T. Lin, Q. Mi, Y. Yu and W. Liu, An Electron-Blocking Interface for Garnet-based Quasi-Solid-State Lithium-Metal Batteries to Improve Lifespan, *Nat. Commun.*, 2024, **15**, 5325.

116 J. Liu, S. Song, J. Wang, X. Mei and H. Zhao, Electron Insulative Interface Based on Schottky Contact Enabling Dendrite-free Solid-state Lithium Metal Batteries, *Adv. Funct. Mater.*, 2025, **35**, 2505836.

117 J. Liu, K. Zha, S. Zhang, Q. Deng, N. Zhang, X. Lu and B. Wei, Interfacial Engineering of Garnet-Type Electrolytes for Solid-State Lithium Metal Batteries, *ACS Appl. Energy Mater.*, 2025, **8**, 7300–7309.

118 L. Zhai, J. Wang, X. Zhang, X. Zhou, F. Jiang, L. Li and J. Sun, Interface Engineering of $Li_{6.75}La_3Zr_{1.75}Ta_{0.25}O_{12}$ via in situ Built LiI/$ZnLi_x$ Mixed Buffer Layer for Solid-State Lithium Metal Batteries, *Chem. Sci.*, 2024, **15**, 7144–7149.

119 J. Wang, X. Han, Y. Feng, S. Chen, H. Yuan, R. Yang, W. Du, C. Hou, X. Liu, T. Tong, W. Zhang, F. Jiang, J. Sun and X. Zhang, In-Situ Construction of a Composite Interlayer for Dendrite-Free $Li_{6.75}La_3Zr_{1.75}Ta_{0.25}O_{12}$ Solid-State Batteries, *Compos. Commun.*, 2024, **46**, 101851.

120 X. Bai, G. Zhao, G. Yang, M. Wang, Q. Lin and N. Zhang, Multifunctional Double Layer Based on Regional Segregation for Stabilized and Dendrite-Free Solid-State Li Batteries, *Adv. Energy Mater.*, 2024, **14**, 2304112.

121 M. Gao, P. Li, S. Fu, S. Yu, Y. Hu, D. Chen, Y. Wei, D. Li, N. Wang, L. Yang and Y. Chen, Constructing a Li_2O/LiZn Mixed Ionic Electron Conductive Layer by Ultrasonic Spraying to Enhance Li/Garnet Solid Electrolyte Interface Stability for Solid-State Batteries, *ACS Appl. Mater. Interfaces*, 2024, **16**, 69253–69261.

122 Y. Yuan, Q. Liu, C. Ji, Z. Xiang, S. Feng and X. Xiong, Artificial Interface Engineering to Achieve High-Performance Garnet-Based Solid-State Lithium Metal Batteries, *J. Mater. Chem. A*, 2025, **13**, 6804–6812.

123 M. Wu, G. Xu, F. Liu, J. Ke, H. Bao, Q. Wang and Z. Ali, Alleviating the Local Charge Accumulation at Li/Garnet Interface Enabling Solid-State Lithium Batteries, *Chem. Eng. J.*, 2024, **500**, 157128.

124 B. Hao, W. Chen, J. Wu, Z.-J. Jiang, X. Chen and Z. Jiang, Long-Term Cycling Stability and Dendrite Suppression in Garnet-Type Solid-State Lithium Batteries via Plasma-Induced Artificial SEI Layer Formation, *Adv. Funct. Mater.*, 2025, **35**, 2502429.

125 J. Meng, Y. Zhang, X. Zhou, M. Lei and C. Li, Li_2CO_3-Affiliative Mechanism for Air-Accessible Interface Engineering of Garnet Electrolyte via Facile Liquid Metal Painting, *Nat. Commun.*, 2020, **11**, 3716.

126 W. Ji, B. Luo, Z. Zhang, Y. Tian, Q. Wang, G. Yu, X. He, Z. Liu, Z. Zhao, R. Zhao, S. Wang, J. Zheng, X. Wang, B. Zhang, J. Zhang, J. Liang and R. Jin, Liquid Metal-Driven Interfacial Electrochemistry: Phase Evolution Mechanisms for Enhanced Li/LLZTO Contact at Room Temperature, *Energy Storage Mater.*, 2025, **81**, 104488.

127 S. Yu, Z. Gong, M. Gao, J. Li, W. Xie, Y. Wei, D. Li, L. Yang, D. Chen, Y. Li and Y. Chen, In-Situ Construction of Nano-Multifunctional Interlayer to Obtain Intimate Li/Garnet Interface for Dendrite-Free All Solid-State Battery, *J. Mater. Sci. Technol.*, 2025, **206**, 248–256.

128 J. Leng, H. Liang, H. Wang, Z. Xiao, S. Wang, Z. Zhang and Z. Tang, A Facile and Low-Cost Wet-Chemistry Artificial Interface Engineering for Garnet-Based Solid-State Li Metal Batteries, *Nano Energy*, 2022, **101**, 107603.

129 S.-S. Chi, Y. Liu, N. Zhao, X. Guo, C.-W. Nan and L.-Z. Fan, Solid Polymer Electrolyte Soft Interface Layer with 3D Lithium Anode for All-Solid-State Lithium Batteries, *Energy Storage Mater.*, 2019, **17**, 309–316.

130 X. Ma, Y. Xu, B. Zhang, X. Xue, C. Wang, S. He, J. Lin and L. Yang, Garnet Si-$Li_7La_3Zr_2O_{12}$ Electrolyte with a Durable, Low Resistance Interface Layer for All-Solid-State Lithium Metal Batteries, *J. Power Sources*, 2020, **453**, 227881.

131 Z. Bi, W. Huang, S. Mu, W. Sun, N. Zhao and X. Guo, Dual-Interface Reinforced Flexible Solid Garnet Batteries Enabled by In-Situ Solidified Gel Polymer Electrolytes, *Nano Energy*, 2021, **90**, 106498.

132 L. Chen, Z. Huang, W. Pang, Z. Jin, Y. Li and C.-A. Wang, Dual Interface Layers for Solid-State Li Metal Battery with Low Interfacial Resistance and Small Polarization Based on Garnet Electrolyte, *Electrochim. Acta*, 2020, **330**, 135352.

133 J. Li, H. Zhang, Y. Cui, H. Da, Y. Cai and S. Zhang, Ultra-Stable High Voltage Lithium Metal Batteries Enabled by Solid Garnet Electrolyte Surface-Engineered with a Grafted Aromatics Layer, *Chem. Eng. J.*, 2022, **450**, 138457.

134 G. Yang, X. Bai, Y. Zhang, Z. Guo, C. Zhao, L. Fan and N. Zhang, A Bridge between Ceramics Electrolyte and Interface Layer to Fast Li^+ Transfer for Low Interface Impedance Solid-State Batteries, *Adv. Funct. Mater.*, 2023, **33**, 2211387.

135 C. Zheng, Y. Lu, Q. Chang, Z. Song, T. Xiu, J. Jin, M. E. Badding and Z. Wen, High-Performance Garnet-Type Solid-State Lithium Metal Batteries Enabled by Scalable Elastic and Li^+-Conducting Interlayer, *Adv. Funct. Mater.*, 2023, **33**, 2302729.

136 G. Zhao, W. Liu, B. Zhang, Z. Zhao, W. Huang, Y. Xu, J. Fang, T. Li and Y. Xu, Ion-Conducting Self-Healing Interlayer Enabling Ultrastable $Li_7La_3Zr_2O_{12}$-Lithium Interphase for High Performance Solid Lithium Metal Batteries, *Renewables*, 2025, **3**, 21–30.

137 A. Gutiérrez-Pardo, F. Aguesse, F. Fernández-Carretero, A. I. Siriwardana, A. García-Luis and A. Llordés, Improved Electromechanical Stability of the Li Metal/Garnet Ceramic Interface by a Solvent-Free Deposited OIPC Soft Layer, *ACS Appl. Energy Mater.*, 2021, **4**, 2388–2397.

138 G. Wang, C. Wei, X. Liu and W. Ding, Efficient Lithium Dendrite Control and Intimate Li/Garnet Interface Built through a Carbonized Metal-Organic Framework Layer, *ACS Appl. Energy Mater.*, 2024, **7**, 2278–2284.

139 Z. Li, X. Wang, X. Lin, X. Ou, J. Luo, Z. Chen, A. Li, J. Zhang, X. Wang and R. Zhao, Ferroelectric Nanorods as a Polymer Interface Additive for High-Performance Garnet-Based Solid-State Batteries, *ACS Appl. Mater. Interfaces*, 2023, **15**, 35684–35691.

140 Y. Liu, J. Meng, M. Lei, Y. Yu, C. Lai and C. Li, Alloyable Viscous Fluid for Interface Welding of Garnet Electrolyte to Enable Highly Reversible Fluoride Conversion Solid State Batteries, *Adv. Funct. Mater.*, 2023, **33**, 2208013.

141 L. Zhang, N. Wang, J. Wang, Y. Dang, R. Zheng, Z. Wang, J. Jiang, Y. Cui, Y. Wu, H. Sun, Q. Zhuang, Y. Liu and X. Sun, A Rigid-Flexible Gel Interlayer with Li^+-Conducting/e^--Insulating Properties for Dendrite-Free Solid-State Lithium Metal Batteries, *Mater. Today*, 2025, **87**, 77–89.

142 M. Cai, J. Jin, T. Xiu, Z. Song, M. E. Badding and Z. Wen, In-situ Constructed Lithium-Salt Lithiophilic Layer Inducing Bi-Functional Interphase for Stable LLZO/Li Interface, *Energy Storage Mater.*, 2022, **47**, 61–69.

143 K. Wang and D. Mollenhauer, First-Principles Studies on the Structure and Stability of the Solid Electrolyte Interphase with LiPON in Solid-State Batteries, *J. Phys. Chem. C*, 2025, **129**, 13160–13168.

144 S. J. Turrell, Y. Liang, T. Cai, B. Jagger and M. Pasta, Origin of Stability in the Solid Electrolyte Interphase formed between Lithium and Lithium Phosphorus Oxynitride, *Chem. Mater.*, 2025, **37**, 3504–3518.

145 S. Tu, B. Zhang, Y. Zhang, Z. Chen, X. Wang, R. Zhan, Y. Ou, W. Wang, X. Liu, X. Duan, L. Wang and Y. Sun, Fast-charging capability of graphite-based lithium-ion batteries enabled by Li_3P-based crystalline solid–electrolyte interphase, *Nat. Energy*, 2023, **8**, 1365–1374.

146 Y. Xia, G. Mao, T. Yao, J. Yang, Y. Zhou, K. Lin, Z. Xu, D. Chen, H. Shao and L. Shen, One-Step Biphasic Interfacial Engineering Stabilizes Single-Crystal Ultrahigh-Nickel Cathodes, *Adv. Funct. Mater.*, 2025, e13107.

147 Z. Gu, D. Song, S. Luo, H. Liu, X. Sun, L. Zhu, W. Ma and X. Zhang, Insights into the Anode-Initiated and Grain Boundary-Initiated Mechanisms for Dendrite Formation in All-Solid-State Lithium Metal Batteries, *Adv. Energy Mater.*, 2023, **13**, 2302945.

148 M. Wu, J. Ke, C. Tan, F. Liu, X. Sun and G. Xu, Depolarization-Induced Potential Equilibrium Reduces Electron Accumulation to Improve Interfacial

Compactness of Garnet Electrolyte with Li Metal, *Electrochim. Acta*, 2025, **536**, 146822.

149 Y. Zhao, X. Lin, Y. Yang, X. Wu, Z. Hu, M. Hua and P. Si, Economic and Effective Construction of a P/Sn Multifunctional Layer on the Li/Garnet Interface via Transformation Reactions, *ACS Sustainable Chem. Eng.*, 2024, **12**, 7092–7104.

150 Y. Xu, Y. Guo, X. Zhang, G. Zhang, K. Fang, Q. Peng, X. Zhang, X. Sun, K. Wang and Y. Ma, Tailoring Highly Ion-Conductive and Stabled PVDF-Based Solid Electrolyte via Surface Coordination Chemistry, *Adv. Funct. Mater.*, 2025, **35**, 2422461.

151 L. Zhao, Y. Du, C. Wang, D. Li, H. Li and Y. Zhao, Rationally Coordinating Polymer Enabling Effective Li-Ion Percolation Network in Composite Electrolyte for Solid-State Li-Metal Batteries, *Energy Storage Mater.*, 2024, **68**, 103360.

152 M. B. Dixit, B. S. Vishugopi, W. Zaman, P. Kenesei, J.-S. Park, J. Almer, P. P. Mukherjee and K. B. Hatzell, Polymorphism of garnet solid electrolytes and its implications for grain-level chemo-mechanics, *Nat. Mater.*, 2022, **21**, 1298–1305.

153 Y. Guo, S. Pan, X. Yi, S. Chi, X. Yin, C. Geng, Q. Yin, Q. Zhan, Z. Zhao, F.-M. Jin, H. Fang, Y.-B. He, F. Kang, S. Wu and Q.-H. Yang, Fluorinating All Interfaces Enables Super-Stable Solid-State Lithium Batteries by In Situ Conversion of Detrimental Surface Li_2CO_3, *Adv. Mater.*, 2024, **36**, 2308493.

154 X. Yin, Y. Guo, S. Chi, Y. Jia, F. Li, J. Qi, X. Yi, S. Wu and Q.-H. Yang, Beyond Polymerization: In Situ Coupled Fluorination Enables More Stable Interfaces for Solid-State Lithium Batteries, *J. Am. Chem. Soc.*, 2025, **147**, 4393–4402.

155 Z. Zhao, Z. Wen, X. Liu, H. Yang, S. Chen, C. Li, H. Lv, F. Wu, B. Wu and D. Mu, Tuning a Compatible Interface with LLZTO Integrated on Cathode Material for Improving NCM811/LLZTO Solid-State Battery, *Chem. Eng. J.*, 2021, **405**, 127031.

156 Y. Fu, X. C. Zhang, F. Z. Xuan, S. T. Tu and Z. D. Wang, Multiple cracking of thin films due to residual stress combined with bending stress, *Comput. Mater. Sci.*, 2013, **73**, 113–119.

157 L. Guan, Y. Shi, C. Gao, T. Wang, J. Zhou and R. Cai, Interfacial contact loss and bending effects on electrochemical-mechanical modeling for all-solid-state Li-ion batteries, *Electrochim. Acta*, 2023, **440**, 141669.

158 S. H. Kang, H. Lee, Y.-J. Hong, S. Myoung, H. Seo, J. Choi, S. Yoon, J. Y. Kim, D. O. Shin, M. J. Lee, Y.-S. Park, Y.-G. Lee and Y. M. Lee, High-Performance, Roll-to-Roll Fabricated Scaffold-Supported Solid Electrolyte Separator for Practical All-Solid-State Batteries, *Small*, 2025, **21**, 2502996.

159 J. Park, J. Kim, J. Kim, M. Kim, T. Song and U. Paik, Sustainable and cost-effective electrode manufacturing for advanced lithium batteries: the roll-to-roll dry coating process, *Chem. Sci.*, 2025, **16**, 6598–6619.

160 K. H. Ayalew, N. Palaniyandy, M. K. Mathe and P. F. Msomi, Garnet-type LLZO electrolytes for solid-state lithium batteries: Interfaces, conductivity, in-situ processing, and industrial prospects, *Chem. Eng. J.*, 2025, **524**, 168098.

161 W. Huang, Z. Bi, N. Zhao, Q. Sun and X. Guo, Chemical Interface Engineering of Solid Garnet Batteries for Long-Life and High-Rate Performance, *Chem. Eng. J.*, 2021, **424**, 130423.

162 X. Liu, X. Kong, W. Xiang, Y. Jiang, B. Xiong, W. Ping, C. Xia, D. Huan and C. Wang, $LiCoO_2$ Sintering Aid Towards Cathode-Interface-Enhanced Garnet Electrolytes, *J. Energy Chem.*, 2023, **84**, 181–188.

163 F. Han, J. Yue, C. Chen, N. Zhao, X. Fan, Z. Ma, T. Gao, F. Wang, X. Guo and C. Wang, Interphase Engineering Enabled All-Ceramic Lithium Battery, *Joule*, 2018, **2**, 497–508.

164 H. Hosokawa, A. Takeda, R. Inada and Y. Sakurai, Tolerance for Li Dendrite Penetration in Ta-Doped $Li_7La_3Zr_2O_{12}$ Solid Electrolytes Sintered with $Li_{2.3}C_{0.7}B_{0.3}O_3$ Additive, *Mater. Lett.*, 2020, **279**, 128481.

165 K. Chen, Y. Shen, Y. Zhang, Y. Lin and C.-W. Nan, High Capacity and Cyclic Performance in a Three-Dimensional Composite Electrode Filled with Inorganic Solid Electrolyte, *J. Power Sources*, 2014, **249**, 306–310.

166 Y. Fan, O. I. Malyi, H. Wang, X. Cheng, X. Fu, J. Wang, H. Ke, H. Xia, Y. Shen, Z. Bai, S. Chen, H. Shao, X. Chen, Y. Tang and X. Bao, Surface-Confined Disordered Hydrogen Bonds Enable Efficient Lithium Transport in All-Solid-State PEO-Based Lithium Battery, *Angew. Chem., Int. Ed.*, 2025, **64**, e202421777.

167 J. Li, J. Long, H. Du, J. Wang, W. Zhao, H. Gong, W. Zou, F. Wang, J. Shi, Y. Zhang, Z. Bai, O. I. Malyi and Y. Tang, Breaking Diffusion Limit in Ester-Flame-Proof Na-Ion Electrolytes Through Solvent Coordination Chemistry, *Angew. Chem., Int. Ed.*, 2025, **64**, e202512950.